8404549

Yeh, Yaw-Huei

FAILURE MECHANISMS OF BURIED PIPELINES UNDER FAULT MOVEMENT AND SOIL LIQUEFACTION

The University of Oklahoma PH.D. 1983

University Microfilms International 300 N. Zeeb Road, Ann Arbor, MI 48106

THE UNIVERSITY OF OKLAHOMA

GRADUATE COLLEGE

FAILURE MECHANISMS OF BURIED PIPELINES UNDER FAULT MOVEMENT AND SOIL LIQUEFACTION

A DISSERTATION

SUBMITTED TO THE GRADUATE FACULTY

in partial fulfillment of the requirements for the

degree of

DOCTOR OF PHILOSOPHY

BY

YAW-HUEI YEH

Norman, Oklahoma

1983

FAILURE MECHANISMS OF BURIED PIPELINES

UNDER FAULT MOVEMENT AND SOIL LIQUEFACTION

APPROVED BY

Thomas M. Murray

Akhtar S. Khan

DISSERTATION COMMITTEE

ABSTRACT

Failure Mechanisms of Buried Pipeline Under Fault Movement and Soil Liquefaction

Lifelines, such as oil and gas transmission lines and water and sewer pipelines have been damaged heavily in recent earthquakes. The damages of these lifelines have caused major, catastrophic disruption of essential service to human needs. Two of the seismic hazards are (a) large fault movement and (b) soil liquefaction.

A. Fault Movement

Although simplified analysis procedures for buried pipelines across tensile strike-slip fault zones have been proposed, the results are not accurate because of several assumptions involved. Furthermore, several other important failure mechanisms and parameters have not been investigated.

In this investigation, a more precise analysis for buried pipeline subjected to tensile strike-slip fault is proposed by modifying some of the assumptions used previously. Following topics are covered:

1) The conditions of using elastic foundation for the far end of the pipe and the ultimate passive soil pressure

near the fault are used to find the behavior of a pipeline crossing an active fault.

2) An iterative method is used to solve the non-linear equations induced from the non-linearity of material and soil characteristics and large displacement.

Based on the analysis results, this study also discusses the design criteria for buried pipeline subjected to various fault movements.

B. Soil Liquefaction

This is an initial research to investigate the performance of a pipeline in a soil liquefaction environment during earthquakes. Therefore, a fundamental idea is introduced to explain the pipe failure mechanisms under such soil liquefaction environment. The pipe is subjected to longitudinal wave propagation at the time of liquefaction of soil deposits. The longitudinal wave propagation (e.g. P-wave) induces axial strains (stresses) that cause pipe buckling/breaking.

A simplified pipe model on a time dependent elastic foundation is proposed to simulate a liquefaction situation that a pipeline is buried in a liquefiable zone during earthquakes and the finite difference technique coupled with a time-increment computer solution is employed to determine the dynamic responses of the proposed model numerically.

ACKNOWLEDGEMENT

The author wishes to express sincere gratitude to his adviser, Professor Leon R.L. Wang, for encourage and constructive criticism throughout the investigation of his dissertation. He is also grateful to Drs. T.M. Murray, A.R. Kukreti, A.S. Khan and A.B. Schwarzkopf for offering valuable suggestions.

Much appreciation is expressed to the University of Oklahoma and to the National Science Foundation (Grant Numbers CEE-8025172 and CEE-8209241) for financial support for this research.

Many thanks are also due to Miss Lori E. Creech and Mr. Thomas Hendrick for their help in proofreading.

Finally, the author also wishes to thank especially his parents for their supports and encouragement.

TABLE OF CONTENTS

LIST OF TABLES

LIST OF FIGURES

CHAPTER I

INTRODUCTION

Lifelines are fulfilling a vital role in conducting and/or distributing energy, communication, transportation and water. The interruption of services provided by these lifelines especially underground lifelines could give much inconveniece to human lives, and could sometimes cause the unexpected disasters. If such disruption occurs during an earthquake, the effect of the loss of vital services will be greatly amplified by impending fire-fighting and preventing essential communications, transportation, etc.

Recent studies(1,26,27,33,38) have shown that buried gas, water and sewer pipelines have been damaged heavily by earthquakes. According to the damage reports of buried pipelines due to earthquakes, the seismic hazards such as fault movement, landslide and ground squeeze are some of the major effects that cause the ruptures or severe distortions of the pipe. Under similar circumstances, ruptures have also occurred at the pipe connections to other structures where the large relative response between them has been observed. For example, the 1972 Managua earthquake(5) caused surficial displacement along four prominent strike-slip faults through the downtown area of the Nicaragua capital. Nearly all water mains crossing the faults ruptured, causing a major damage of the city water distribution system. In a similar fashion, surface faults and landslides caused by the 1971 San Fernando earthquake ruptured water, gas, and sewage lines seriously along the Sylmar segment of the San Fernando fault.

Ruptures or severe distortions (including pull-out failure of segmented pipe) might also result from the relative pipe movements in liquefied soils, and from the relative movements at abrupt interfaces between rock or stiff soils and much softner soils. During the earthquake of June 16, 1964, in Niigata, Japan(26,33), extensive damage to engineering structures occurred as a result of liquefaction of the sandy soil on which they were supported. Many structures settled more than 3 ft, and the settlement was often accompanied by severe tilting of buildings. In addition to settlement failure of buildings there was a kind of damage due to the floating of underground structures. Consequently, about 68% of the underground distribution lines were damaged. The general failure modes of buried pipelines observed after this earthquake were (a) pull-out of joints, (b) breaking of caulking, (c) pull-out of joints between caulking and lead pipes and (d) breaking of control valves and pipes. A similar situation also occurred to most areas of Hokkaido, Japan during the 1968 Tokachi-Oki Earthquake(39). Soil liquefaction was still the main cause of severely damaged buried pipelines in the stricken regions.

In general, two of the major seismic hazards(18) that can signicantly affect portions of a buried pipeline transmission system are: (a) Ground rupture and differential movement along fault zone and (b) soil liquefaction. To mitigate the damages of buried pipelines resulting from these two major seismic hazards, the effective analyses and consideration are required for the construction of buried pipelines.

To account for the pipe behaviors under each different seismic environment as previously mentioned, two distinct analyses were employed in this research. They are: (a) Non-linear static analysis for fault movement, and (b) finite difference method for soil liquefaction, respectively. The first analysis which includes the concepts of a beam on an elastic foundation and the non-linearity of passive earth pressure etc., is used to determine the resistant capacity of buried pipeline to the large fault movement (mainly by tensile strike slip). Due to the fact that equilibrium conditions are insufficient to determine pipeline stresses, the application of compatibility requirement would be quite essential for solving the problems related to fault movement. In addition, it is difficult to find an explicit expression for axial force along the pipe, therefore an iterative method is required. With regard to the problem of soil liquefaction, a finite differrence method was introduced to find the dynamic responses and/or buckling of the buried pipeline passing through a soil liquefiable zone. In order to simulate the phenomenon of soil liquefaction, the stiffness of surrounding soil of the pipe is assumed to be a time varying (decreasing) variable instead of a constant.

For both cases, a further parametric study to investigate the influences of all possible parameters to a buried pipeline was performed.

CHAPTER II

BACKGROUND OF RESEARCH

2.1 Preface

In a highly active seismic zone it is essentially impossible for a major pipeline transmission system to avoid seismic effects. In theory, a pipeline might be alined to avoid all regions with anticipated fault movements and high liquefaction potential to mitigate the hazard. However, in practice, constraints caused by environmental concerns, urban areas, and the need for contiguous real estate for right-of-way, provide very limited choices for the route. Often a route selected may pass through regions of active fault or with high liquefaction potential. For instance, in Southern California any pipeline from the coastal area to the interior must at least cross the San Andreas fault zone as well as several lesser known fault zones. In Niigata city, Japan, most of the city area is supported on sand deposits which are prone to cause soil liquefaction. It is unavoidable to place pipeline network system crisscrossing the liquefiable zone.

Therefore, differential pipe movements resulting from fault movements and soil liquefaction often must be accounted for in design. The following describes the research background on buried pipelines under these adverse environments.

2.2 Fault Movement

Generally fault displacement is associated with three types of faults, namely: strike-slip, normal-slip and reverse-slip as shown in Figure 2.1. By reviewing the earthquake reprots(20,38), it is noted that the vertical separations of fault motions range from 1-ft to 5-ft, but the horizontal displacements due to strike-slips could be up to 21-ft. Hall and Newmark(11) have pointed out that vertical fault motions (including normal-slip and reverse-slip) are generally not serious for metal pipe, since the pipe normally has the capability to produce a 4-ft or 5-ft vertical displacement without undue difficulty. In this respect, large abrupt differential horizontal ground movements (strike-slip) which result at an active fault probably present the most severe earthquake effect on a buried pipeline. If the fault movement is large, the buried pipeline may break through the surrounding soil. Survivability in this environment requires the pipeline to undergo large inelastic deformations without rupture. At the present time, the researchers(11,17,18,25,28,29) have concentrated on investigating the behavior of shallow buried pipe in soil subjected to large strike-slip fault movement.

For a pipeline crossing a strike-slip, it may be elongated or contracted longitudinally. It is convenient to define a strike-slip causing pipe elongation as tensile strike-slip, as shown in Fig.2.2. For the other case, a compressive strike-slip which causes the buried pipeline to contract or buckle is shown in Fig.2.3.

In 1975 Newmark and Hall(25) developed a procedure to analyze the effect of fault movement on an underground pipeline. Fig.2.2 shows the schematic diagram on the effects of shallow buried pipe resulting from horizontal fault displacement (tensil strike-slip). In this analysis, Newmark and Hall(25) adopted the soil friction on pipe to slip derived directly from earth pressure at rest (static pressure). No consideration on passive soil resistance was given. Furthermore, Newmark and Hall(24) used small deflection theory to calculate pipeline elongation. They found that the resistant capacity of a buried pipeline to fault movement is dependent upon the soil characteristics, angle of crossing a fault, slip length and property of material (ductility) etc. and the fault movement resisting capacity is maximized by minimizing the longitudinal, lateral, and uplift resistance between the surrounding soil and the pipe. Thus, without considering the passive resistance of soil, which is larger than the static earth pressure, would be unconservative.

Later, Kennedy et al.(17,18) extended Newmark and Hall's procedure to determine the pipe resistant capacity to fault movement by taking uniform passive soil pressure and large deflection theory into consideration. They assumed that the pipeline shown in Fig.2.2, is a flexible cable and is deformed into a single constant curvature curve approached asymtotically to the undeformed portion of the pipeline. In this model, only axial tensile force at the point of inflection, was used for equilibrium. Under these circumstances (the pipe behaving like a cable), lateral forces from the soil on the pipe are in equilibrium with the axial tension developed in the pipe. No bending moment was considered. A free-body diagram of the curved pipe is shown in Fig.2.4. The equation of force equilibrium in y-direction is presented below:

$$\Sigma F_y = 0$$

$$F_a \sin Q = \int_0^Q p_p \cos\phi \, ds \qquad (2.1)$$

where $ds = R d\phi$ and p_p is constant, thus

$$F_a \sin Q = p_p R \sin Q$$

or

$$R = F_a / p_p = 1/k \qquad (2.2)$$

where R = radius of curvature of the deformed pipe

k = curvature of the deformed pipe

F_a = the axial tension in the pipe

p_p = the lateral force (soil pressure) per unit length

In this case, the force equilibrium of the pipe can be maintained. But if the faulting direction is opposite to that indicated in Fig.2.2, the buried pipeline is subjected to a longitudinal compression other than axial tensile force. Under such a situation, Eqn.2.1 is unable to satisfy the condition of force equilibrium any more. Such a phenomenum can be seen clearly from Fig.2.5.

To be realistic, the internal forces imposed to the pipeline at the point of inflection should include axial and shear forces. Futhermore, the omission of the bending stresses (curvature effect) in the equilibrium and in the failure consideration could be unconservative. Preliminary analyses(42,43) have confirmed such observations. Another assumption in Newmark/Kennedy's paper is that the far ends (away from the point of inflection) of the pipeline which approach tangentially to the referenced displacement lines is not exactly correct. Actually, the response behavior of buried pipeline at far ends to fault movement should be similar to beams on an elastic foundation.

Recently, Audibert and Nyman(2) have performed experiments on the soil resistance against horizontal motion of pipes. They found that the passive soil resistance was not uniformly distributed along the perimeter and was much greater than the earth pressure at rest. They also found that such soil pressure-displacement relationship was non-linear showing a greater increase of displacement at a higher earth pressure. To study the true failure mechanisms of buried pipelines due to faulting, the effects of higher and non-uniform soil pressure should be considered.

More recently, O'Rourke and Trautmann(28,29) made a study of the deformation of both continuous and segmented pipelines due to permanent fault movement. A finite element discrete model of a hypothetical pipeline crossing a fault was proposed to describe pipeline response to fault displacement using ANSYS Program developed by Swanson Analysis Systems. Both axial and lateral springs were used at the nodes. The analysis is based on an influenced (deformed) length of pipeline due to fault movement. Here the influenced length which is the deformed portion of pipeline (segment AC or AE shown in Fig.2.2) was set 120-ft in their finite element model disregarding to the amount of fault movements. However, from the preliminary analyses(42,43), it was shown that a larger fault movement will require a longer influenced length of the pipe. Therefore, it might lead to an incorrect design because the model of O'Rourke et al. did not account for the variation of the deformed length of pipeline.

2.3 Soil Liquefaction

The cause of liquefaction of sands has been studied, either qualitatively or quantitatively, for many years(21,30,33,34,35). Those studies were confined to a certain extent of geotechnical problems. No one has investigated analytically the failure mechanism of a buried pipe within the liquefied mediums.

After reviewing the damage reports for the 1964 Niigata Earthquake(33), it was found that engineering structures were damaged extensively as a result of liquefaction of the sandy soil on which they were supported. With regard to the underground pipelines subjected to soil liquefaction, the general failure modes can be found as pull-out, breaking, buckling, and crushing. An obvious example is the buckling damage of lifelines in a liquefied region during the Tangshan Earthquake(37). Recently, attempts have been made to correlate pipeline damage due to geological and other conditions(16,19) (e.g. pipe size etc.), but the influence of soil liquefaction to underground pipeline has been excluded in their investigation.

Although Kennedy et al.(18), mentioned that most of the pipeline design considerations for fault crossings can also be applicable for crossing liquefiable soil regions, they have not analyzed the problem analytically. Qualitatively, they recommended a number of ways to mitigate the hazard for new construction of pipelines crossing liquefiable soil regions. They also pointed out that the buoyancy force of liquefied soil surrounding the pipe might play an important role in the failure of pipeline. In practice, the soil liquefiable zone covers a large area; and the buried depth for the shallow buried pipeline is around 3 to 5 feet. Therefore, the effects due to vertical differential movement of the pipe and the buoyancy force of liquefied soil are not expected to be severe. Moreover, such effects, as mentioned previously, are unable to give a good explanation for the buckling failure of buried pipeline.

To be realistic, consider a critical situation (as shown in Fig.2.6a) in which a buried pipeline is subjected to axial compression produced by seismic tremors, and the surrounding mediums of the pipe within the liquefiable zone is liquefied during the earthquake. In such case, the surrounding soil that has lost all shear strength due to seismic waves, behaves like a viscous fluid, and the pipe could be considered partially supported. The pipeline could be buckled if the induced seismic axial load along the pipe is beyond tolerable sustained load of the pipe, its critical load.

Many researches on the static and dynamic buckling of columns(7,13,14,15,32,40) have been analytically and experimentally undertaken for several decades. The approaches to find the dynamic responses of elastic columns included Bessel function method(13,14), stability analysis via Lyapunov's direct method (15) or Mathieu equation(23,40), finite difference method(32) and other experimental methods, etc. The extent of the previous studies only covered the case of the elastic column simply supported at both ends. Furthermore, no one incorporated the effects of soil foundation and flexible end supports (i.e. both end moment and vertical displacement not equal to zero at the boundaries of the liquefied zone) in their analyses. Note that the stiffness of the soil foundation varies (decreases) with time within the liquefiable region. For practical purposes, a further investigation to correlate the dynamic response of an infinitely long elastic column with actual seismic ground excitation should be required, but no study on this was investigated.

A situation to the breaking failure of the pipe submerged in the liquefied medium will occur if the pipe is axially subjected to large tensile forces instead of compressive forces. Fig.2.6b shows the breaking failure of the pipe as mentioned.

Note that the axial pipe load (tension and compression) may be resulted from the longitudinal propagation of P-wave through the entire pipeline, which produces the relative displacement between the end portions of the pipe outside the liquefied area. As to soil liquefaction, it may be attributed to the upward propagation of shear waves from the underlying soil layers.

It is the other objective of this research, i.e. to study in some details the failure mechanisms of buried pipelines under soil liquefaction condition due to earthquakes.

2.4 Specific Objectives and Scope

The objectives of this research are to systematically analyze the seismic response behaviors and failure mechanisms for buried pipelines subjected to fault movement and soil liquefaction, and to develop effective design guidelines for the buried lifeline systems under the above mentioned adverse environments.

The scope of this research will include the following tasks.

(1) Parametric responses and failure mechanisms of buried lifelines under large fault movement environments.

(2) Parametric responses and failure mechanisms of buried lifelines under soil liquefaction environments.

(3) Development of design guidelines for buried lifelines under various seismic environments.

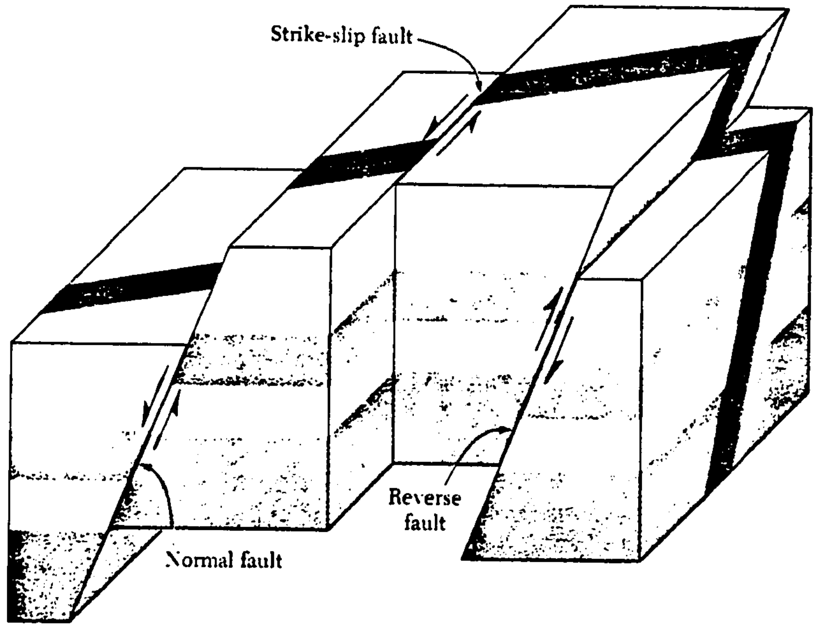

Fig.2.1 Diagram showing the three main types of fault motion. (Courtesy from Bruce A. Bolt)

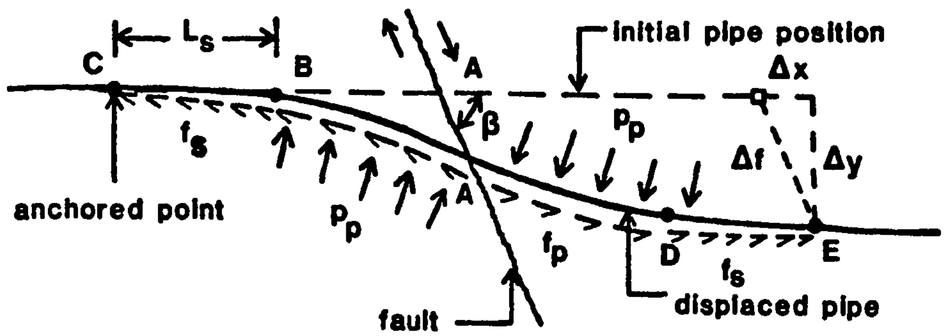

Fig.2.2 Pipeline response to tensile strike-slip fault movement.

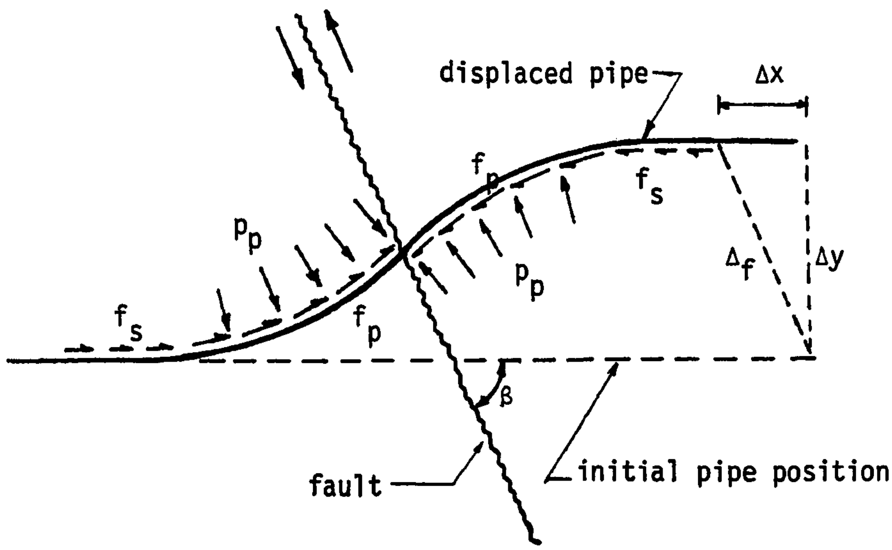

Fig.2.3 Pipeline response to compressive strike-slip fault movement.

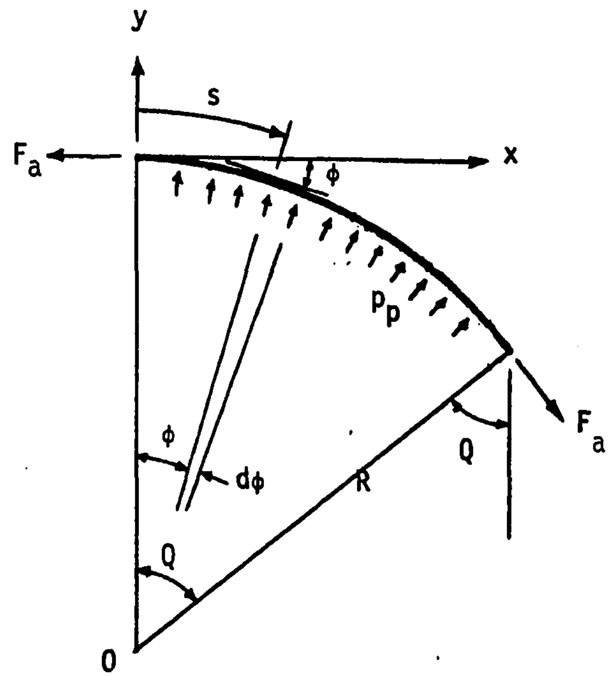

Fig.2.4 Concept of Kennedy et al. - the pipe behaves like a cable in the case of tensile fault movement (strike-slip).

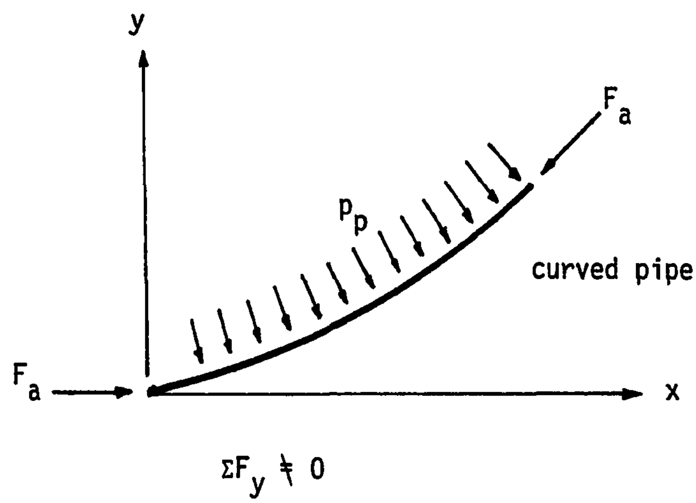

Fig.2.5 Inconsistency on force equilibrium of pipeline subjected to compressive fault movement (strike-slip).

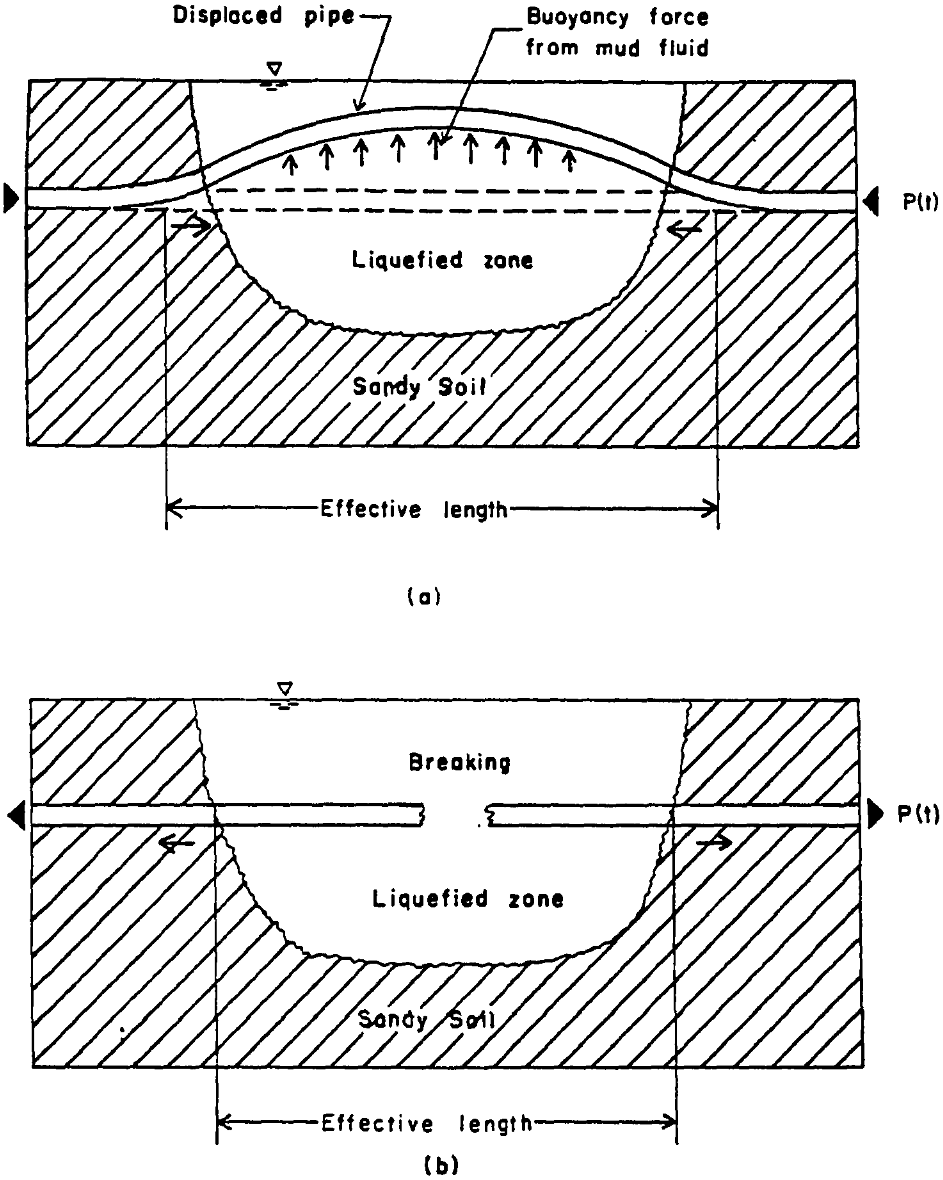

Fig.2.6 Pipe failure modes due to soil liquefaction.

CHAPTER III

ANALYSIS FOR BURIED PIPELINE SUBJECTED TO FAULT MOVEMENT

3.1 Preface

In the consideration of the influences of large fault movement to buried pipelines, only static analysis associated with large deformation theory will be investigated because observed pipe failure phenomena occurs in static state. Based on ,the reports from many invesigators(11,17,18,25,28,29), the resistant capacity of a buried pipeline to fault movement is dependent upon the soil characteristics, the angle of crossing a fault, the slip length, the property of the pipe material, etc.

To improve the existing results for the strike-slip faults, it is necessary to include a shear force at the point of inflection of the curved pipe crossing the fault zone and a boundary condition related to a semi-infinite beam on an elastic foundation at some distance from the fault zone, as shown in Fig.3.1. Note that the combined axial force and bending effects in the failure criteria as well as the geometry effect from the large deflection in the equilibrium equation will be included in the analysis.

Using the yielding of the ductile material of the pipeline to accommodate the large fault movement, the problem is two-fold non-linear: geometry non-linearity and material non-linearity. It will , moreover, have an implicit relationship with other parameters. In this regard, it is necessary to employ a numerical iteration procedure to determine the fault movement resisting capacity for the pipeline.

3.2 Buried Pipeline Subjectecd To Fault Movement

Fig.3.1 shows a lateral fault movement resulting in a horizontal displacement of "Δ_f". This displacement moves one side of the buried pipe a distance "Δx" parallel with the initial axis of the pipeline, and a distance "Δy" perpendicular to the initial axis relative to the other end of the pipe, in which

$$\Delta x = \Delta_f \cos\beta \;;\quad \Delta y = \Delta_f \sin\beta \qquad (3.1)$$

where "β" is an angle crossing the fault. This movement will require the pipe to elongate between points "C" and "E", and will result in an axial tensile strain in the pipe.

The pipe elongation is resisted by sliding friction forces, "f", between the pipe and surrounding soil. Because of the resistance provided by these friction forces, the pipe elongation does not take place uniformly over the entire distance between anchors or the points where its internal stress decreases to zero. At the region immediately adjacent to the fault, the axial strain (or stress) of the pipe is maximum.

The lateral component of movement, "Δy", forces the pipe to displace laterally with respect to the surrounding soil. This lateral displacement is accommodated by the pipe pushing the soil aside with the soil placing a lateral pressure on the pipe which is termed as passive earth pressure. For shallow buried pipeline, the uplift resistance of the soil is small and the pipe can lift upward with relative freedom to accommodate the vertical fault movement. Thus, the study will be centered on the effects of strike-slip (horizontal fault movement) to the buried pipe.

3.3 Geometrical Configuration

From Fig.3.1, the lateral fault movement displaces the buried pipeline to a new deformed shape with a double curvature curve over the transition zone. It would be adequate to take one half of the pipe into consideration due to its anti-symmetrical curve. As shown in Fig.3.1, the one half of the deformed pipe consists of the curved segment and the semi-infinite segment on an elastic foundation at the left hand side of the point "B". Within the transtion region of "AB", the point "A" , taken as point of inflection, is moved about one half of "Δ_f". The entire curved pipe is assumed to be bent into a single curve with constant curvature. The curved pipe also tangentially approaches the rest of the semi-infinite portion at point B. The major portion of the buried pipe, which is not involved in large displacement, is considered as a semi-infinite long beam supported on an elastic foundation.

For general consideration, a scheme indicating the response of the buried pipeline to tensile strike-slip fault movement is shown in Fig.3.1.

3.4 Material Properties

In general, three grades of steel, X-70, X-65, and X-60 are considered as the pipe material in the pipeline construction. A stress-strain curve for X-65 pipe is shown in Fig.3.2. The stress-strain curve is approximated by a tri-linear curve having an initially elastic portion to an "effective" yield point, "σ_1", (or called first yield point) somewhat greater than the actual yield point, then a second linear part with a much smaller slope to the ultimate strain "ε_2", followed by a constant yield stress to the point of failure. The ultimate strain is assumed to be either 0.04 or 10 times the first yield strain.

The parameters used in the calculations are shown in Fig.3.3. The properties for several kinds of material used in these analyses are listed in Table 3.1. Here the "effective" yield point is denoted by "σ_1" at which the strain is "ε_1". The stress at a strain of 0.04 (or $10\varepsilon_1$) is indicated by symbol "σ_2". The slope of the stress-strain curve between these two points corresponds to a modulus "E_2". For convenience, on the stress-strain curve, the first linear part is called the elastic region, and the second linear portion may be referred to as the inelastic region.

3.5 Soil Characteristics

There are two distinct kinds of lateral soil pressure: active earth pressure, and passive earth pressure. First, consider that the soil exerts a push against a retailing wall which tends to slip laterally. This kind of pressure is known as active lateral pressure of the soil. Next, imagine that the retaining wall moves toward the soil. The pressure which the soil develops in response to this movement toward it is called passive resistance pressure. It may be much larger than the active pressure.

For a buried pipe subjected to a strike-slip movement, it is reasonable to consider that lateral pressure applied to the pipe from the surrounding soil are passive soil pressure.

Recently, Audibert and Nyman(2) have performed experiments on the soil resistance against horizontal motion of pipe. They found that the soil pressure- displacement relationship was nonlinear, showing a greater increase of displacement (y) at larger earth pressure (p). They also pointed out that in most cases the p - y curves reach a well defined plateau at a large lateral displacement. For example, the lateral earth pressure will gradually approach the ultimate value of the soil resistance as the buried pipe, with 3-ft depth of embedment, moves beyond 1-in. laterally. The relationship between p and y was shown in Fig.3.4. By overviewing the deformed pipe over the transition region, nearly the entire curved portion of the pipe is forced to displace enormously (far beyond 1-in. long) with respect to the initial pipe position. Thus it becomes possible to determine the ultimate passive resistace of the surrounding soil. Based upon a number of previous investigations(2,9,36), the ultimate load bearing capacity of soil can be employed to represent the ultimate passive resistance to the buried pipe subjected to large fault movement. Eqn.(3.2) gives an expression for the ultimate load bearing capacity of the soil.

$$q_u = \gamma Z N_q \qquad (3.2)$$

where γ = unit weight of soil

Z = depth to center of pipe

N_q = Brinch Hansen bearing capacity factor

If the outside diameter of the pipe is designated as D, the ultimate passive soil resistance per unit length can be expressed as

$$p_p = q_u D \qquad (3.3)$$

The appropriate value of N_q can be chosen from Fig.3.5, which shows the variations of N_q with the normalized depth

Z/D for different values of the internal angle of friction of the soil "ϕ_0".

As a result of fault movements, the pipe also moves longitudinally with respect to the surrounding soil within the transition zone. Longitudinal friction forces are developed between the soil and pipe, resisting this movement. Thus the longitudinal friction forces on the pipe are expressed in Eqn.3.4.

$$f_p = p_p \tan\phi_p \tag{3.4}$$

in which "ϕ_p" is a inter-friction angle between the soil and the pipe, approximately 20-degree for a smooth wall of steel pipe buried in sand(11).

For the majority of the pipe length affected by faulting, the pipe almost remains straight and is not subjected to large lateral passive soil pressures. For this portion of the pipe, the friction force "f_s", per unit length is given by

$$f_s = \pi D q \tan\phi_p \tag{3.5}$$

in which q = the average static soil pressure on the pipe as approximated by

$$q = 0.5(1+K_0)\gamma Z \tag{3.6}$$

in which "K_0" represents the coefficient of lateral soil pressure at rest. For loose to moderately dense sands, "K_0" is approximated by 0.5.

The friction force, "f_p" or "f_s", has a considerable effect on the capacity of buried pipe to withstand fault movement. From the preliminary studies(42,43), the small friction force will allow the pipe to elongate longer to accommodate the offset of fault movement. Thus, it is extremely beneficial to keep the friction factor as low as possible.

3.6 Pipe on Elastic Foundation

As elucidated in Sect.3.3, the majority of the pipe length affected by faulting is not involved in large lateral displacement and is considered as a semi-infinitely long beam supported on the elastic foundation. Fig.3.8 shows the region in which the pipe is considered as a beam on an elastic foundation. A theoretical development of stress analysis for this kind of pipe was based on the Hetenyi's derivation(12) to determine the deflection curve of the pipe and the induced internal forces at the tangential point B as shown in Fig.3.1. It must be noted that the buried pipe is treated as a prismatic rod through the entire pipe length, and the shell failure mode is not included in this analysis.

3.6.1 Spring Constant of Elastic Foundation

A straight beam supported along its entire length by an elastic medium and subjected to vertical forces acting in the principal plane of the symmetrical cross section is shown in Fig.3.6. Because of this action, the beam will deflect, producing continuously distributed reaction forces in the supporting medium. Under this circumstance, the fundamental assumption is that the supporting medium behaves like a spring which follows Hooke's Law. The intensity of the reaction force "q" at any point is proportional to the deflection of the beam "y" at that point, i.e. $q = ky$. The reaction forces will be assumed to be acting vertically and opposing the deflection of the beam. "k" is the soil stiffness which is equivalent to a spring constant.

As depicted in Sect.3.5, the soil reaction force mobilized on the pipe (i.e. the pipe push the surrounding soil aside) is considered the passive soil resistance which is expressed in Eqn.3.7

$$p = ky \tag{3.7}$$

Based upon the notions of Audibert and Nyman(2), the relationship between "p" and "y" is nonlinear as shown in Fig.3.4, i.e. the corresponding equivalent soil stiffness varies with "y". Within the region of the pipe on an elastic foundation, no large pipe displacement is involved. In this regard, it is reasonable at the present time to designate the slope of initial tangent on p-y curve as the effective (initial) spring constant "k_i", namely

$$p = k_i y \tag{3.7a}$$

In addition, in the transition zone as shown in

Fig.3.1, the soil stiffness corresponding the ultimate soil resistance per unit pipe length "k_u" can be obtained in the following manner. From Eqn.3.3, the ultimate passive soil pressure was given for large lateral displacement as:

$$p_p = \gamma Z \ D \ N_q \qquad (3.3)$$

Also

$$p_p = k_u \ y_u \qquad (3.7b)$$

in which "y_u" is the ultimate displacement, approximately 0.02Z for large diameter pipe, and "k_u" is the corresponding equivalent soil stiffness as shown in Eqn.3.8.

$$k_u = 50 N_q \gamma D \qquad (3.8)$$

A graph shows the distinction between "k_u" and "k_i" appearing in Fig.3.7.

To express "k_i" in the similar form as Eqn.3.8, an adjustment to Eqn.3.8 is required. Eqn.3.9 gives an expression for the initial soil stiffness of "k_i".

$$k_i = c_k \ N_q \gamma D \qquad (3.9)$$

where "c_k" is a coefficient of soil stiffness, dependent upon the soil characteristics. It is apparent that the denser the soil, the steeper the intial tangent of p - y curve, as shown in Fig.3.4. In other words, a denser soil will give a larger value of coefficient "c_k".

3.6.2 Governing Differential Equation

The governing differential equation for a beam on an elastic foundation is derived by using conventional notations and assumptions of strength of materials. Consider an infinitely small element shown in Fig.3.9, the vertical equilibrium yields:

$$V - (V + dV) + kydx - wdx = 0 \qquad (3.10)$$

Hence

$$dV/dx = ky - w \qquad (3.11)$$

Making use of the relations $V=dM/dx$ and $EI(d^2y/dx^2)=-M$, and differentiating it twice, we obtain the governing differential equation

$$EIy'''' + ky = w \qquad (3.12)$$

where the prime denotes differentiation with respect to "x", "EI" is the flexural rigidity of the beam and "k" the equivalent spring constant as indicated in Eqn.3.9. If no load is applied, i.e. w=0, the above equation will take the form

$$EIy'''' + ky = 0 \qquad (3.13)$$

3.6.3 Solutions

Let

$$\lambda^4 = \frac{k}{4EI} \qquad (3.14)$$

Thus the general homogeneous solution for Eqn.3.13 is shown as below.

$$y = e^{\lambda x}(C_1\cos\lambda x + C_2\sin\lambda x) + e^{-\lambda x}(C_3\cos\lambda x + C_4\sin\lambda x)$$

(3.15)

where C_1,C_2 ,C_3 and C_4 are constants which can be determined from the boundary conditions of the pipe.

For a beam of infinite length, it is reasonable to assume that in an infinite distance from the beginning point of the semi-infinite beam the deflection of beam must approach zero, that is, if $x \to \infty$, then $y \to 0$. This condition can be fulfilled only if in the equation above the terms connected with "$e^{\lambda x}$" vanish, which necessitates that in the case under discussion C_1=0, and C_2=0. Hence the deflection curve of the beam will take the form

$$y = e^{-\lambda x}(C_3\cos\lambda x + C_4\sin\lambda x) \qquad (3.16)$$

From the boundary condition at point "B" in Fig.3.8, it shows

$$y = 0 \quad \text{as } x = 0$$

Thus C_3=0, and Eqn.3.16 becomes

$$y = C_4 e^{-\lambda x}\sin\lambda x \qquad (3.17)$$

Since $M=-EIy''$, the end moment at point B which should be in equilibrium with the interface moment transmitted from the nonlinearly deflected pipe region (transition zone), can be obtained by differentiating Eqn.3.17 twice and letting $x=0$. The following equation is the expression for the second derivative of "y" with respect to "x".

$$y'' = -2C_4 \lambda^2 e^{-\lambda x} \cos\lambda x \tag{3.18}$$

Let x=0, and M=-EIy'', then

$$M_B = 2C_4 EI \lambda^2 \tag{3.19}$$

Thus

$$C_4 = M_B /(2EI \lambda^2) \tag{3.20}$$

where "M_B" is to be determined at the interface from the non-linearly deflected pipe.

By substituting Eqn.3.20 into Eqn.3.17, and taking the successive derivatives of "y" with respect to "x", the expressions for "y", "θ_B" and "V_B" are obtained.

$$y = \frac{M_B}{2EI\lambda^2} e^{-\lambda x} \sin\lambda x \tag{3.21}$$

$$\theta_B = \frac{M_B}{2\lambda EI} \tag{3.22}$$

$$V_B = -\lambda M_B \tag{3.23}$$

in which "θ_B" is the pipe rotation at point "B", and "V_B" is the internal shearing force transmitted from the non-linearly deflected portion of the pipe.

3.7 Effect Due To Large Lateral Displacement

In the region near a fault, the buried pipe is displaced enormously against the surrounding medium due to large fault movement. According to the report(20) on the San Francisco Earthquake of 1906, the amount of horizontal displacement due to strike-slip could be up to 21 feet. It is obvious that the buried pipe within this region becomes quite vulnerable to resisting large fault movement. Under this circumstance, the pipe could fail by tension, compression and bending etc. In general, the significant effects resulting from fault movement consist of axial straining and bending of the pipe near the fault (Fig.3.1). A detailed structural analysis of the pipeline over the transition zone (i.e. segment BD) was performed for the case of strike-slip based on large deformation theory. This analysis was incorporated with the previously mentioned soil force-displacement relationship, using an iteration method to determine the resistant capacity of a buried pipeline to fault movement, and to investigate the parametric effects on the pipe.

Furthermore, some additional assumptions are made: the curvature of the pipe remains essentially constant, and the surrounding soil of the pipe is considered as a homogeneous medium throughout the entire transition zone. Under the large deformation situation, the concepts of a beam on an elastic foundation can not be applied because of the effects of large lateral displacement.

3.7.1 Force Equilibrium for Curved Beam

The analysis starts with the following equations of statics:

$$\Sigma F_x = 0 \; ; \quad \Sigma F_y = 0 \; ; \quad \Sigma M_o = 0 \; .$$

Fig.3.10 shows a state of force equilibrium for the curved pipe under the influences of faulting. First of all, consider the force equilibrium in the x-direction.

$$\Sigma F_x = 0$$

$$F_2 = F_1 \cos Q - V_1 \sin Q - \int_0^Q f_p R \cos\Phi d\Phi + \int_0^Q p_p R \sin\Phi d\Phi \tag{3.24a}$$

After some steps of mathematical manipulation, it becomes

$$F_2 = F_1 \cos Q - V_1 \sin Q - f_p R \sin Q + p_p R(1 - \cos Q) \tag{3.24b}$$

where F = Axial force along the pipe

V = Shearing force

R = Radius of curvature of the curved pipe

Q = Subtending angle to the arc AB of the curved pipe

Next is the equilibrium for y-direction, that is,

$$\Sigma F_y = 0.$$

$$-V_2 = F_1 \sin Q + V_1 \cos Q - \int_0^Q f_p R \sin\Phi d\Phi - \int_0^Q p_p R \cos\Phi d\Phi \tag{3.25a}$$

or

$$V_2 = -F_1 \sin Q - V_1 \cos Q - f_p R(\cos Q - 1) + p_p R \sin Q \tag{3.25b}$$

Refer to Fig.3.10 again, the moment equilibrium about point "O" is given as below. For $\Sigma M_o = 0$,

$$M_2 = F_1 R - \int_0^Q R(f_p R d\phi) - F_2 R$$

$$= (F_1 - F_2)R - f_p R^2 Q \qquad (3.26)$$

In considering of global configuration of the pipeline affected by the faulting, Fig.3.1 shows that the pipe was rotated horizontally a small angle at the connected point B. Due to this effect, an adjustment to the above equations is displayed in the following expressions. Refering to the geometric confugiration of the pipe as shown in Fig.3.11, the revised equations are

$$F_B = F_A \cos Q - V_A \sin Q - f_p R \sin Q + p_p R(1-\cos Q) + V_B \sin\theta_B \qquad (3.27)$$

$$\bar{V}_B = -F_A \sin Q - V_A \cos Q - f_p R(\cos Q-1) + p_p R \sin Q \qquad (3.28)$$

$$M_B = (F_A - F_B)R - f_p R^2 Q \qquad (3.29)$$

Note that $\bar{V}_B = V_B \cos\theta_B$, and $V_B = \lambda M_B$ (change sign for opposite direction in Eqn.3.23). Substitue Eqn.3.27 into Eqn.3.29, it gives

$$M_B = R\{F_A - F_A \cos Q + V_A \sin Q + f_p R \sin Q$$

$$-p_p R(1-\cos Q) - V_B \sin\theta_B\} - f_p R^2 Q \qquad (3.30a)$$

or

$$M_B/R = F_A(1-\cos Q) + V_A \sin Q + f_p R(\sin Q - Q)$$

$$- p_p R(1-\cos Q) - \lambda M_B \sin\theta_B \qquad (3.30b)$$

After rearranging terms in the above equation, then

$$F_A = \{M_B(1/R+\lambda\sin\theta_B) - V_A \sin Q$$

$$-f_p R(\sin Q - Q) + p_p R(1-\cos Q)\}/(1-\cos Q) \qquad (3.31)$$

Similarly to Eqn.3.28

$$\lambda M_B \cos\theta_B = (p_p R - F_A)\sin Q - V_A \cos Q - f_p R(\cos Q - 1)$$

or

$$V_A = \{(p_p R - F_A)\sin Q - \lambda M_B \cos\theta_B + f_p R(1-\cos Q)\}/\cos Q \qquad (3.32)$$

Putting this expression of V_A into Eqn.3.31, gives

$$F_A = p_p R + \{M_B(1/R+\lambda\sin\theta_B + \lambda\cos\theta_B \tan Q)$$

$$- f_p R(\tan Q - Q)\}/(1-\cos Q-\sin Q\tan Q) \qquad (3.33)$$

in which the variables of R, M_B, θ_B and Q still remain unknown. Four more independent equations are required to find the axial force of the pipe at the fault crossing location.

3.7.2 Geometric Condition of Faulting Length

Figure 3.11 shows a geometric configuration of the deformed pipe subjected to strike-slip. The following derivation is established to correlate the faulting length and the angle of crossing a fault with the curvature of the deformed pipe throughout the transition zone, based on their geometry. Let " Δ_f " and "β" be the faulting length and the angle of crossing a fault, respectively. Then, the procedure is given as below.

$$DE = EA'\tan\theta_B$$

$$EA' = AA'\cos(\beta - \theta_B)$$

Thus $DE = AA'\cos(\beta - \theta_B)\tan\theta_B$

Next,

$$BG = AE - EF$$

Since

$$EF = DF - DE = BF\tan\theta_B - AA'\cos(\beta - \theta_B)\tan\theta_B$$

$$AE = AA'\sin(\beta - \theta_B)$$

Therefore

$$BG = AA'\{\sin(\beta - \theta_B) + \cos(\beta - \theta_B)\tan\theta_B\} - BF\tan\theta_B$$

But BF=AG=RsinQ, thus

$$BG = AA'\{\sin(\beta - \theta_B) + \cos(\beta - \theta_B)\tan\theta_B\} - R\sin Q\tan\theta_B$$

Note that BG=R-RcosQ, and $AA' = \Delta_f/2$. Substituting these expressions into the above equation, yields

$$R(1-\cos Q) = 0.5\Delta_f\left\{\sin(\beta-\theta_B)+\cos(\beta-\theta_B)\tan\theta_B\right\} - R\sin Q\tan\theta_B$$

Consequently, an explicit expression for the radius of curvature R is obtained in terms of Q, Δ_f and β

$$R = \frac{0.5\Delta_f\left\{\sin(\beta-\theta_B)+\cos(\beta-\theta_B)\tan\theta_B\right\}}{1 - \cos Q + \sin Q\tan\theta_B} \qquad (3.34)$$

This equation reveals that the radius of curvature "R" is proportional to the amount of fault movement if the rest of the parameters are set as constants.

3.7.3 Relationship Between "R" and "M"

In the preceding articles of this chapter, the analysis of the pipeline within the transition zone was performed under using large deformation theory. This indicates that the approximate expression "d^2y/dx^2" for the curvature of the deformed pipe is no longer valid. However, the Bernoulli-Euler theory defines the basic moment-curvature relationship of a beam element in the following form:

$$1/R = M/\bar{E}I = d\Phi/ds \qquad (3.35a)$$

or

$$M = \bar{E}I/R \qquad (3.35b)$$

Substitution of "M" into Eqn.3.33 gives

$$F_A = p_p R + \left\{\bar{E}I/R(1/R+\lambda\cos\theta_B\tan Q+\lambda\sin\theta_B)\right.$$
$$\left. - f_p R(\tan Q-Q)\right\}/(1-\cos Q-\sin Q\tan Q) \qquad (3.36)$$

where s = Arc length along the deformed pipe

Φ = Slope of the deformed pipe

$\bar{E}$ = Initial or reduced modulus of elasticity, depending upon bending stress level.

I = Moment of inertia of the pipe

$= 0.25\pi\{D^4 - (D-t)^4\}$

t = Thickness of the pipeipe wall

Since $\theta_B = M_B/2\lambda\bar{E}I$ as shown in Eqn.3.22, then

$$\theta_B = 1/(2\lambda R) \qquad (3.37)$$

By using Eqns.3.34 and 3.37, it is possible to eliminate two of the three unknowns from the expression for "F_A" as shown in Eqn.3.36. One additional condition is needed to compute "F_A".

3.7.4 Compatibility Requirement

In addition to the static equilibrium condition, it is necessary in any structural analysis that all conditions of compatibility be satisfied. These conditions refer to the continuity of the displacements throughout the structure and are sometimes referred to as conditions of geometry. Normally, these conditions employed, are similar to the equilibrium conditions, to satisfy the uniqueness of displacement at all concerned points of the structure.

For a pipeline crossing a fault, the application of compatibility requirement is very essential since the analysis of force equilibrium is insufficient to solve the problem. Fig.3.11 shows a geometric configuration of the buried pipeline subjected to strike-slip fault movement. Under such a fault movement, the pipe will undergo deformations and, as a consequence, the portion A'B of the pipe will be displaced to a new position, AB. The considerable difference between the segments A'B and AB, is known as geometric elongation. The total elongation obtained from integrating axial strain along the semi-infinite pipe must be compatible with the geometric elongation which will be shown in Eqn.3.40 later. For convenience, the integration of axial strain is designated as permissible elongation. Using Fig.3.11, a procedure to acquire the amount of geometric elongation is presented as below.

$$A'B = BD - A'D = BF/\cos\theta_B - A'E/\cos\theta_B$$

But

$$BF = AG = R\sin Q$$

$$A'E = 0.5\Delta_f \cos(\beta - \theta_B)$$

Therefore, the initial pipe length A'B before faulting is

$$A'B = \frac{R\sin Q - 0.5\Delta_f\cos(\beta-\theta_B)}{\cos\theta_B} \tag{3.38}$$

The arc length of the curved pipe is

$$AB = R*Q \tag{3.39}$$

From their geometry, it shows

$$\Delta_G = 2(AB - A'B)$$

By substituting Eqns.3.38 and 3.39 into the above expressions, the geometric elongation is expressed as follows.

$$\Delta_G = 2(R^*Q - R\sin Q + 0.5\Delta_f \cos\beta) \qquad (3.40)$$

In regard to calculating permissible elongation, the material properties of the pipe play a very important role when applying high axial stress along the pipe. It is apparent that a ductile pipe loaded in one direction will undergo a larger deformation before failing than a brittle pipe. Fig.3.12 shows the free-body diagrams for calculating permissible elongation. The strain can be defined in terms of the axial stress by the appropriate stress-strain curve that appeared in Fig.3.3. The maximum axial stress in the pipe occurs at the fault crossing, and is reduced at other locations by the longitudinal friction forces on the pipe. In addition, different values of longitudinal friction forces are specified for the sections of the curved pipe and the pipe on elastic foundation. Thus the elongation is most easily defined as the summation of the elongations in three regions as indicated in Fig.3.12, and defined below:

Region I : In this region, the pipe stress is in the inelastic zone and the soil is in the ultimate passive stage.

Region II : The pipe stress is within elastic limit, but the soil is still in the ultimate passive stage.

Region III: The pipe stress is elastic and the soil is at its rest state.

Table 3.2 described their locality characteristics in these three regions as mentioned above.

a. Region I (Pipe: inelastic and Soil: passive)

By applying Eqn.3.24b the axial force along the segment "s_1" is

$$F^i = F_A \cos\phi - V_A \sin\phi - f_p R\sin\phi + p_p R(1-\cos\phi) \tag{3.41}$$

The "F^i" will be equal to "F_T" if "ϕ" increases to "Q_1". Thus "Q_1" can be determined from above equation. Note that $F_T = \sigma_1 A_p$, in which "A_p" is the cross-sectional area of the pipe. The arc length corresponding to "Q_1" is obtained by its geometry,

$$s_1 = Q_1 R \tag{3.42}$$

and

$$\sigma^i = F^i / A_p$$

Thus

$$\sigma^i = \frac{1}{A_p} \left\{F_A \cos\phi - V_A \cos\phi - f_p R\sin\phi + p_p R(1-\cos\phi)\right\} \tag{3.43}$$

The elongation in this region is acquired by integrating the pipe strain along "s_1".

$$\Delta e_1 = \int_0^{s_1} \left\{(\sigma_1 / E_1) + (\sigma^i - \sigma_1)/E_2\right\} ds$$

Since $ds = Rd\phi$, and E_2, A and R are constants, then

$$\Delta e_1 = (R/E_2 A_p)\int_0^{Q_1}\left\{F_A \cos\phi - V_A \sin\phi - f_p R\sin\phi + p_p R(1-\cos\phi)\right\} d\phi$$

$$+ RQ_1 \sigma_1 (1/E_1 - 1/E_2)$$

After integration, it becomes

$$\Delta e_1 = (R/E_2 A_p)\ F_A \sin Q_1 + (V_A + f_p R)(\cos Q_1 - 1) + p_p R(Q_1 - \sin Q_1)$$

$$+ RQ_1 \sigma_1 (1/E_1 - 1/E_2) \qquad (3.44)$$

By applying Eqns.3.24b,3.25b and 3.26, the internal forces at the intermediate point "T" are listed as follows.

$$F_T = F_A \cos Q_1 - V_A \sin Q_1 - f_p R\sin Q_1 + p_p R(1-\cos Q_1) \qquad (3.45)$$

$$V_T = -F_A \sin Q_1 - V_A \cos Q_1 + f_p R(1-\cos Q_1) + p_p R\sin Q_1 \qquad (3.46)$$

$$M_T = (F_A - F_T)R - f_p R^2 Q_1 \qquad (3.47)$$

b. Region II (Pipe: elastic and Soil: passive)

A similar procedure is applied to region II. The axial pipe stresses along the segment "s_2" are obtained by applying Eqn.3.24b.

$$\sigma^{ii} = \left\{F_T \cos\phi - V_T \sin\phi - f_p R\sin\phi + p_p R(1-\cos\phi)\right\}/A_p \qquad (3.48)$$

The elongation in this region can be acquired from the following equation.

$$\Delta e_2 = \int_0^{s_2} (\sigma^{ii}/E_1)ds$$

By substituting Eqn.3.48 into the above equation, gives

$$\Delta e_2 = \frac{R}{E_1 A_p} \int_0^{Q_2} \left\{ F_T \cos\phi - V_T \sin\phi - f_p R\sin\phi + p_p R(1-\cos\phi) \right\} d\phi$$

or

$$\Delta e_2 = (R/E_1 A_p) \left\{ F_T \sin Q + (V_T + f_p R)(\cos Q_2 - 1) + p_p R(Q_2 - \sin Q_2) \right\} \tag{3.49}$$

It should be noted that the slope of the stress-strain curve is "E_1" within the elastic range. The axial pipe stress at point "B" can be found either from Eqn.3.24b, or Eqn.3.48 if set $\phi = Q_2$.

c. <u>Region III (Elastic Beam on Elastic Foundation Region)</u>

To determine the magnitude of elongation in this region, a simple equation incorporating the influence of static earth pressure is expressed as below.

$$\sigma^{iii} = \sigma_B - \int_0^{s} (f_s/A_p)ds$$

$$= \sigma_B - sf_s/A_p \tag{3.50}$$

Here it would be reasonable to treat 'ds' as 'dx' along the pipe because lateral displacement of the pipe in this region is small, and no significant effects on geometric deformation occurs. However, the axial pipe stress must be reduced to zero at some distance from point "B" under the effects of "f_s". It is assumed that zero stress of the pipe occurs at the distance "L" from the connected point "B". In this respect, the value of "L" is easily determined by letting $\sigma^{iii}=0$ and s=L in Eqn.3.50.

$$\sigma_B - f_s L/A_p = 0$$

Thus

$$L = \sigma_B A_p/f_s \tag{3.51}$$

As a consequence, the third part of the permissible elongation can be calculated as:

$$\Delta e_3 = \int_0^L (\sigma^{iii}/E_1)dx \tag{3.52}$$

The substitution of "σ^{iii}" in above equation will give

$$\Delta e_3 = \frac{1}{E_1}\int_0^L (\sigma_B - sf_s/A_p)dx$$

or

$$\Delta e_3 = \frac{1}{E_1}(\sigma_B L - f_s L^2/2A_p) \tag{3.53}$$

The permissible elongation throughout the smi-infinite pipe is thus determined by summing up all amounts of elongation computed from Eqns.3.44,3.49 and 3.52. Hence,

$$\Delta L = \Delta e_1 + \Delta e_2 + \Delta e_3$$

Note that the total permissible elongation, resulting from the integration of internal strains throughout the entire pipeline, must be 2 times of "ΔL". Thus

$$\Delta_P = 2\,\Delta L \tag{3.55}$$

To satisfy the condition of compatibilty, the geometric elongation (Eqn.3.40) must be compatible with permissible elongation as shown in Eqn.3.55, that is

$$\Delta_G = \Delta_P \tag{3.56}$$

The additional requirement provided in Eqn.3.56 is added to solve the problem related to a buried pipe deformed by fault movement as mentioned previously.

Table 3.1 Material Properties for Buried Pipe

	X-65	X-70
E_1 (ksi)	30000	30000
E_2 (ksi)	453.7	601.9
σ_1 (ksi)	72.0	72.0
ε_1 (in./in.)	.0024	.0024
σ_2 (ksi)	81.8	85.0
ε_2 (in./in)	.024 (.04)	.024 (.04)
M_{y1} (k-in.)	53850.92	53850.92
M_p (k-in.)	78942.94	82031.18

* Refer to Fig.3.3.

E_1 = First modulus of elasticity

E_2 = Second modulus of elasticity.

M_{y1} = Elastic resisting moment of the pipe corresponding to "σ_1".

M_p = Plastic resisting moment of the pipe with diameter of 42 in. and thickness of 0.562 in.

Table 3.2 Characteristics of locality along the left portion of the pipeline

Region	σ	E	f	p	stress state
I (AT)	$\sigma_1 \sim \sigma_2$	E_2	f_p	p_p	inelastic
II (TB)	$0 \sim \sigma_1$	E_1	f_p	p_p	elastic
III (BC)	$0 \sim \sigma_1$	E_1	f_s	q	elastic

* Refer to Fig.3.12.

Region "AT" and "TB" inside the transition zone.

Region "BC" is the zone of beam on elastic foundation.

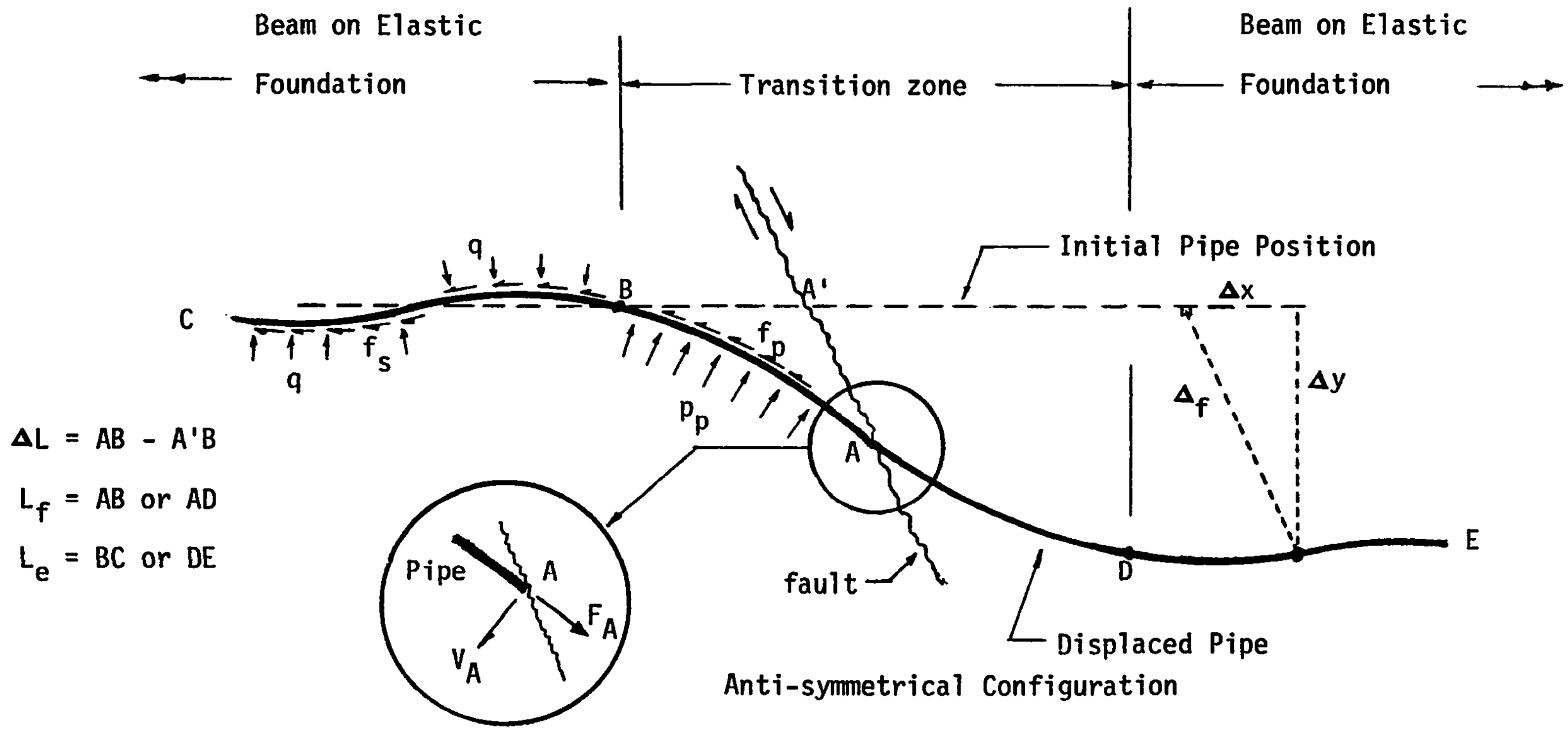

Fig.3.1 Pipeline response to tensile strike-slip fault movement.

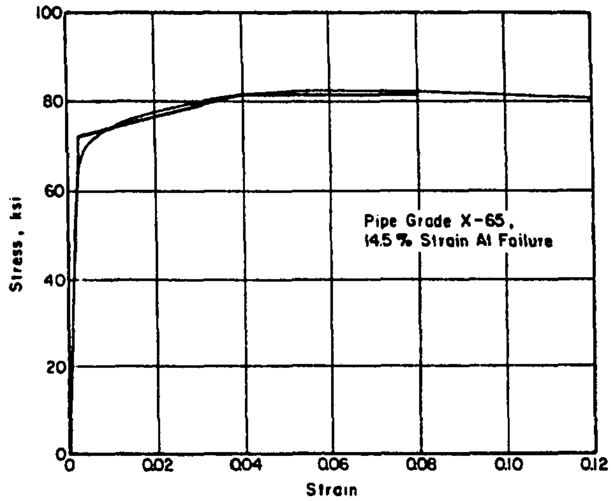

Fig.3.2 Uniaxial Stress-Strain Curve
(After Newmark and Hall, 1975)

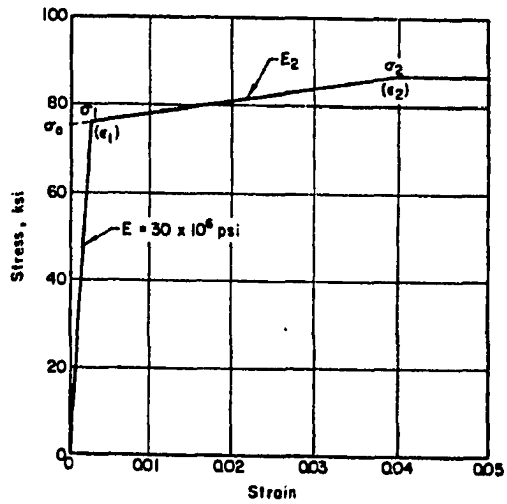

Fig.3.3 Notation used for Stress-Strain curve
(After Newmark and Hall, 1975)

LEGEND

1. No. on curve indicates cover ratio.
2. ↓ indicates ultimate pressure p_u

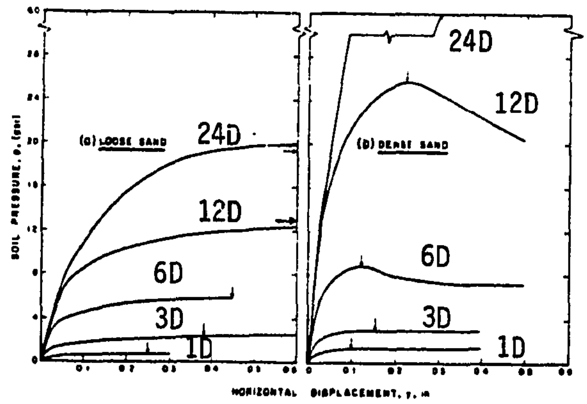

Fig.3.4 p - y curves for 1 in. model conduit embedded in (a) Loose Carver sand; (b) Dense Carver sand (After Audibert and Nyman, 1977)

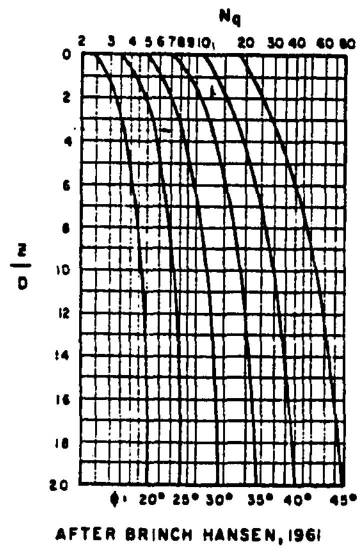

Fig.3.5 Variations of bearing capacity factor N_q with normalized depth of embedment, for different values of angle of internal friction ϕ_0

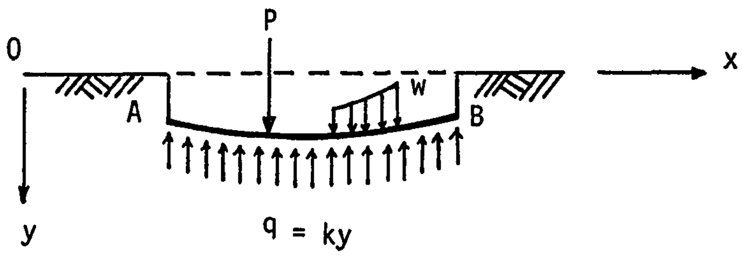

Fig.3.6 Finite-long beam on Elastic Foundation

k_i = Initial tangent stiffness

k_u = Stiffness corresponding to ultimate soil pressure

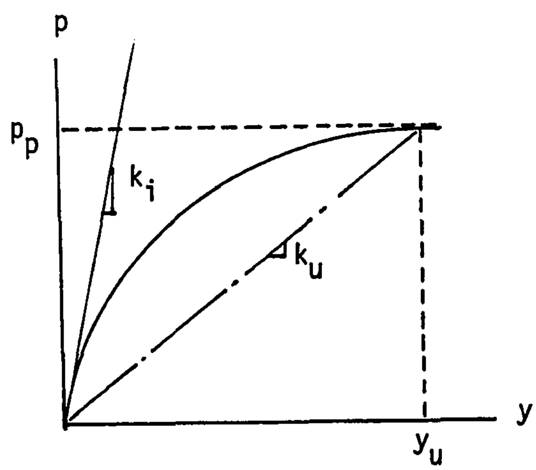

Fig.3.7 Soil Pressure - Displacement Relationship

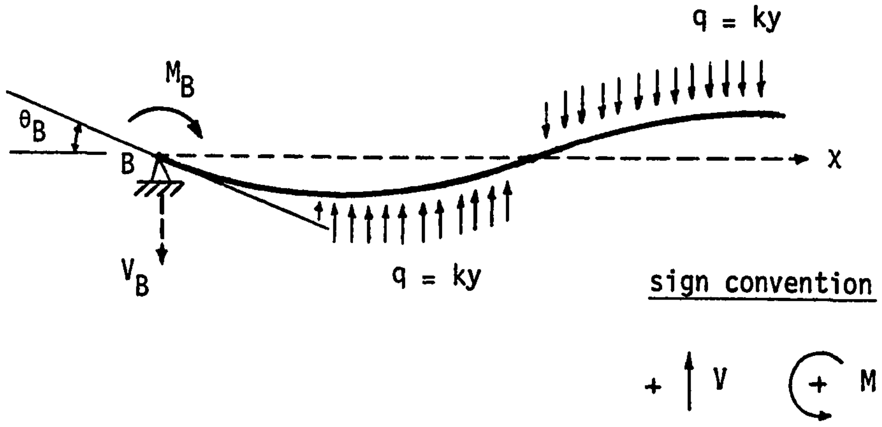

Fig.3.8 Semi-infinite beam on elastic foundation

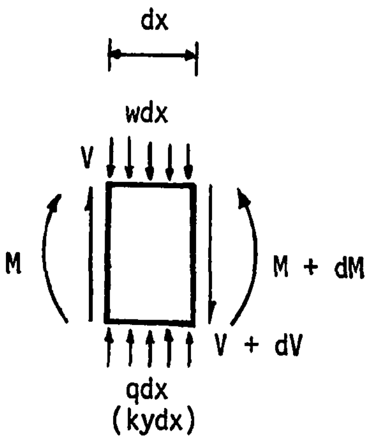

Fig.3.9 Forces acting on differential element.

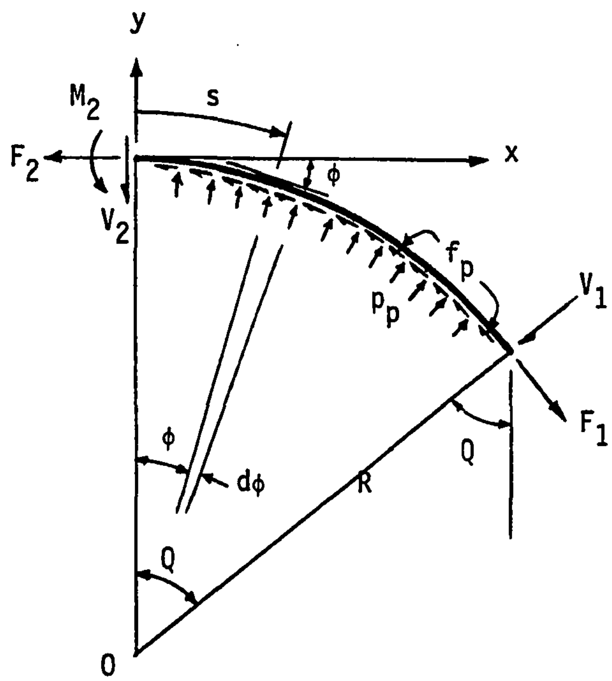

Fig.3.10 Force equilibrium for curved beam.

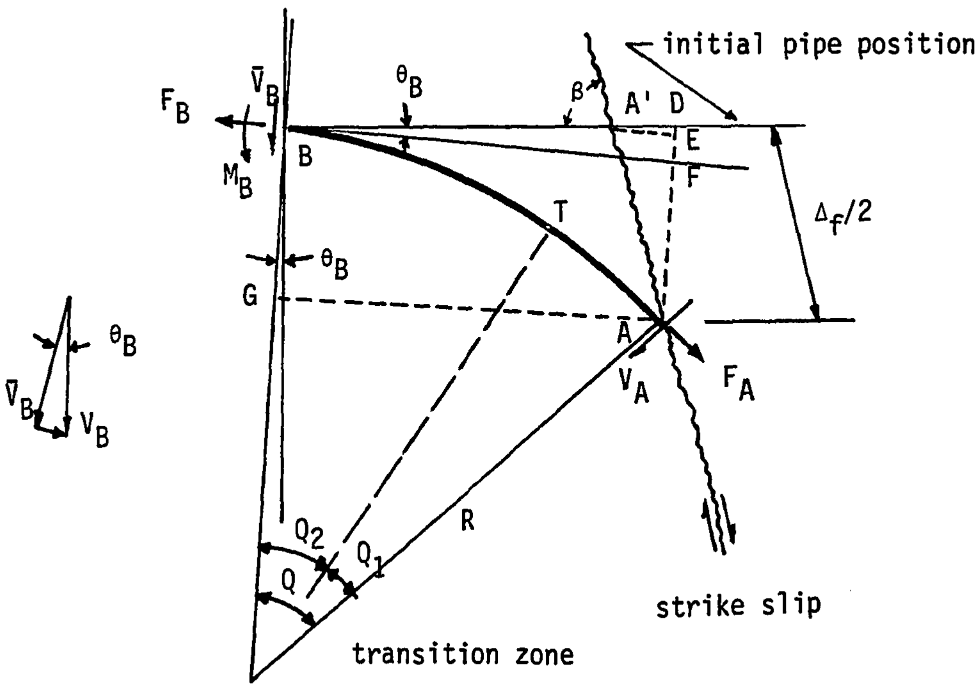

Fig.3.11 Geometric configuration of buried pipeline subjected to strike-slip movement.

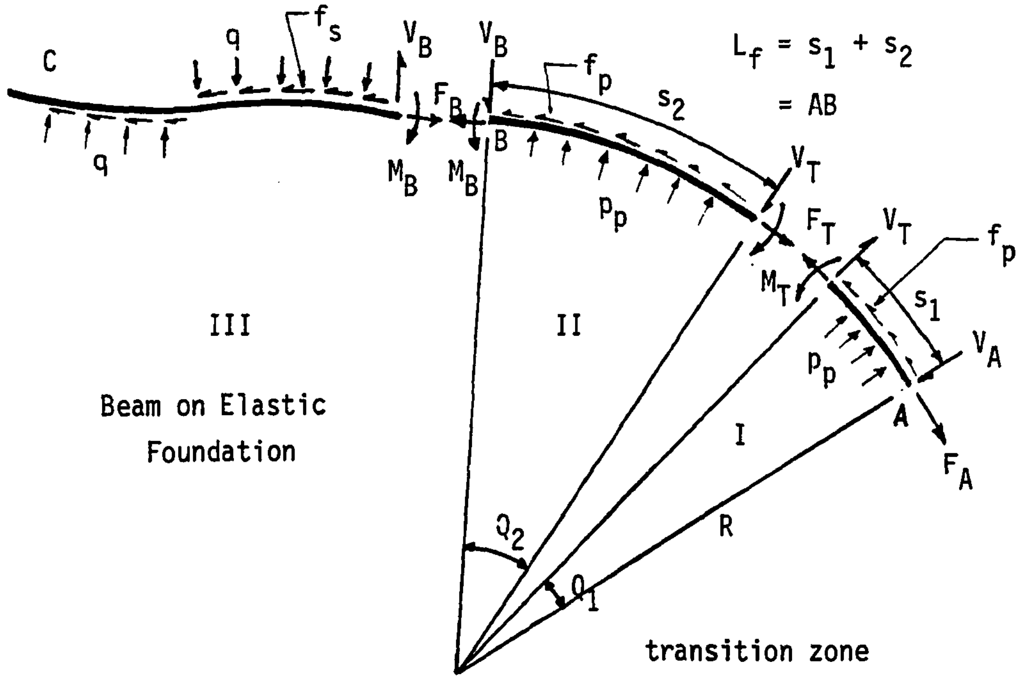

Fig.3.12 Diagram of free-body for calculating the permissible elongation of buried pipeline. (Refer Fig.3.11)

CHAPTER IV

NUMERICAL SOLUTIONS FOR FAULT MOVEMENT EFFECTS

4.1 Preface

In determinating the resistant capacity of a buried pipeline to a large fault movement, a difficulty arises. The axial pipe forces can not be expressed explicitly in terms of the radius of curvature "R" or the subtending angle, "Q", of curved segment of the pipe. An iterative procedure is thus introduced herein to solve the problem correlated with some implicit parameters mentioned earlier.

The numerical iterative procedure is based on the formulations given in CHAPTER III - ANALYSIS FOR BURIED PIPELINE SUBJECTED TO FAULT MOVEMENT. Essentially, the iterative procedure is to match the compatibility requirements for pipe deformation under the influence of fault movemnet.

In addition, the effects of various parameters affecting the resistant capacity of the buried pipeine to fault movement are also examined in this investigation. Those parameters include the angle of crossing a fault, the magnitude of fault movement, the ductility of pipe material, the elastic and bearing capacity and longitudinal resistant characteristics (friction angle), of soil etc.

Finally, a design criterion for constructing a buried pipeline crossing an active fault is established by considering the influence of axial force on the plastic moment of the steel pipe.

4.2 Iterative Procedure

The iterative procedure consists of a sequence of calculations in which the geometric elongation may not be equal to the permissible elongation in each iteration. In the calculation of each iteration, a suitable value of "Q" is given to compute the resulting values of geometric and permissible elongations. This process is repeated by changing "Q" value until the requirement of compatibility is satisfied, i.e. the geometric elongation is almost equal to the permissible elongation. The allowable error is set at 2% during calculation.

The computer program listing is given in the Appendix "C". The flow chart of the program is shown in Fig.4.1.

The computational procedures are given below.

STEP (1) INPUT GIVEN DATA

In this step, the required data includes:

a) angle of crossing a fault

b) magnitude of fault movement

c) friction angle between soil/pipe

d) unit weight of soil

e) Brinch Hansen bearing capacity factor

f) buried depth

g) pipe diameter (42-in.)

h) wall thickness of the pipe (0.562-in.)

i) yield stresses of pipe material

STEP (2) COMPUTE SOIL PRESSURE AND FRICTION

Eqns.(3.3)-(3.6) were used to calculate the resulting value of the ultimate passive soil resistance and longitudinal skin friction between the soil/pipe as the pipe was displaced laterally by faulting. Note that the appropriate value of Brinch Hansen bearing capacity factor can be chosen from Fig.3.5, which shows the variation of the factor with the normalized depth Z/D for different values of the internal angle of friction "ϕ_0".

STEP (3) SELECT ADEQUATE SUBTENDING ANGLE "Q" TO DETERMINE THE AXIAL PIPE FORCE

To initiate the process, an initial trial value of "Q" must be assumed; it will have to be increased or decreased depending on the outcome of the compatibility. The final Q-value should represent the best description to the requirement of compatibility, i.e. the geometric elongation and the permissible elongation (integration of pipe strains) are nearly equal. After finding the final value of "Q", the induced axial forces of the pipe can be determined using Eqn.3.33. Three initial trial values of "Q" (or "AST" used in computer program) for this study are listed below.

1) Q = 3-degree if Δ_f < 10-ft.

2) Q = 5-degree if 10 $\leqslant \Delta_f \leqslant$ 22.5-ft.

3) Q = 7.5-degree if Δ_f > 22.5-ft.

The initial angle increment "$\Delta\alpha$" (or "AL" used in the computer program) is designated as 0.02-degree, and the refined angle increment is set equal to one half or one third of the initial angle increment. Furthermore, as shown in Fig.4.2, no axial pipe stress is allowed to exceed the second yield stress "σ_2", during the calculation. In such case, the pipe is considered 'Fail' at point "A".

The implicit parameter "R" in Eqn.3.34 can be estimated by assuming suitable values of "θ_B", the pipe rotation at conjunction point "B" of the pipe. This estimation of "R" can also be adjusted gradually in each iteration until the requirement of compatibility is satisfied.

STEP (4) DETERMINE GEOMETRIC AND PERMISSIBLE ELONGATIONS

The amount of geometric elongation is acquired simply by applying Eqn.3.40. Three equations (3.44, 3.49, 3.53) are required to determine the permissible elongation. The three equations are integrations of axial pipe strain at three distinct stress stages as indicated in Sect.3.7.4, in which the stress-strain curve of the pipe material are approximated by the piece-wide-linear form as shown in Fig.3.2 or Fig.3.3.

STEP (5) COMPARE GEOMETRIC AND PERMISSIBLE ELONGATIONS (ITERATIVE PROCEDURE)

To satisfy the compatibility requirement, the permissible elongation should be equal to the geometric elongation. If these two quantities are not equal (2% accuracy), STEPS (3)-(5) should be repeated, by changing the value of "Q" until the requirement of compatibility is satisfied.

Technically, if the deviation indicator "$(\Delta_p - \Delta_G)/\Delta_P$ " is less than 25%, the angle increment "$\Delta\alpha$" will be refined to one half or one third of the initial angle increment for better approaching the match point "M" as shown in Fig.4.3.

STEP (6) EFFECTIVE MODULUS OF ELASTICITY FOR MOMENT CURVATURE RELATIONSHIP

The Modulus of Elasticity "E" will be reduced in some amount if the induced moment at point "B" is greater than the first yield moment, "M_{y1}", of the pipe. Based on the stress-strain curve shown in Fig.4.4, two-stage reduced modulus of elasticity "E_r" for a typical steel pipe shown in Fig.4.5 can be expressed in the following manners.

i) $M_{y1} \leqslant M_B \leqslant M_{y2}$

$$E_r = M_B / \{ M_{y1}/E_1 + (M_B - M_{y1})/E_2 \} \qquad (4.1)$$

ii) $M_{y2} \leqslant M_B \leqslant M_p$

$$E_r = E_{r2} \, (M_p - M_B)/(M_p - M_{y2}) \qquad (4.2)$$

where M_B = Induced moment at point "B".

M_{y1} = First yield moment of the pipe.

M_{y2} = Second yield moment of the pipe.

M_p = Plastic resisting moment of the pipe.

E_{r2} = Reduced modulus of elasticity corresponding to the second yield point.

Note that the modulus of elasticity "E" is kept constant (E_1) if "M_B" is less than "M_{y1}", and becomes to zero if "M_B" is beyond the value of "M_p".

STEP (7) PRINT THE RESULTS

The results consist of four categories:

a) The resulting axial stresses, shear stresses and bending stresses.

b) Geometric lengths and elongations.

c) Angles of rotation.

d) Stress ratios.

4.3 Design Criteria

In the case of a buried pipeline crossing an active fault, the pipe is simultaneously subjected to both axial and bending forces in the transition zone, especially at conjunction point "B" of the pipe (Fig.3.1). Normally, the presence of axial force tends to reduce the bending moment capacity of a steel pipe due to axial force - bending moment interaction effects. For the condition of fault movement, an investigation of the influence of axial pipe forces on the resisting bending moment is presented below:

Fig.4.6 shows the stress-distribution in a steel pipe at various stages of deformation caused by thrust and moment. Due to the axial tensile force, yielding on the tension side precedes that on the compression side. Eventually, plastification occurs. However, since part of the area resists the axial force, the stress block no longer contains equal compression and tension areas (as was the case with pure bending). Thus, as shown in Fig.4.6, the total stress-distribution (sketch "a") may be divided into two parts: a part that is associated with the axial load (sketch "b") and a part that corresponds with the bending moment (sketch "c").

$$A_1 = 0.5(R_e^2 - R_i^2)\,\alpha_o \qquad (4.3)$$

$$P = 4A_1\sigma_2 \qquad (4.4)$$

Thus, the subtending angle for the mid arc of the cross-sectional area of the pipe can be expressed as below.

$$\alpha_o = \frac{P}{2\sigma_2} / (R_e^2 - R_i^2) \qquad (4.5)$$

in which "σ_2" is the second yield stress, "R_e" and "R_i" are outside and inside radii of the pipe, respectively.

As shown in Fig.4.7, the distance from the centroid of "A_2" to mid-axis is determined by the following equations.

$$\bar{y}_{pc} = \frac{2\int_0^{\bar{\alpha}} R_c(\cos\theta)(t\,ds)}{2\int_0^{\bar{\alpha}}(t\,ds)}$$

$$= R_c(\sin\bar{\alpha})/\bar{\alpha} \tag{4.6}$$

where t = wall thickness of pipe

ds = differential arc length = $Rd\theta$

R_c = average value of R_e and R_i

$\bar{\alpha} = \pi/2 - \alpha_o$

The corresponding bending moment "M_{pc}" is given by the following expressions which include the effect of axial tensile force:

$$A_2 = (R_e^2 - R_i^2)\,\bar{\alpha} \tag{4.7}$$

$$M_{pc} = A_2\,\sigma_2\,(2\bar{y}_{pc}) \tag{4.8}$$

Substitution of Eqns.4.6 and 4.7 into Eqn.4.8, gives

$$M_{pc} = (R_e^2 - R_i^2)\sigma_2(2R_c \sin\bar{\alpha})$$

$$= \left\{t(D - t)^2\sigma_2\right\}\sin\bar{\alpha} \tag{4.9}$$

in which "D" is outside diameter of the pipe.

Note that the plastic moment of a steel pipe can also be determined by setting P=0 in Eqn.4.4. As shown in Fig.4.7, the distance from the centroid of the half cross-sectional area to the mid-axis is obtanied by applying Eqn.4.6. Let $\bar{\alpha}=\pi/2$, therefore

$$\bar{y} = \frac{R_c \sin(\pi/2)}{\pi/2} = \frac{2R_c}{\pi} \tag{4.10}$$

$$M_p = (\pi R_c t)\,\sigma_2\,(2\bar{y})$$

$$= 4R_c^2 t\,\sigma_2 \tag{4.11}$$

where $R_c=(D-t)/2$, then

$$M_p = t(D-t)^2\,\sigma_2 \tag{4.12}$$

It is apparent that when the axial force is zero, $M=M_p$, and the moment capacity is zero as the axial force reaches the value $P=P_y$.

In addition, a nondimensional form of the interaction equation for steel pipe can be obtained in the following derivations. From Eqns.4.9 and 4.12

$$M_{pc}/M_p = \sin\bar{\alpha} \tag{4.13}$$

But $\bar{\alpha}=\pi/2 - \alpha_o$, and substitution of Eqn.4.5 into the above equation gives

$$\bar{\alpha} = \frac{\pi}{2} - \frac{P}{2\sigma_2} / (R_e^2 - R_i^2)$$

$$= \frac{\pi}{2}(1 - \frac{P}{P_y}) \qquad (4.14)$$

Substituting Eqn.4.14 into Eqn.4.13 gives

$$M_{pc}/M_p = \sin\bar{\alpha} = \cos\left\{\frac{\pi}{2}(\frac{P}{P_y})\right\} \qquad (4.15)$$

This is the interaction equation for steel pipe subjected to both axial tensile force and bending moment.

With the aid of the interaction equation as shown above, the design procedure is presented as follows.

i) Obtain the resulting values of axial and bending stresses from the iterative procedure as mentioned earlier.

ii) Calculate the resisting moment "M_{pc}" by replacing the resulting value of axial stress of Eqn.4.15.

iii) Compare "M_{pc}" with resulting moment "M". The design criteria for steel pipe is satisfied if "M_{pc}" is greater than the resulting bending moment.

4.4 Results and Conclusions

A series of additional parametric analyses are presented to better define the influences of pipe design parameters on the fault movement effects for a buried pipe-line. the parameters for the sequence of analyses are listed in Table 4.1. In each analysis, only one of the parameters is investigated to find its effects on the buried pipeline; the rest are kept constant. For all analyses, the pipe used is 42-in. (1071-mm) diameter, 0.562-in. (14.3-mm) wall thickness, X-70 material placing in loose to moderately dense sand with 110 pcf (1760 kg/m^3) unit weight of soil.

The additional structural properties of a X-70 pipe are listed below. (Refer to Fig.3.3 and Table 3.1)

σ_1 = 72000 psi

σ_2 = 85000 psi

E_1 = 30,000,000 psi

E_2 = 345,745 psi

ε_1 = 0.0024

ε_2 = 0.04

Note that the case of a pipe submerged in a saturated sand has not been taken into consideration.

4.4.1 Effect of Fault Movement (Analysis No.1)

To investigate the effects of fault movement, six different fault movements were selected as data for the numerical analysis mentioned earlier. The values of selected movements are 5, 10, 15, 20, 25 and 30-ft. In this parametric study, the conditions are:

Fault crossing angle = 70-degree

Pipe diameter = 42 in.

Pipe thickness = 0.562 in.

Soil/pipe friction angle = 20-degree

Buried depth = 3 ft.

Coefficient of soil stiffness = 1000

Using the iterative analysis computer program (Appendix C), the axial and bending stresses for various fault movement have been obtained and shown in Fig.4.8. It is seen from Fig.4.8 that the resulting axial and bending stresses increase with an increase in fault movement. The notations used in Fig.4.8 are defined as follows.

$$r_1 = (\sigma_a^A)/\sigma_2 \qquad r_2 = (\sigma_a^B)/\sigma_2$$
$$r_3 = M_B/M_p \qquad r_4 = M_{pc}/M_p \tag{4.16}$$

where σ_a^A = Axial pipe stress at point "A", ksi.

σ_a^B = Axial pipe stress at point "B", ksi.

σ_2 = Second yield stress as shown in Fig.3.3, ksi.

M_B = Induced moment at point "B".

M_p = Plastic resisting moment of steel pipe.

M_{pc} = Resisting moment of steel pipe associated with axial load "P".

It is clear from Fig.4.8 that the induced axial forces at point "A" and "B" show a smaller increase in axial stress as the fault movement goes beyond 15 feet. It is also found from Fig.4.8 that the resulting bending moment expressed in non-dimensional form of "r_3" increases with an increase in fault movement. The numerical results of resulting stresses are given in Table 4.2 for "ε_2=0.04".

Note that for the pipe with "ε_2=0.04", the axial pipe stress at point "A" (76.22 ksi) has exceeded the first yield stress (72 ksi) at 20-ft fault movement. In other words, the pipe will behave inelastically and undergo a large deformation with a small increase in stress.

As indicated in Table 4.2, the bending stresses at point "B" have exceeded the first yield stress as the fault movement goes beyond 25-ft. In this respect, the reduced modulus of elasticity "E_r" shown in Fig.4.5 should be used.

Fig.4.9a-4.9d plot horizontal fault movement versus pipeline response parameters "ΔL", "L_f", "L_e" and "R". Here "ΔL" is the half elongation of the pipe, "L_f" is the length of curved pipe near the fault (curve length of "AB" on Fig.3.1), "L_e" is the length of axially stressed pipe next to the transition zone (length "BC" on Fig.3.1) and "R" represents the radius of curvature of curved pipe "AB". It is observed from Fig.4.9(a)-(d) that the resulting values of the first three parameters increase with the increase of fault movement, while "R" varies inversely with fault movement. Table 4.3 shows the calculated results of "ΔL", "L_f", "L_e" and "R" for the pipe material of "ε_2=0.04".

In Sect.4.3, the design criteria for a steel pipe is based on the resisting moment capacity taking the axial force - bending moment interaction effect as shown in Eqn.4.15. It is clear that the larger the induced axial force is in the pipe, the smaller the resisting moment "M_{pc}" will be. Therefore, under the effect of induced axial force, the pipe would be conidered safe if the resisting moment "M_{pc}" is greater than the resulting moment "M_B" imposed by the fault movement. Normalizing by the plastic moment, "M_p" of the pipe section, the dimensionless moment capacity ($r_4 = M_{pc}/M_p$) must be greater than the dimensionless response moment ($r_3 = M_B/M_p$).

As indicated in Fig.4.8, "r_3" increases, while "r_4" decreases with the magnitude of fault movement and two curves intersect at a fault movement equal to 11.5-ft. For fault movement smaller than 11.5-ft, the resisting moment is greater than the response moment and the pipeline is considered to be safe under the conditions. On the contrary, the pipeline fails if the fault movement is greater than 11.5-ft.

4.4.2 Effect of Angle Crossing A Fault (Analysis No.2)

The effect of the angle of a pipeline crossing a fault from 55 to 90-degree has been investigated and the results are shown in Table 4.4-4.5 and Fig.4.10-11. The rest of conditions listed in Analysis 2 of Table 4.1 are kept constant in this investigation. From Fig.4.10, for a constant fault movement of 15-ft, increasing crossing angles results in a significant decrease in axial pipe stress. As shown in Table 4.4, it is interesting to point out that for an angle above 70-degree, the resulting axial stresses along the pipe are less than the first yield stress of "σ_1", hence they are within the elastic range. In regard to the bending stress at point "B", it increases steadily with increasing crossing angle. For angles greater than 80-degree, the modulus of elasticity will have to be reduced due to the high bending stress (greater than 72-ksi) at point "B". As shown in Fig.4.10, the corresponding value of the intersection point of the curves "r_3" and "r_4" is 79-degree. Therefore, if the pipe (D=42-in., t=0.562-in.) is designed to resist large fault movement, e.g. 15-ft long, it is recommended that the crossing angle should not be less than 79-degree.

Fig.4.11 show the crossing angle correlation with pipeline response parameters "ΔL", "L_f", "L_e" and "R". The pipe elongation, radius of curvature of curved pipe and the affected length of the pipe on an elastic foundation become smaller as the crossing angle increases gradually.

4.4.3 Effect of Friction Angle between Soil and Pipe (Analysis No.3)

The resistance of the pipe to slip in the soil medium in which it is buried, is significantly affected by the angle of friction between the pipe and the medium. Various soil/pipe frictional angles (5-50 degrees) are used to investigate their influences to the behavior of a pipeline crossing a fault with 15-ft movement and 70-degree crossing angle. The additional conditions are 3-ft for buried depth and 1000 for the coefficient soil stiffness.

Resulting axial and bending stresses of the pipe under the effect of various friction angles between soil/pipe are shown in Fig.4.12-13 and Table 4.6-4.7. As shown in Fig.4.12, for the case of "$\varepsilon_2 = 0.04$", the axial pipe stresses at point "A" increase tremendously with the increase of "ϕ_p" less than 20-degree. However, for angles of "ϕ_p" beyond 20-degree, the rate of increase of stress (which has already exceeded "σ_1" as shown in Table 4.6) becomes smaller.

As shown by the stress(σ_a^B)-angle(ϕ_p) curve in Fig.4.12, the axial pipe stress at point "B" decreases with increasing of "ϕ_p" for friction angles greater than 30-degree. The reasons why such a phenomenum may occur may be due to the effect of longitudinal friction along the curved segment of the pipe. Normally, the larger friction angle will produce greater longitudinal friction to offset the axial pipe stresses.

From Table 4.7, the data show that the pipe elongation is almost independent of the friction angle between the pipe/soil. The quantities of affected length of the pipe on elastic foundation decrease with the increase of "ϕ_p". In addition, the resulting curves "L_f" and "R" on Fig.4.13 reveal similar pattern of decrease with decreasing " " for frictional angles greater than 30-degree as the curve of stress(σ_b^B)-angle(ϕ_p) in Fig.4.12.

To determine the resistant capacity of the pipe to the frictional angle between soil/pipe, it can be done by finding the value corresponding to the intersection point of the curves "r_3" and "r_4" shown in Fig.4.12. Here the corresponding value is 12.5-degree.

4.4.4 Effect of Buried Depth (z') (Analysis No.4)

In this analysis, the effects of five different buried depths are investigated; 1, 2, 3, 5 and 10-ft. The values of another parameters are 15-ft fault movement, 70-degree crossing angle, 20-degree frictional angle between soil/pipe and 1000 for the coeficient of soil stiffness. Note that the buried depth (z') is measured from ground surface to the top of the pipe. In addition, the corresponding values of the Brinch Hansen bearing factor to various buried depths are listed Table 4.14. The results of pipe stresses and pipeline response parameters are shown in Table 4.8-9 and Fig.4.14-15.

As shown in Fig.4.14, the axial pipe stress at point "A" increases with increasing buried depth, and exceeds the first yield stress for depths greater than 5-ft as shown in Table 4.8. But the axial pipe stress at point "B" never enters the inelastic range, (i.e. less than first yield stress). The difference of axial pipe stresses between point "A" and "B" increases with an increase in buried depth. As indicated in Eqn.3.5-3.8, the greater values of buried depth will produce larger longitudinal friction forces between pipe/soil, and thus reduce the axial pipe stress at point "B", as compared with the axial stress at point "A".

It is very obvious from Fig.4.14 that the bending moment, "r_3", at point "B" increases significantly with buried depth. In this respect, the resistant capacity of deep-buried pipe to fault movement is essentially less than that of shallow-buried pipe.

In the present case, as shown in Fig.4.15(a), the changes in pipe elongation under the same fault movement (15-ft) with several buried depths are very small. On the contrary, the resulting values of "L_f", "L_e" and "R" decrease enormously with buried depth. These occurrences can be characterized by Fig.4.15(a)-4.15(d). Note that the numerical results of this analysis are listed in Tables 4.8-4.9.

To ensure a safe design for pipe under the conditions indicated in Table 4.1, it is desirable to bury the pipe within a depth of 2.15-ft according to the analytical data appearing in Fig.4.14.

4.4.5 Effect of Coefficient of Soil Stiffness (c_k) (Analysis No.5)

In this procedure, the quantities of other parameters which were kept constant throughout the analysis, are listed in Table 4.1, with the exception of "c_k" which had values of 500, 1000, 2000, 4000, 6000 and 8000. The expression for the coefficient of soil stiffness is given in Eqn.3.9. The computed results are described in Fig.4.16-17 and Table 4.10-11.

From Fig.4.16, it is observed that little change in axial pipe stress results from changing the coefficient of soil stiffness. However, results of analysis show that increasing the coefficient of soil stiffness considerably decreases the bending moment at the conjunction point "B", i.e. increases the resistant capacity of the buried pipe to fault movement. The analysis results related to axial and bending stresses of the pipe were given in Table 4.10.

This analysis also shows that the pipe elongation has little relation to the coefficient of soil stiffness, and the resulting values of "L_f", "L_e" and "R" are slightly affected by changing the coefficient of soil stiffness. These can be observed from Fig.4.17.

As shown in Fig.4.16, the value corresponding to the intersection point of curves "r_3" and "r_4" is 7200. With the value of "c_k" equal to or greater than 7200, the 42-D pipe can resist 15-ft fault movement under the conditions 70-degree crossing angle, 20-degree soil/pipe frictional angle and 3-ft buried depth.

4.4.6 Effect of Pipe Diameter (Analysis No.6)

Six different pipe diameters are used to examine their influences to the behavior of the pipeline crossing an active fault. The values of six pipe diameters are 8", 12", 24", 30", 36" and 42". The thickness of pipe wall is kept as 0.562-inch for all different pipe sizes. The reference values of other influential parameters are 15-ft fault movement, 70-degree crossing angle, 20-degree frictional angle between soil/pipe, 4.75-ft buried depth (measured from ground surface to the center of the pipe) and 1000 for the coefficient of soil stiffness. The computed results are delineated in Fig.4.18-19 and Table 4.12-13.

From Fig.4.18, it is found that little change in axial pipe stress and resisting moment "M_{pc}" result from changing the pipe diameter. On the contrary, the computed results show that the induced bending moment at the conjunction point "B" increases considerably with an increase in the pipe diameter. The numerical results of analysis related to axial and bending stresses of the pipe are listed in

Table 4.12. As shown in Fig.4.19, the analysis shows that the pipe elongation and the affected length of the pipe on the elastic medium have little relation to the pipe diameter. Both influential parameters of "L_f" and "R" almost linearly increase with an increase in pipe diameter.

To determine the resistant capacity of the pipe to the pipe diameter, it can be carried out by finding the value corresponding to the intersection point of the curves "r_3" and "r_4" shown in Fig.4.18. As indicated in Fig.4.18, the pipe with the diameter smaller than 17" can be considered safe under those conditions as Analysis No.6 listed in Table 4.1.

4.4.7 Summary

The reference values for the affecting parameters in this study are listed below.

a) Fault movement = 15 ft.

b) Crossing angle = 70-degree

c) Soil/pipe frictional angle = 20-degree

d) Buried depth = 3 ft.

e) Coefficient of soil stiffness = 1000

f) Pipe diameter =42 inches

In each parametric analysis, only one of the parameters as listed above is investigated to find its effects on the buried pipeline; the rest of parameters are kept constant during calculation. Therefore, the resisting capacity of the pipe to each parameter are described as follows.

a) Fault movement $\leq$ 11.5 ft.

b) Crossing angle $\geq$ 79-degree

c) Soil/pipe frictional angle $\leq$ 12.5-degree

d) Buried depth $\leq$ 2.15 ft.

e) Coefficient of soil stiffness $\geq$ 7200

f) Pipe diameter $\leq$ 17.0 inches

TABLES IN CHAPTER IV

Table 4.1 The sequence of analyses and constant values of the related parameters.

Analysis number	Δ_f	β	ϕ_p	z'	c_k	D
1	x	70	20	3	1000	42
2	15	x	20	3	1000	42
3	15	70	x	3	1000	42
4	15	70	20	x	1000	42
5	15	70	20	3	x	42
6	15	70	20	3	1000	x

Note: The values of variable (x) in each analysis are listed as follows.

1) Analysis No.1 - Effects of Fault Movements
Δ_f = 5, 10, 15, 20, 25, 30-ft

2) Analysis No.2 - Effects of Angles of Crossing A Fault
β = 55, 60, 65, 70, 75, 80, 85, 90-degree

3) Analysis No.3 - Effects of Frictional Angles between Soil and Pipe
ϕ_p = 5, 10, 15, 20, 30, 40, 50-degree

4) Analysis No.4 - Effect of Buried Depth
z' = 1, 2, 3, 5, 10-ft

5) Analysis No.5 - Effects of Coefficients of Soil Stiffness
c_k = 50, 100, 250, 500, 750, 1000

6) Analysis No.6 - Effects of Pipe Diameters
D = 8, 12, 24, 30, 36, 42"

Table 4.2 Resulting pipe stresses (Analysis No.1) due to various fault movements. ($\varepsilon_2 = 0.04$)

Δ_f	σ_a^A	σ_a^B	σ_b^B	r_1	r_2	r_3	r_4
5	38.65	32.90	53.87	.455	.387	.491	.821
10	54.49	46.93	64.10	.641	.552	.584	.647
15	68.23	59.22	68.65	.803	.697	.626	.459
20	76.22	66.02	71.92	.897	.777	.656	.344
25	80.62	69.00	72.05	.942	.812	.657	.291
30	83.14	71.33	72.11	.978	.839	.657	.250

* σ_a^A : Axial pipe stress at point "A", ksi

σ_a^B : Axial pipe stress at point "B", ksi.

σ_b^B : Bending stress at point "B", ksi

Note: $r_1 = (\sigma_a^A)/\sigma_2$ $\qquad$ $r_2 = (\sigma_a^B)/\sigma_2$

$r_3 = M_B/M_p$ $\qquad$ $r_4 = M_{pc}/M_p$

Where M_{pc} = Resisting moment associated with axial load "P".

M_p = Plastic moment of steel pipe.

M_B = Resulting moment at point "B"

Table 4.3 Resulting data of pipeline response parameters (Analysis No.1) due to various fault movements. (ε_2 = 0.04)

Δ_f	ΔL	L_f	L_e	R
5	1.819	63.08	1534.58	974.51
10	3.757	82.19	2189.39	819.00
15	5.770	97.28	2762.70	764.71
20	7.849	109.58	3079.68	730.02
25	10.012	117.78	3219.00	679.80
30	12.232	125.32	3327.55	646.15

* Unit: feet

ΔL: Half elongation of pipe

L_f : Half length of curved pipe

L_e : Affected length of the pipe on elastic medium

R : Radius of curvature of the pipe

Table 4.4 Resulting pipe stresses (Analysis No.2) due to various crossing angles. (ε_2= 0.04)

β	σ_a^A	σ_a^B	σ_b^B	r_1	r_2	r_3	r_4
55	78.25	69.54	63.66	.921	.818	.580	.282
60	76.16	67.30	65.14	.896	.792	.594	.321
65	73.29	64.32	66.67	.862	.757	.608	.373
70	68.23	59.22	68.65	.714	.697	.626	.459
75	60.74	51.77	71.25	.714	.609	.650	.576
80	53.04	44.26	72.04	.624	.521	.657	.684
85	42.86	34.45	72.12	.504	.405	.658	.804
90	28.63	21.35	72.30	.337	.251	.659	.923

Table 4.5 Resulting data of pipeline response parameters (Analysis No.2) due to various crossing angles. (ε_2= 0.04)

β	ΔL	L_f	L_e	R
55	9.11	92.42	3244.24	824.67
60	8.05	94.62	3139.48	806.01
65	6.94	96.34	3000.50	787.49
70	5.77	97.28	2762.70	764.71
75	4.56	97.41	2415.26	736.81
80	3.33	95.79	2065.03	691.87
85	2.08	92.16	1607.18	627.64
90	0.83	86.22	995.85	543.01

* Unit : "Degree" for angle, "feet" for length.

Table 4.6 Resulting pipe stresses (Analysis No.3) due to various frictional angles between soil and pipe. (ε_2 = 0.04)

ϕ_p	σ_a^A	σ_a^B	σ_b^B	r_1	r_2	r_3	r_4
5	31.83	29.82	72.15	.374	.351	.658	.852
10	45.75	41.57	72.05	.538	.489	.657	.719
15	57.17	50.63	71.25	.673	.596	.650	.593
20	68.23	59.22	68.65	.803	.697	.626	.459
30	79.44	64.99	66.67	.934	.765	.608	.361
40	83.76	62.79	41.55	.985	.739	.608	.399
50*	>85.0	--	--	>1.0	--	--	--

Unit : "Degree" for angle, "ksi" for stress.

Table 4.7 Resulting data of pipeline response parameters (Analysis No.3) due to various frictional angles between soil and pipe. (ε_2 = 0.04)

ϕ_p	ΔL	L_f	L_e	R
5	5.85	86.16	5787.95	609.97
10	5.81	91.79	4003.20	685.84
15	5.78	95.38	3208.56	736.83
20	5.77	97.28	2726.70	764.71
30	5.76	98.81	1911.20	787.50
40	5.76	98.80	1270.58	787.43
50*	--	--	--	--

Unit : "Degree" for angle, "feet" for length.

* Axial tensile failure occurs at the point of inflection "A" as "ϕ_p" = 50-degree.

Table 4.8 Resulting pipe stresses (Analysis No.4) due to various buried depths. ($\varepsilon_2 = 0.04$)

z' (ft)	σ_a^A	σ_a^B	σ_b^B	r_1	r_2	r_3	r_4
1	50.64	44.64	46.18	.596	.525	.421	.679
2	59.78	52.35	58.04	.703	.616	.529	.567
3	68.23	59.22	68.65	.803	.697	.626	.459
5	78.09	67.08	72.42	.922	.789	.660	.325
10*	>85.00	--	--	>1.00	--	--	--

z' : Buried depth measured from the ground surface to the top of a buried pipe.

Table 4.9 Resulting data of pipeline response parameters (Analysis No.4) due to various buried depths. ($\varepsilon_2 = 0.04$)

z'	ΔL	L_f	L_e	R
1	5.66	119.98	3596.83	1136.83
2	5.72	106.36	3093.61	904.60
3	5.77	97.28	2726.70	764.71
5	5.96	74.21	2202.13	462.15
10*	--	--	--	--

Unit : Feet

* Axial tensile failure occurs at the point of inflection "A" as z'=10-ft.

Table 4.10 Resulting pipe stresses (Analysis No.5) corresponding to various coefficients of soil stiffness. (ε_2 = 0.04)

c_k	σ_a^A	σ_a^B	σ_b^B	r_1	r_2	r_3	r_4
500	68.00	59.49	71.67	.800	.700	.653	.454
1000	68.23	59.22	68.65	.803	.697	.626	.459
2000	68.03	58.63	63.65	.800	.690	.580	.468
4000	67.47	57.64	58.83	.794	.678	.536	.484
6000	67.92	57.82	55.94	.799	.680	.510	.481
8000	68.05	58.04	51.52	.800	.681	.471	.478

Table 4.11 Resulting data of pipeline response parameters (Analysis No.5) due to various coefficients of soil stiffness. (ε_2 = 0.04)

c_k	ΔL	L_f	L_e	R
500	5.80	91.61	2775.28	692.89
1000	5.77	97.28	2762.70	764.71
2000	5.75	101.89	2734.94	824.76
4000	5.72	106.72	2689.01	892.35
6000	5.71	109.84	2697.44	938.54
8000	5.70	112.21	2726.42	974.88

Table 4.12 Resulting pipe stresses (Analysis No.6) due to various diameters of the pipe. (ε_z= 0.04)

D	σ^A_a	σ^B_a	σ^B_b	r_1	r_2	r_3	r_4
8"	69.17	63.07	32.58	.814	.742	.281	.394
12"	68.37	61.97	42.16	.804	.729	.372	.413
24"	67.31	59.85	58.53	.792	.704	.528	.448
30"	67.51	59.51	62.97	.794	.700	.571	.454
36"	67.43	58.92	66.32	.793	.693	.603	.464
42"	68.23	59.22	68.65	.803	.697	.626	.459

Table 4.13 Resulting data of pipeline response parameters (Analysis No.6) due to various diameters of the pipe. (ε_z= 0.04)

D	ΔL	L_f	L_e	R
8"	6.14	61.26	2772.74	306.98
12"	6.07	65.94	2793.09	355.82
24"	5.91	79.33	2763.48	512.59
30"	5.86	85.66	2761.02	595.50
36"	5.81	91.54	2742.30	678.51
42"	5.77	97.28	2762.70	764.71

Unit : feet for length.

Note: The buried depth "z" measured from ground surface to the center of pipe is kept as 57-in. for all the pipe diameters.

Table 4.14 Values of Brinch Hansen bearing factor

z'(in.)	z(in.)	N_q
12	33	8.80
24	45	9.40
36	57	9.80
60	81	10.90
120	141	12.80

Note: z = Depth to the center of pipe
= z' + D/2

D = Diameter of the pipe
= 42 inches.

z' = Buried depth to top of pipe

FLOW CHART FOR FAULT MOVEMENT

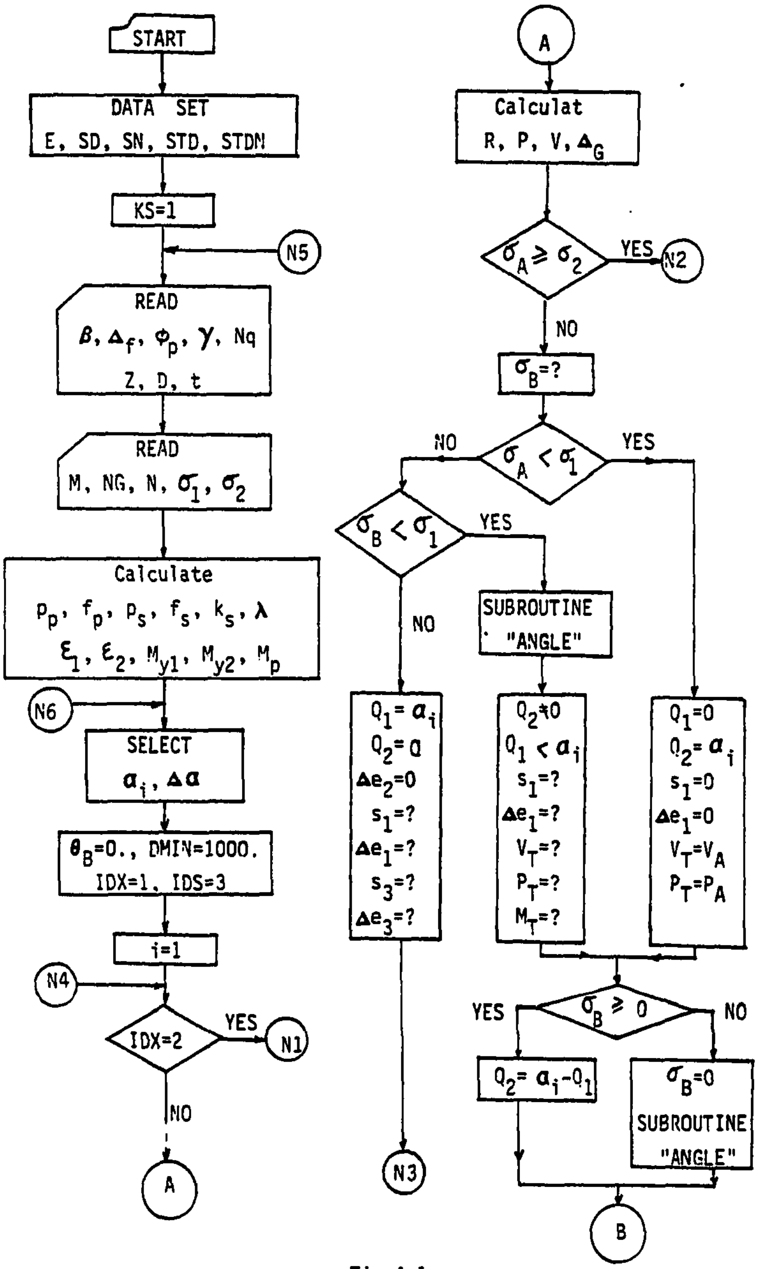

Fig.4.1

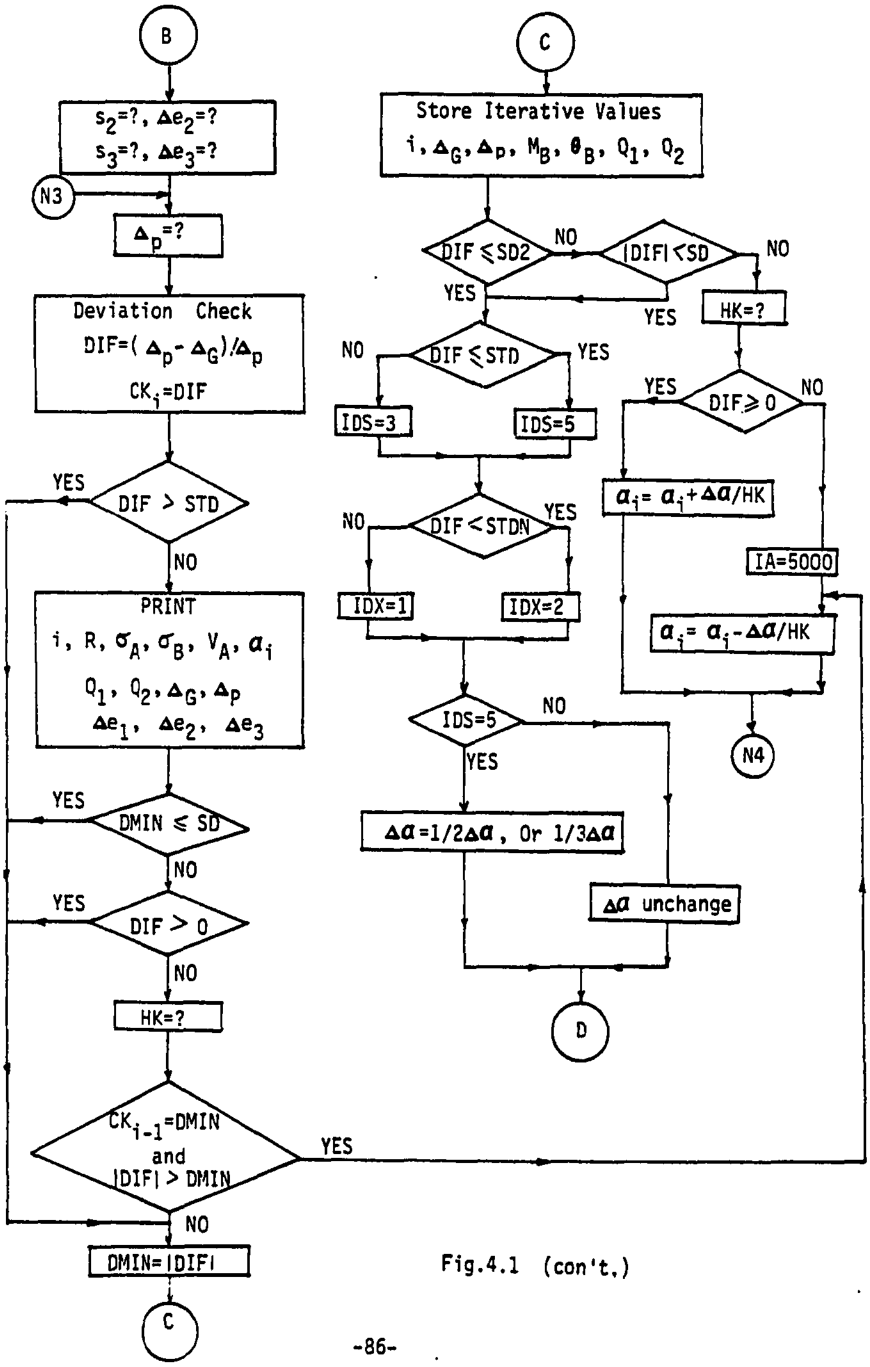
B
s2=?, Δe2=?
s3=?, Δe3=?
N3
Δp=?
Deviation Check
DIF=(Δp- ΔG)/Δp
CKi=DIF
DIF > STD
YES
NO
PRINT
i, R, σA, σB, VA, αi
Q1, Q2, ΔG, Δp
Δe1, Δe2, Δe3
DMIN ≤ SD
DIF > 0
HK=?
CKi-1=DMIN
and
|DIF| > DMIN
DMIN=|DIF|
C
Store Iterative Values
i, ΔG, Δp, MB, θB, Q1, Q2
DIF ≤ SD2
|DIF| < SD
HK=?
DIF ≤ STD
IDS=3
IDS=5
DIF ≥ 0
αi= αi+Δα/HK
IA=5000
αi= αi-Δα/HK
N4
DIF < STDN
IDX=1
IDX=2
IDS=5
Δα=1/2Δα, Or 1/3Δα
Δα unchange
D

Fig.4.1 (con't.)

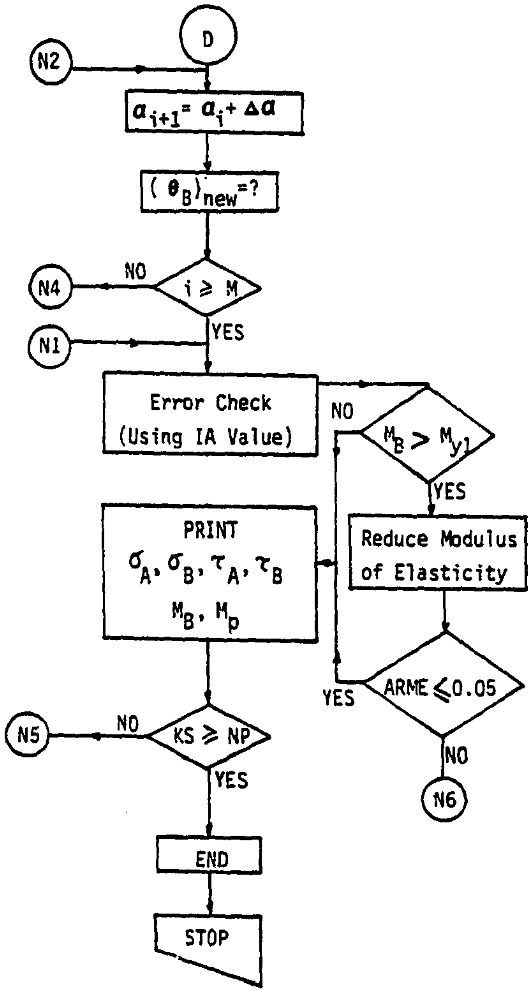
D
N2
$a_{i+1} = a_i + \Delta a$
$(\theta_B)_{new} = ?$
NO
N4
$i \geq M$
YES
N1
Error Check
(Using IA Value)
NO
$M_B > M_{y1}$
YES
Reduce Modulus
of Elasticity
PRINT
$\sigma_A, \sigma_B, \tau_A, \tau_B$
M_B, M_p
YES
ARME $\leq$ 0.05
NO
N6
N5
NO
KS $\geq$ NP
YES
END
STOP

Fig.4.1 (Con't.)

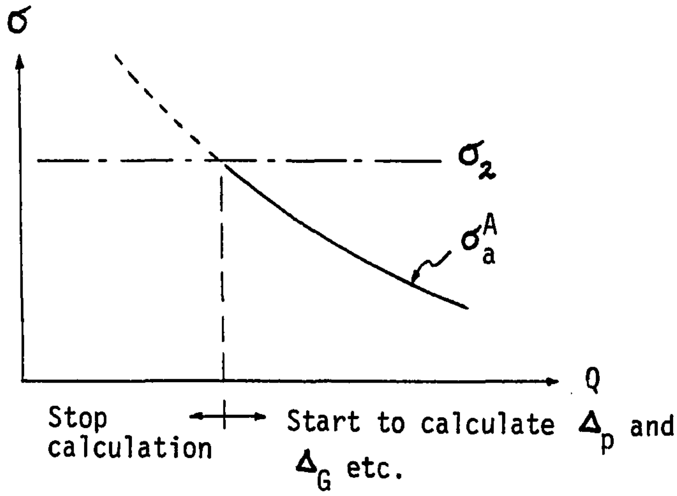

Fig.4.2 Relationship between the induced axial stress at point "A" and the Subtending angle "Q"

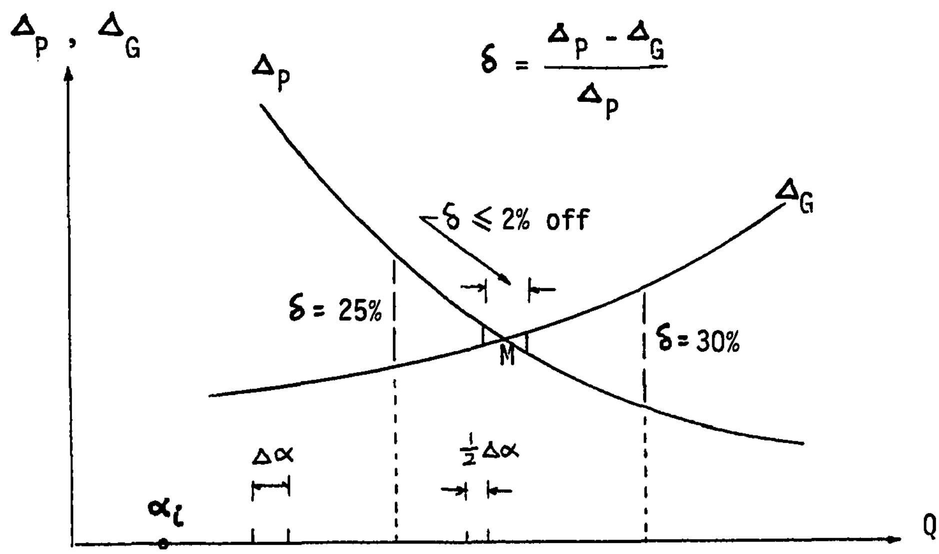

$$\alpha_i = \begin{cases} 3^\circ & \text{if } \Delta_f \leqslant 10' \\ 5^\circ & \text{if } 10' \leqslant \Delta_f \leqslant 22.5' \\ 7.5^\circ & \text{if } \Delta_f < 22.5' \end{cases}$$

Fig.4.3 Iterative Provedure for Fault Movement.

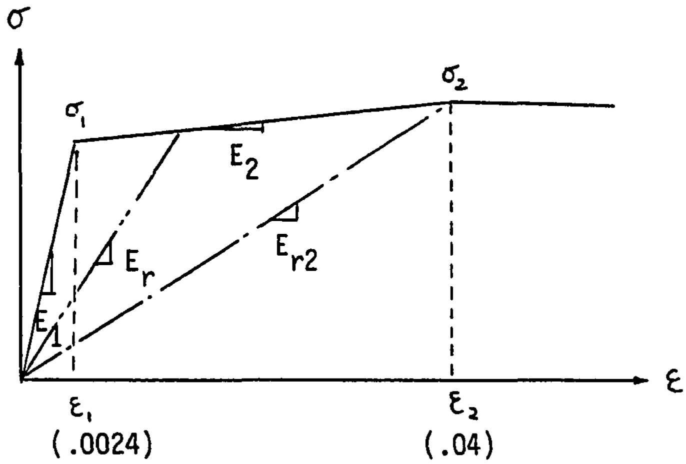

Fig.4.4 Stress-strain curve of steel pipe.

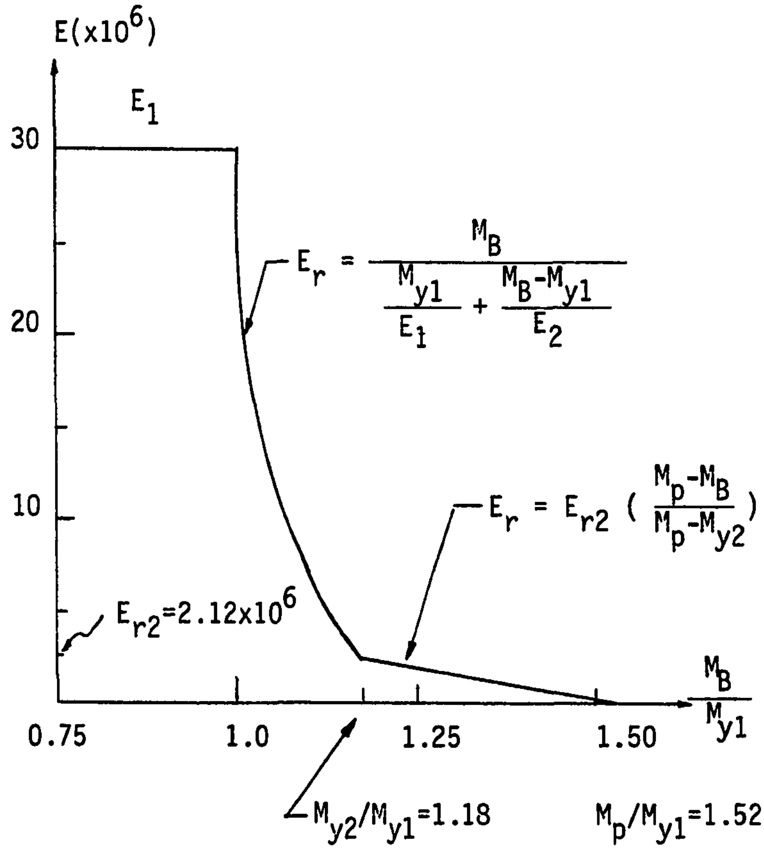

Fig.4.5 Relationship between the Modulus of Elasticity (E) and the Moment Ratio (M/M_{y1}).

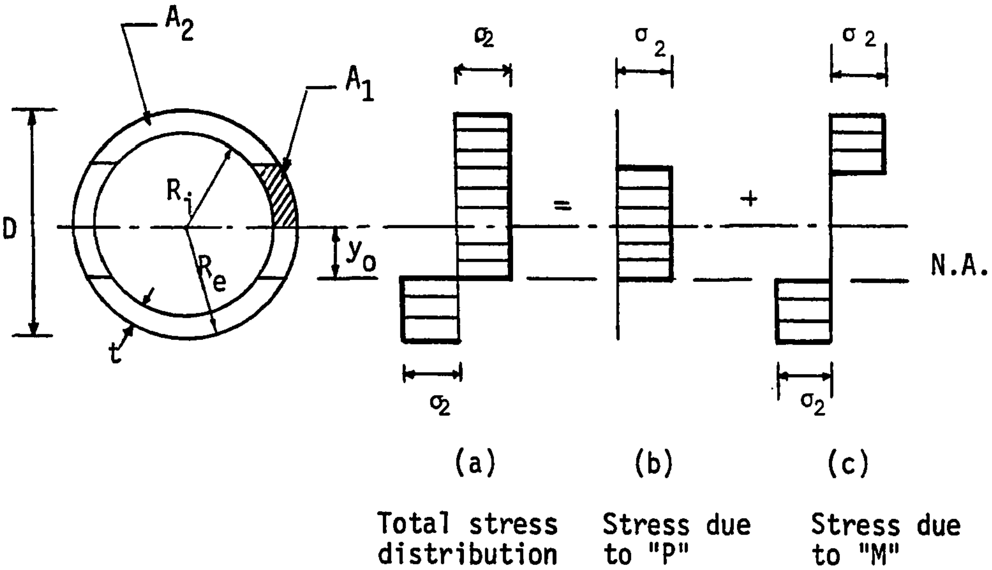

Fig.4.6 Representation of completely plastic cross section of a pipe subjected to bending and axial force.

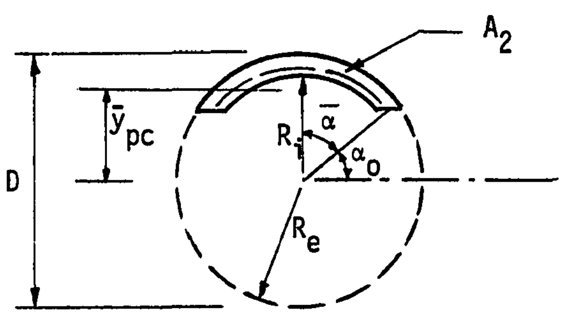

$R_c = (R_i + R_e)/2$

Fig.4.7 Free-body diagram of the pipe element "A_2".

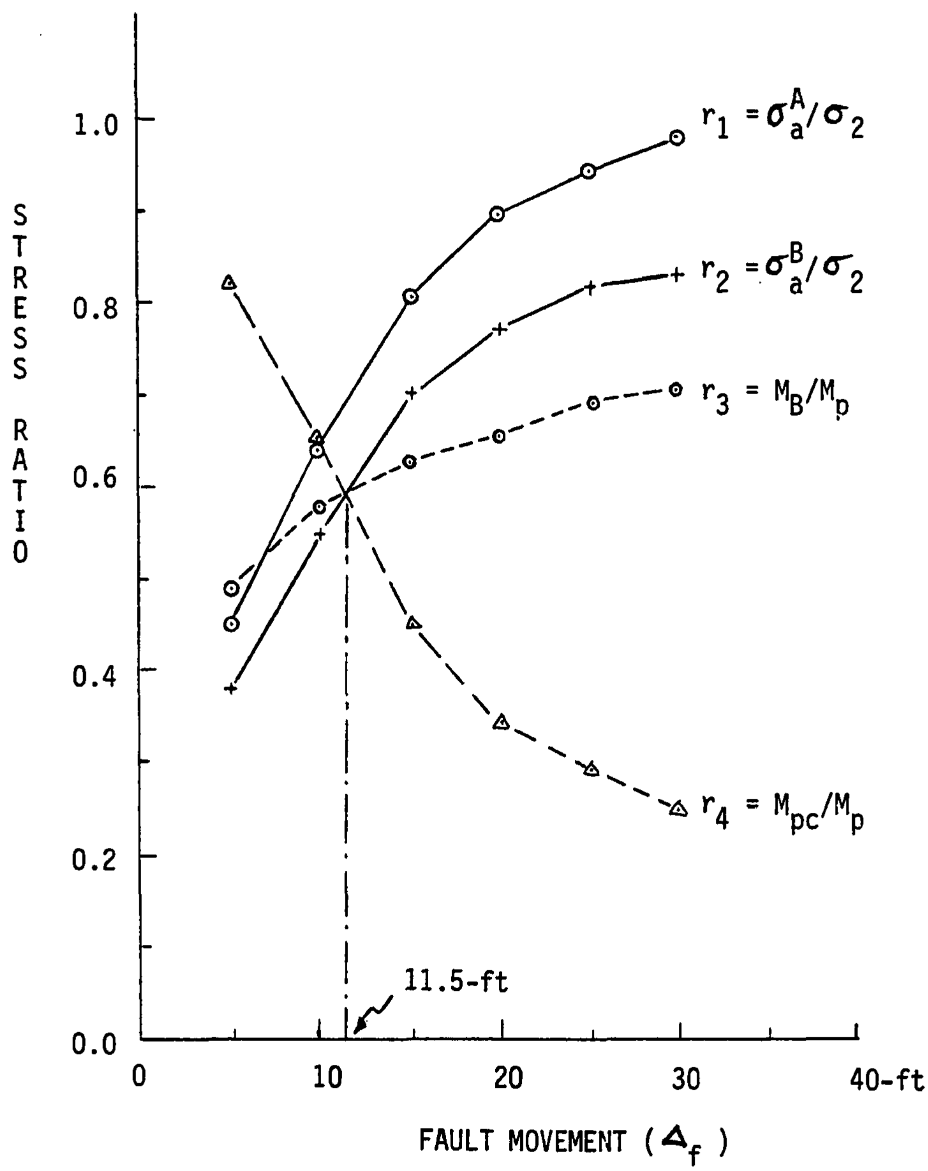

Fig.4.8 Stress Ratio vs. Fault Movement ($\varepsilon_2 = 0.04$).
(Analysis No.1)

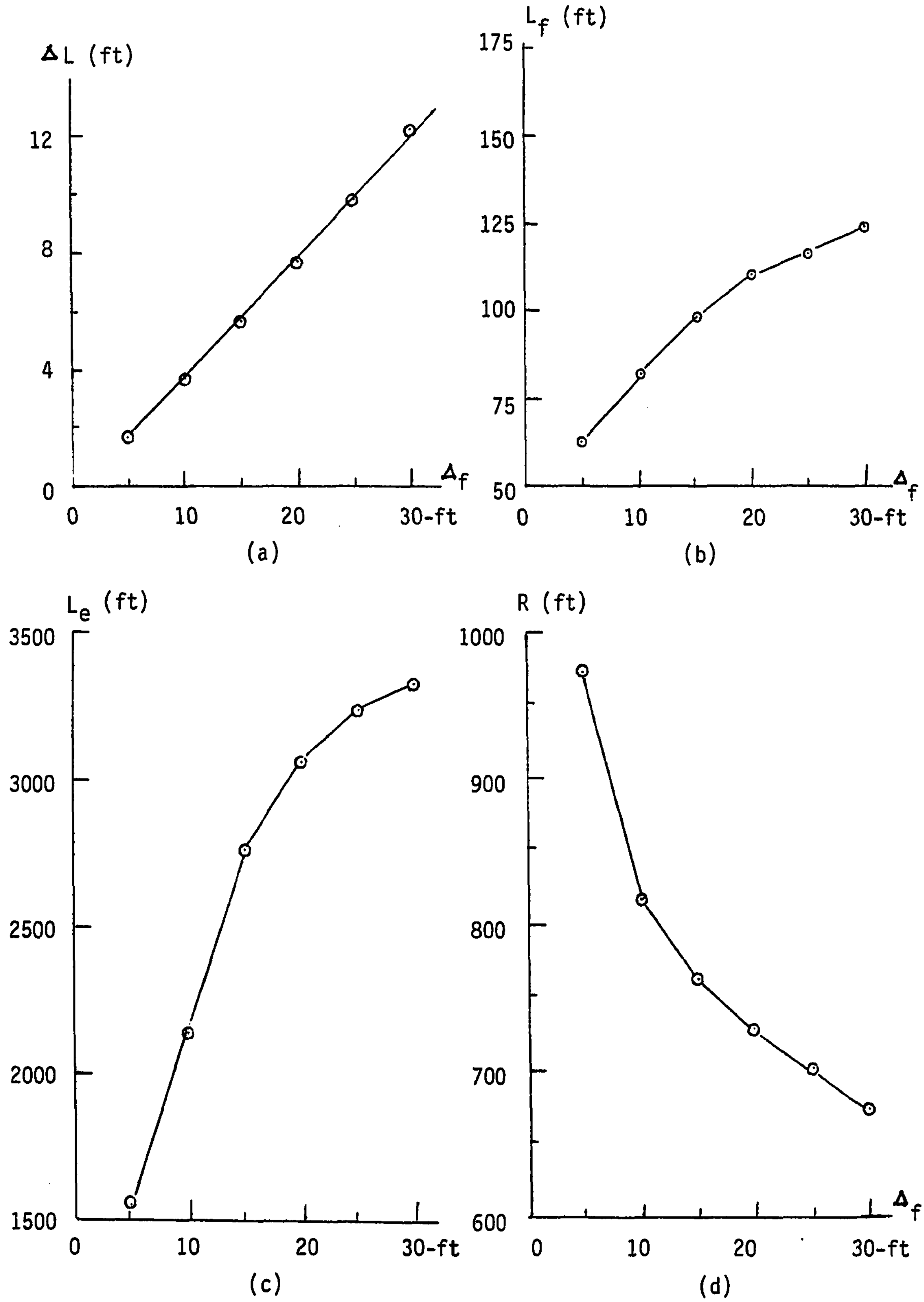

Fig.4.9 Plots of Δ_f vs. ΔL, L_f , L_e and R.
(Analysis No.1)

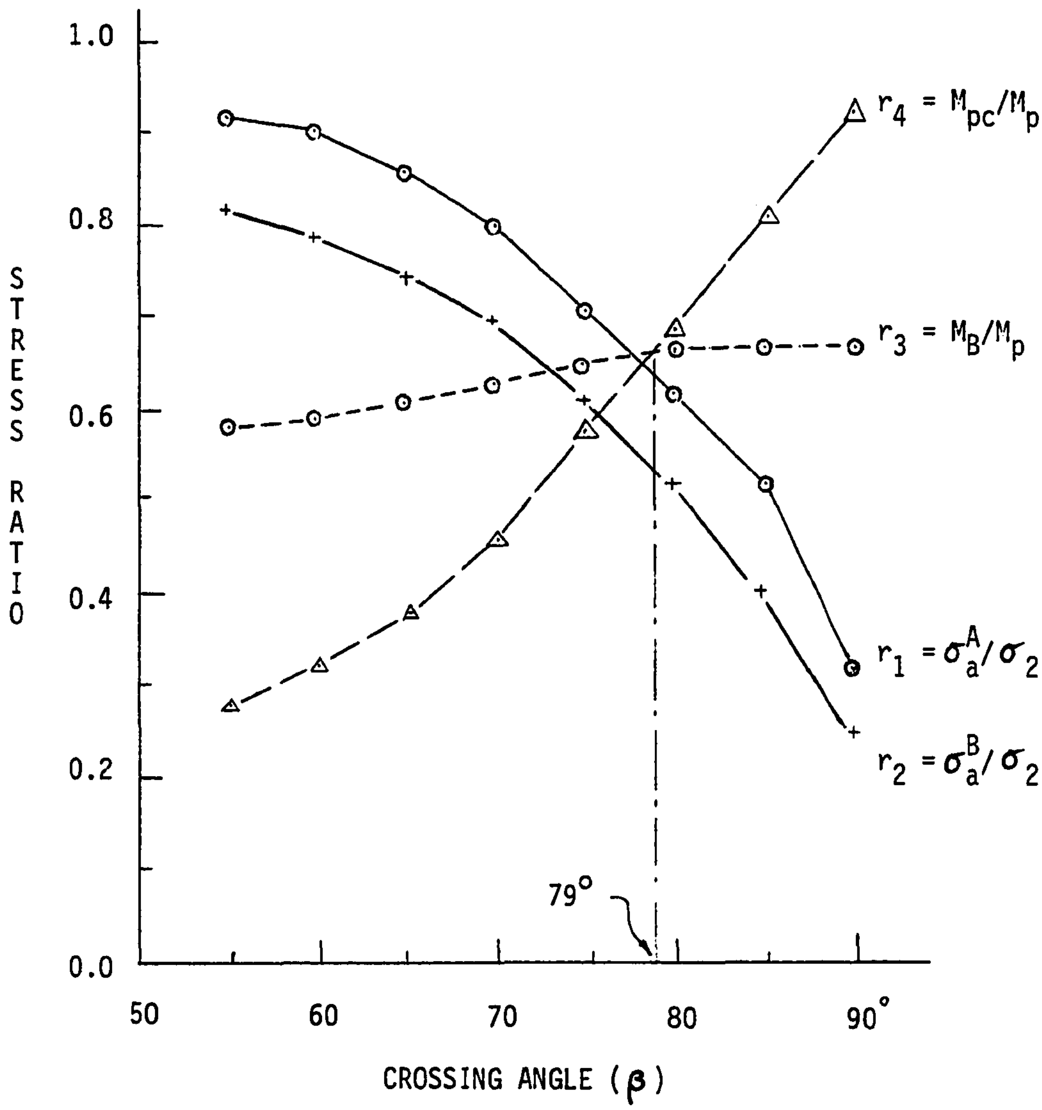

Fig.4.10 Stress ratio vs. Crossing Angle
(ε_2 = 0.04)
(Analysis No.2)

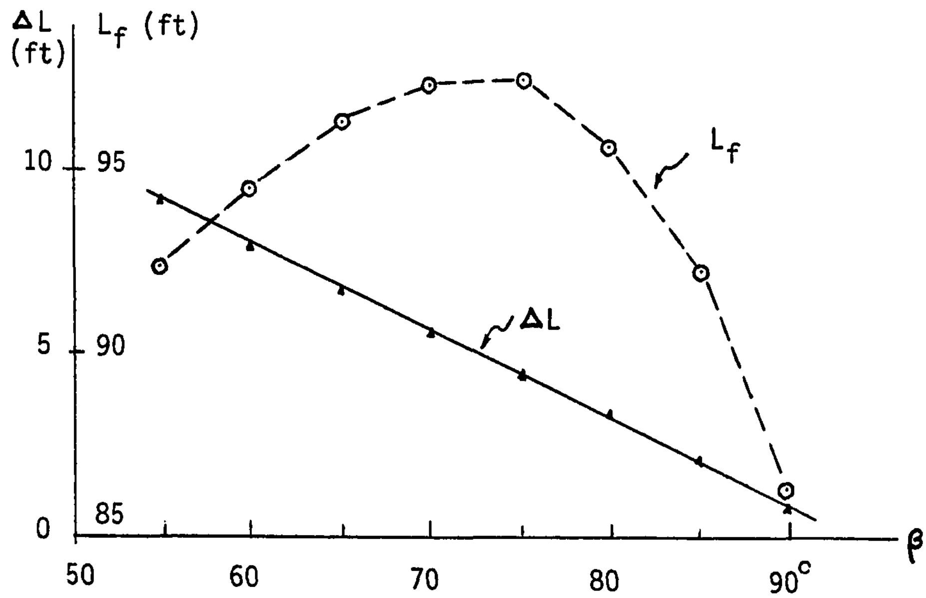

(a)

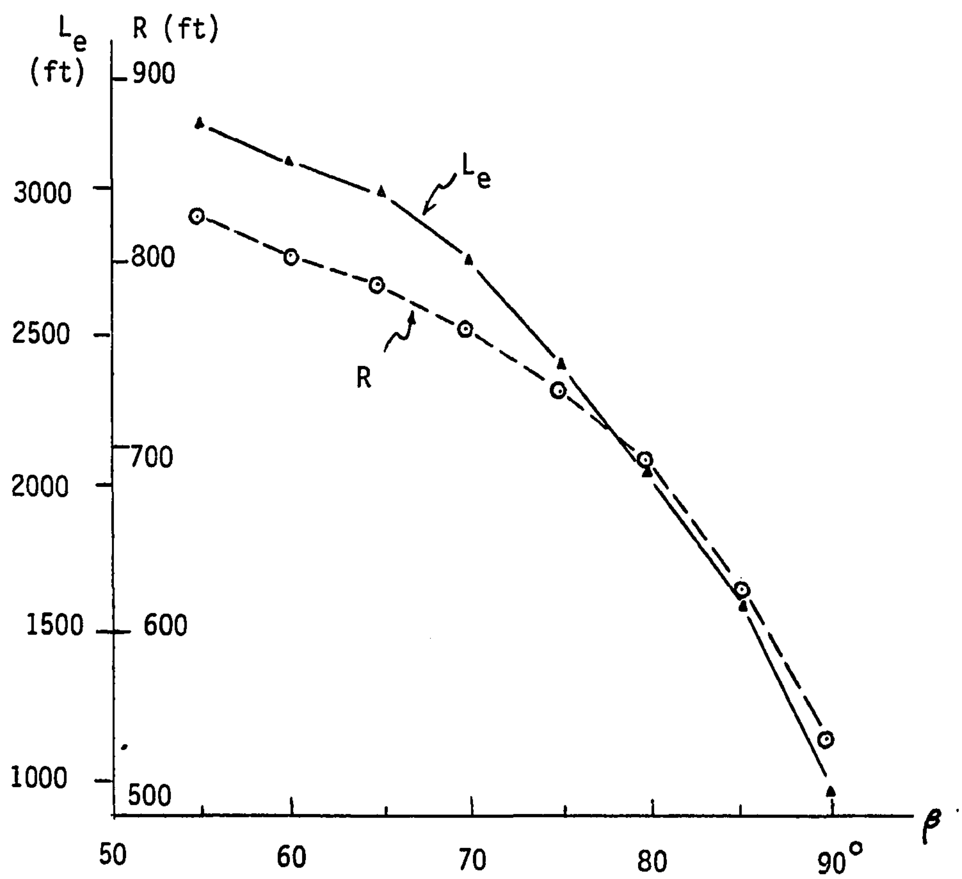

(b)

Fig.4.11 Plots of crossing angle vs. ΔL, L_f , L_e and R.
(Analysis No.2)

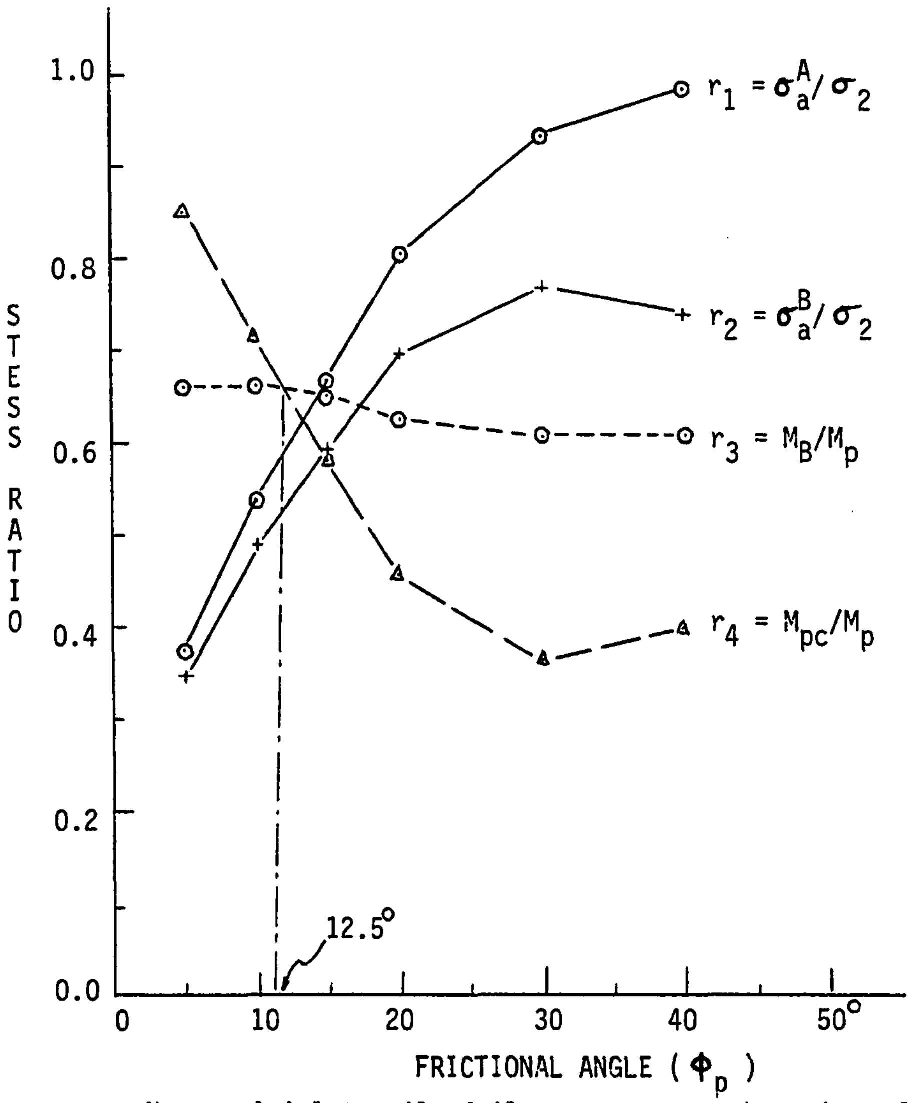

Note: Axial tensile failure occurs at the point of inflection "A" as Φ_p=50°.

Fig.4.12 Stress Ratio vs. Frictional Angle (ε_2 = 0.04).
(Analysis No.3)

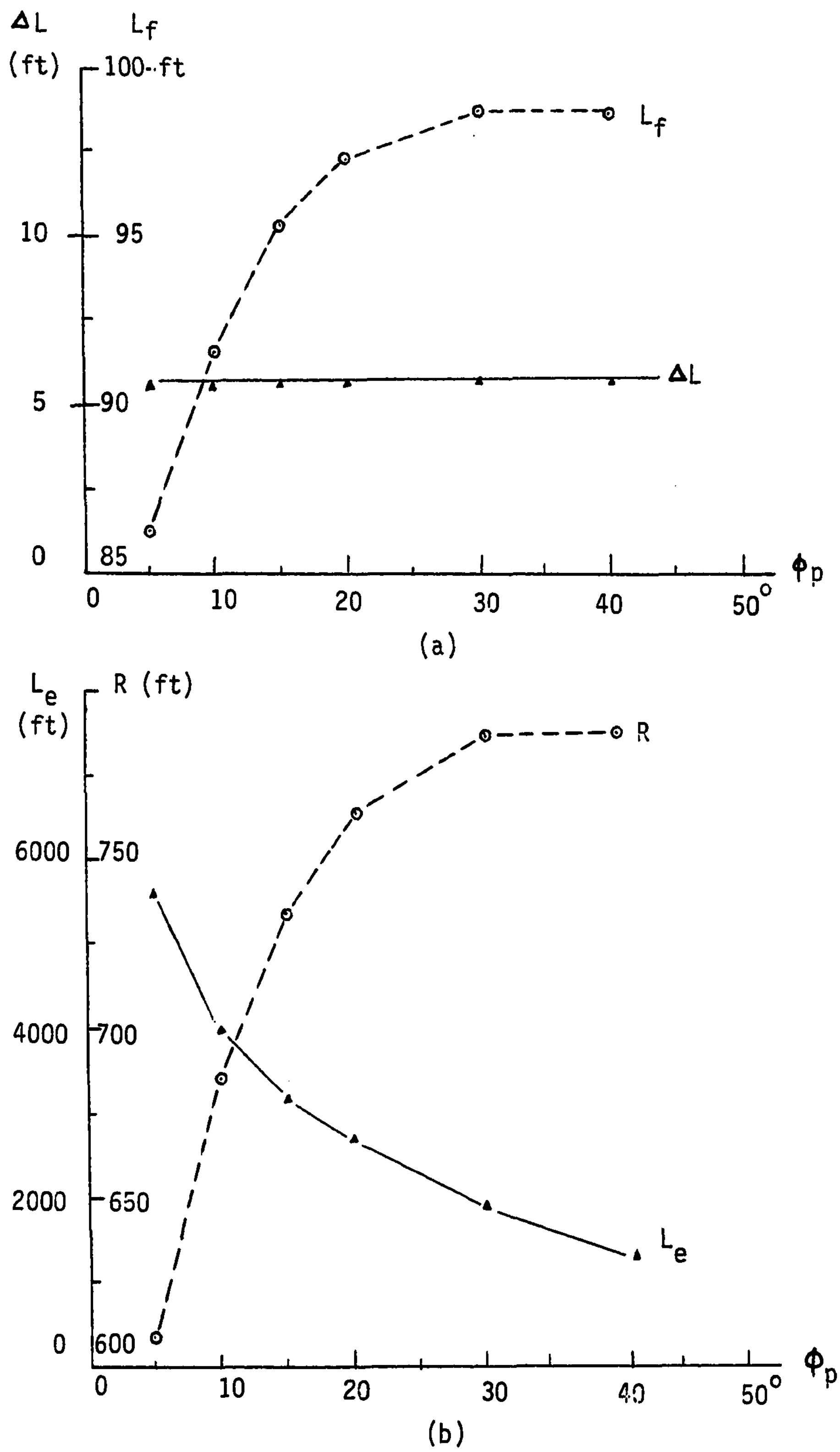

Note: Axial tensile failure occurs at the point of inflection "A" as ϕ_p=50°.

Fig.4.13 Plots of skin friction angle vs. ΔL, L_f , L_e and R. (Analysis No.3)

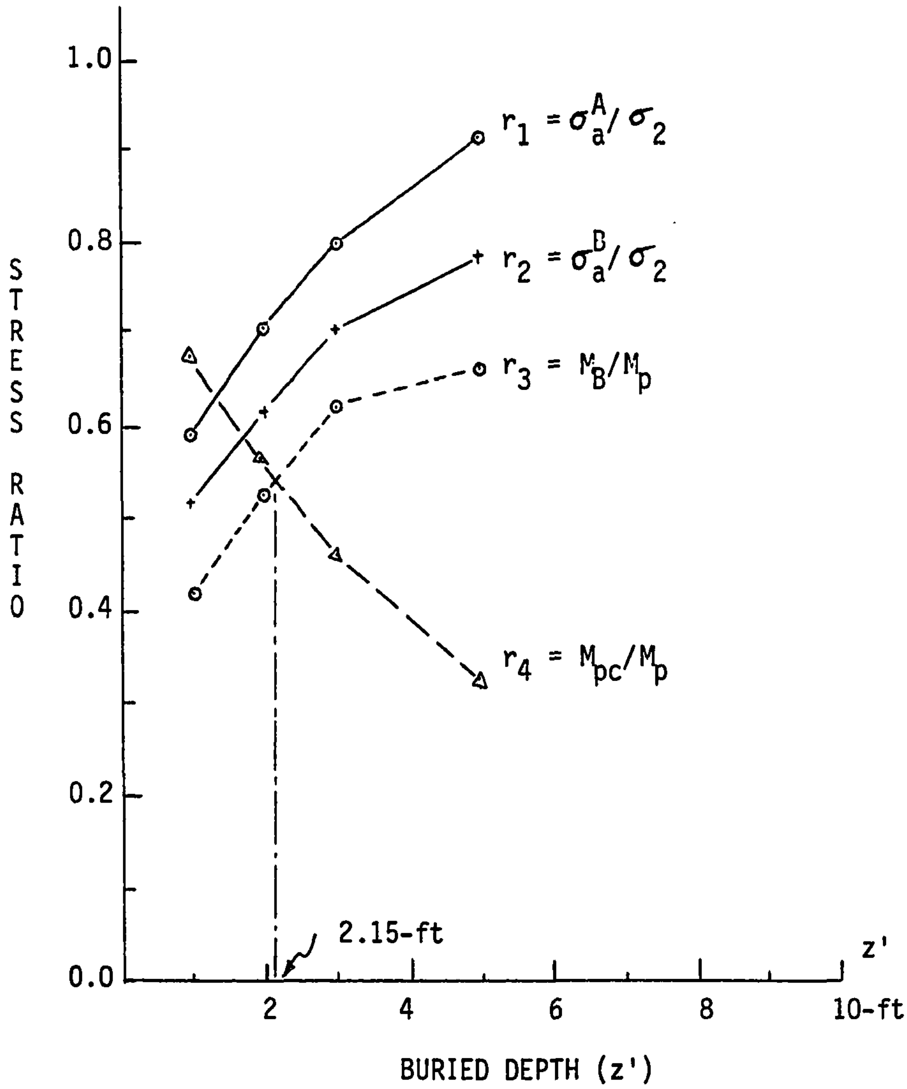

Note: Axial tensile failure occurs at the point of inflection "A" as z'=10-ft.

Fig.4.14 Stress Ratio vs. Buried Depth ($\varepsilon_2 = 0.04$). (Analysis No.4)

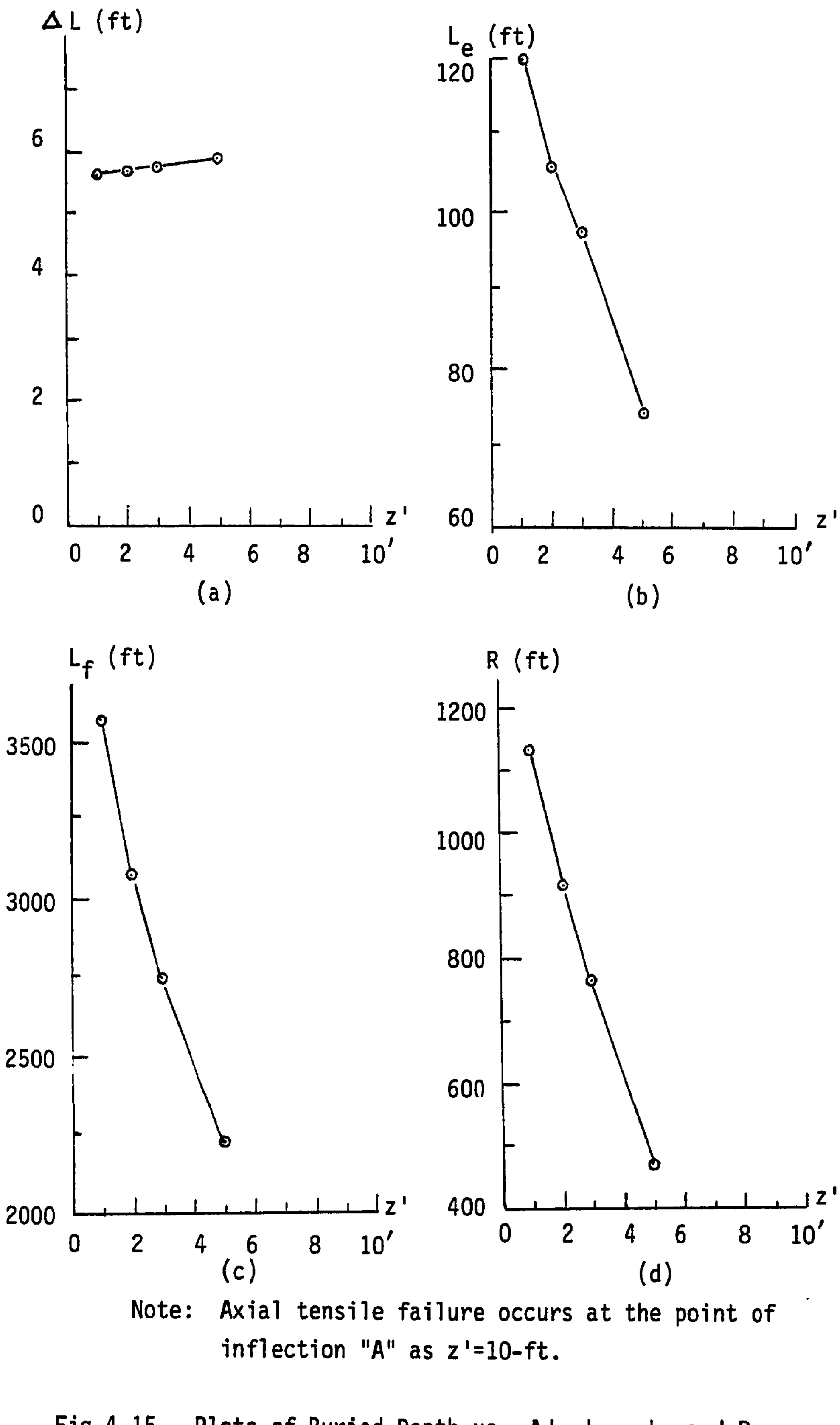

Note: Axial tensile failure occurs at the point of inflection "A" as z'=10-ft.

Fig.4.15 Plots of Buried Depth vs. ΔL, L_f , L_e and R. (Analysis No.4)

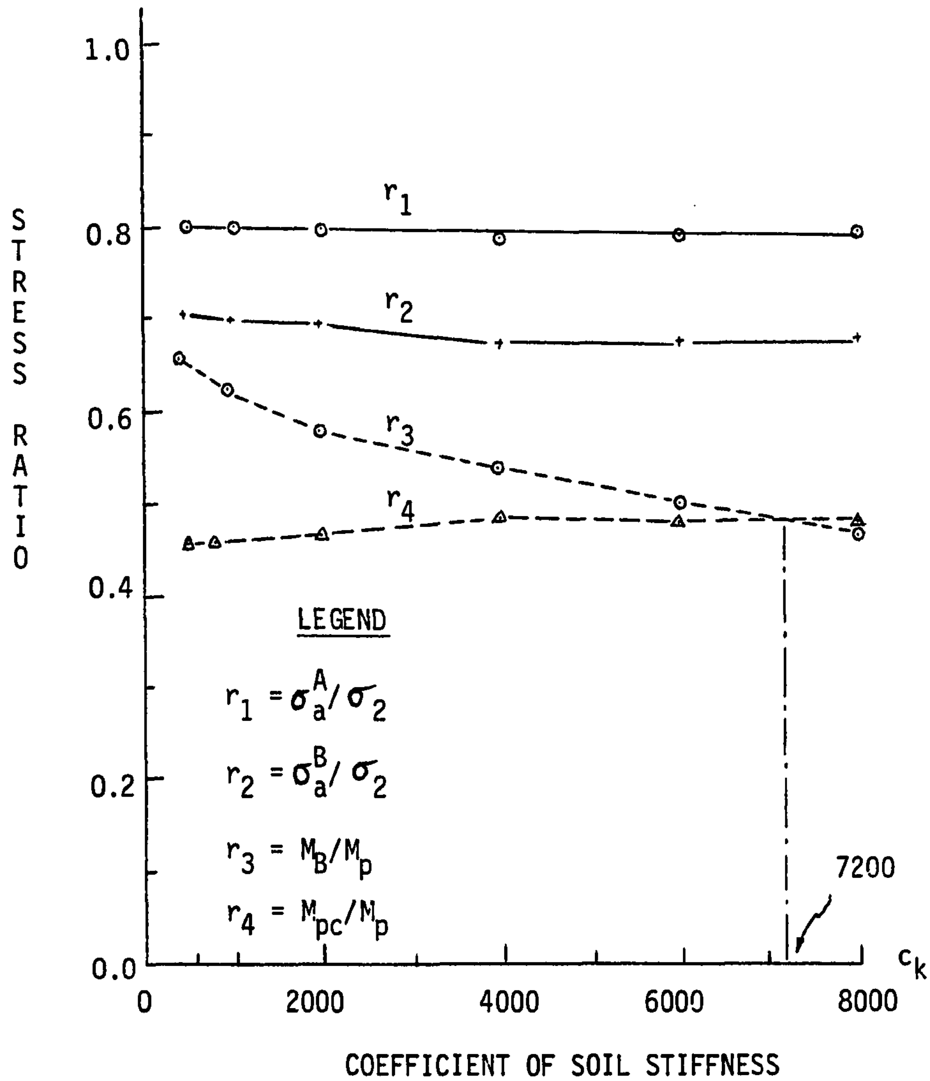

Fig.4.16 Stress Ratio vs. Coefficient of soil Stiffness.
(ε_2 = 0.04)
(Analysis No.5)

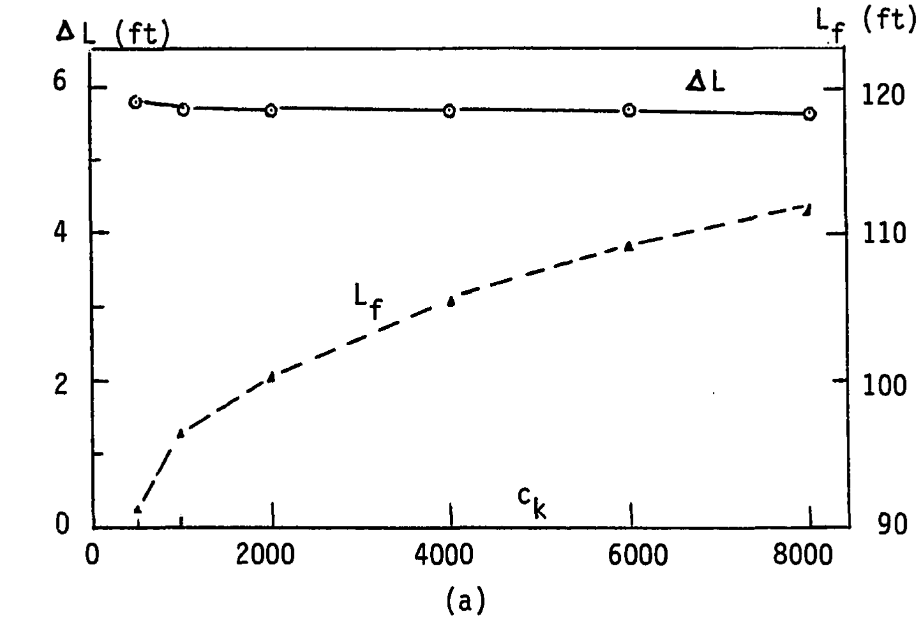

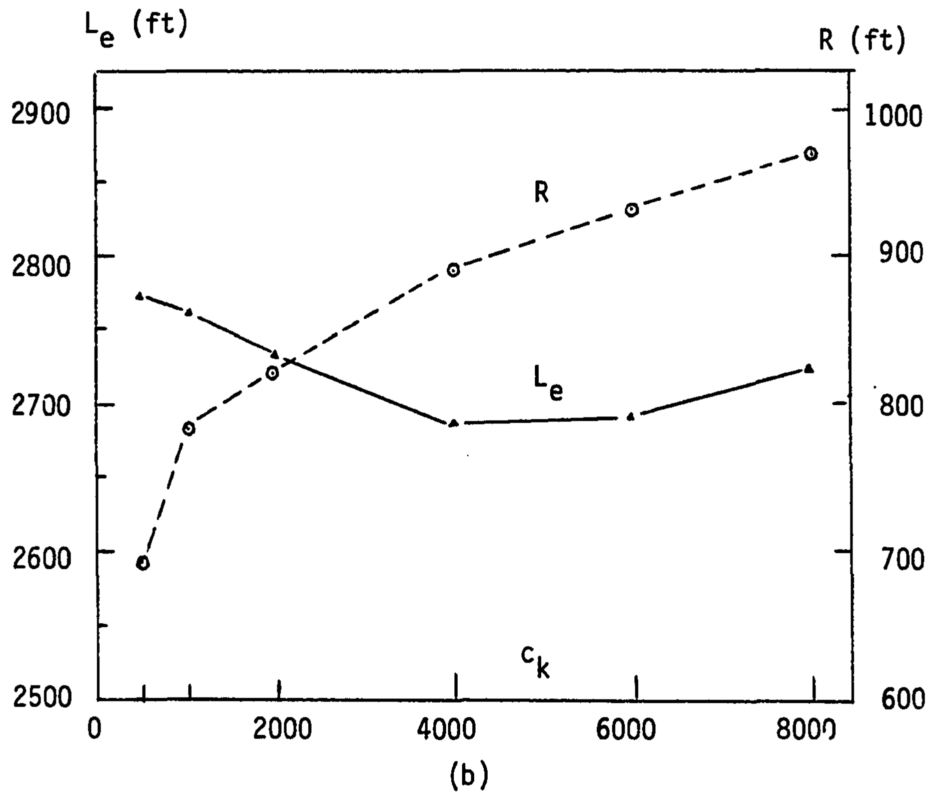

Fig.4.17 Plots of c_k vs. ΔL, L_f , L_e and R.
(Analysis No.5)

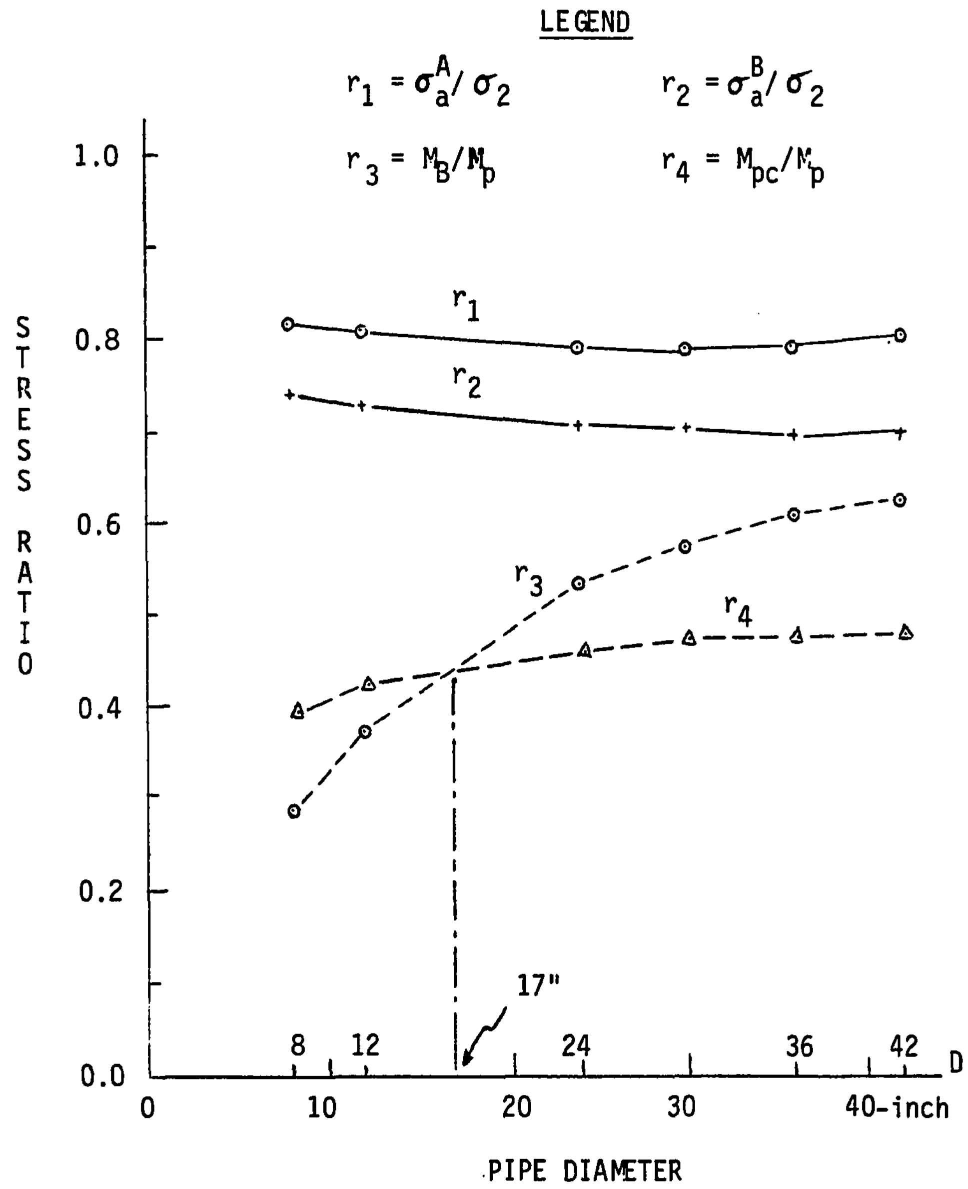

Fig.4.18 Stress Ratio vs. Pipe Diameter (ε_2 = 0.04).
(Analysis No.6)

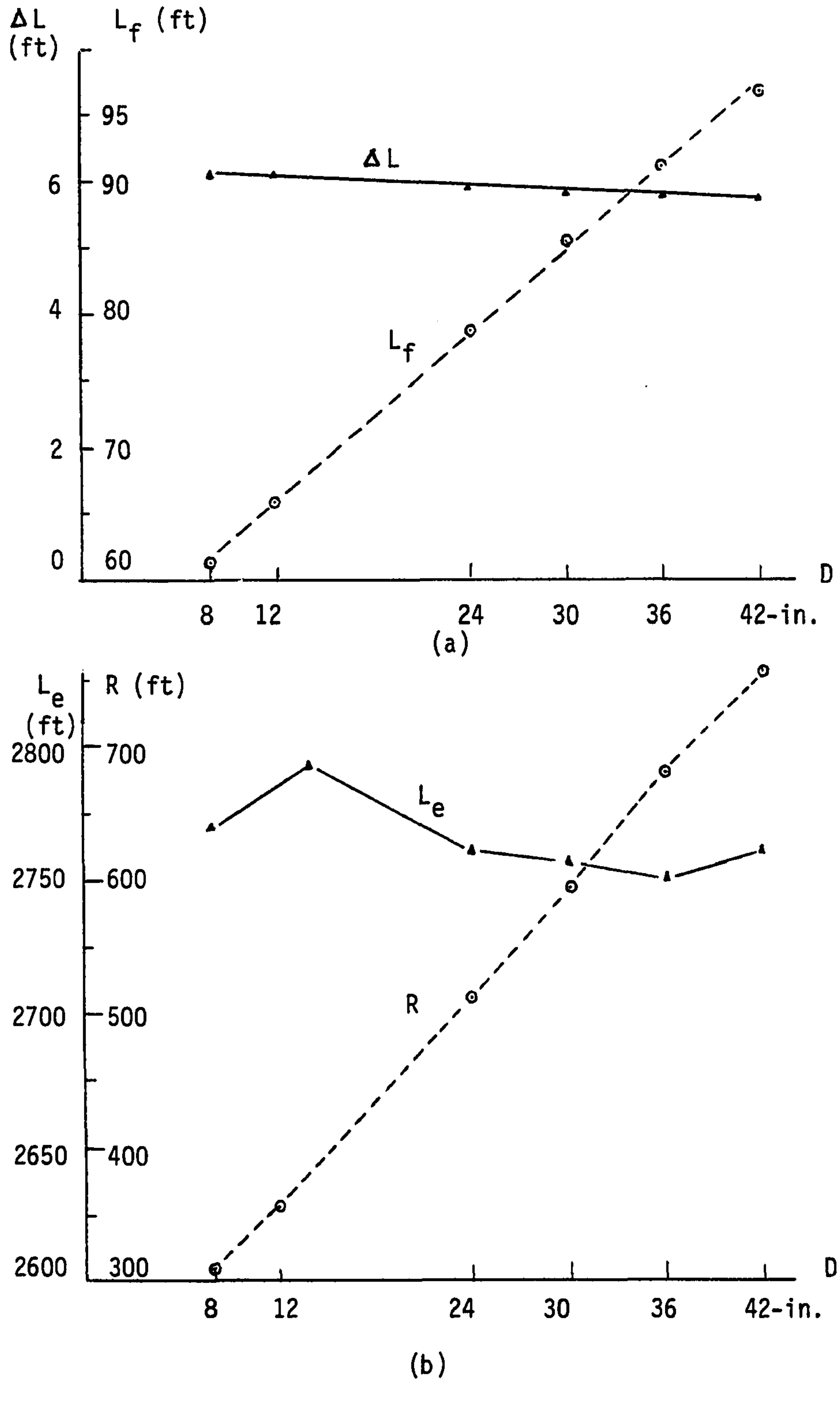

Fig.4.19 Plots of Pipe Diameter vs. ΔL, L_f , L_e and R. (Analysis No.6)

CHAPTER V

SEISMIC ANALYSIS FOR BURIED PIPELINE UNDER A SOIL LIQUEFACTION ENVIRONMENT

5.1 Preface

In the past several years, the prediction of the behavior of saturated soils during earthquakes has become an important concern in regard to foundations of nuclear power plants and major pipeline transmission systems, especially for medium dense and dense deposits. Various procedures (6,10,31,33,34,35) on such predictions have been developed, including analytical and experimental methods.

For the case of a major pipeline transmission system buried in soil deposits that may be susceptible to liquefaction, its seismic environments can be considered in the following manner. In the liquefiable zone, the seismic waves propagating faster through firm soils along the pipe axis cause an incoherent movement at both edges of the pipe submerged in liquefied mediums. Therefore, a buried pipe through the liquefied area is subjected to seismic incoherent motions which generate longitudinal and lateral forces.

When liquefied, soil acts as a dense, viscous fluid, thus the buried pipeline within the liquefiable zone can result in subtantial vertical movement due to its buoyancy. Fig.2.6 shows two possible failure modes (i.e. breaking and buckling of a pipe) induced by seismic waves in a liquefied soil region. The effective length shown in Fig.2.6 associated with the liquefied zone is considered to be an important parameter.

A simplified model of a beam-column (buried pipe) on two elastic foundations (one for liquefiable and the other for non-liquefiable zone) is proposed. To obtain an exact solution for the buckling load of a buried pipeline under such a environment as mentioned above will be very diffcult. A finite difference method incorporating the variation effects of soil stiffness during an earthquake was introduced to study the dynamic buckling of a infinitely long buried pipe. In addition, the proposed method was also able to account for the influences of longitudinal and lateral inertia forces and lateral deformations.

Finally, a parametric analysis is investigated to study the effects of various parameters to the pipe performance.

5.2 Soil Liquefaction

One of the major causes of destruction during an earthquake is the failure of the ground structure. The ground may fail due to fissures, abnormal or unequal movements, or loss of strength. The loss of strength may take place in sandy soils due to an increase in pore pressure. This phenomenon, termed liquefaction, can occur in loose and saturated sands. The increase in pore pressure causes a reduction in the shear strength. If the soil has lost all shear strength, liquefaction occurs and the soil in the liquefied zone behaves like a viscous fluid.

The strength of sandy soil is due to internal friction only. For a saturated sand, its shear strength is expressed as

$$s = (\sigma_n - u) \tan\phi_0 \qquad (5.1)$$

where s = Shear strength

σ_n = Normal pressure on any plane at depth Z

u = Pore pressure

ϕ_0 = Angle of internal friction

It is apparent that the soil will lose its strength if there is an increase in pore pressure "u". Until "u" is equal to "σ_n", then the soil is liquefied.

H.B. Seed and other investigators(34,35) have pointed out that for many deposits, a major part of the soil deformations may be attributed to the upward propagation of shear waves from underlying layers , thus, a soil element, such as that shown in Fig.5.1a, may be considered to be subjected to a series of cyclic shear strains or stresses that reverse many times during the earthquake (Fig.5.1b and 5.1c) and cause the buildup of pore pressure.

A study on liquefaction characteristics of soils was made by Peacock and Seed(30) in 1968. Figures 5.2a-5.2c show a part of the test results describing the process of liquefaction. From Fig.5.2a, it is obvious that there is a gradual increase in pore pressure until the effective confining pressure has pratically been reduced to zero. At this point, the resulting deformations become extremely large, and the soil has essentially liquefied. Generally, the liquefaction denotes a condition where a soil will undergo continued deformation at a constant low residual stress or with no residual resistance.

5.3 Soil Characteristics

The results of a series of simple shear tests(30) performed on the liquefaction of loose sands are shown in Fig.5.3. It is apparent from this figure that, for a sand at a given void ratio under a given initial effective confining pressure, the number of stress cycles required to cause liquefaction increases as the applied pulsating shear stress decreases. In a practical situation, the pulsating shear stresses are induced by the upward propagation of shear waves from the underlying layers as shown in Figures 5.1a-5.1c. A similar relationship between the number of stress cycles causing liquefaction and the pulsating shear stress was found in the tests under cyclic-loading-triaxial conditions(34). Fig.5.4 shows such a relationship obtained from the simple shear tests by Seed and Lee(34).

To account for the actual soil liquefaction in field conditions during an earthquake, the liquefaction study of large saturated sand samples excited on a shaking table seems to be much more realistic than that of the cyclic triaxial loading and simple shear test commonly used. Based upon a part of the shaking table test results presented by Finn(10,31), the resistance to liquefaction decreases with increasing acceleration amplitude (as shown in Fig.5.5). Since the shear stresses induced in the sample are a function of the acceleration amplitude, this decrease in the resistance to liquefaction with increasing acceleration amplitude was anticipated. These results are in general agreement qualitatively with the data obtained from triaxial(34) and simple shear tests(30).

With regard to the behavior of dense sand under cyclic stress applications, the test results(34) indicated a similar relationship between the number of stress cycles required to cause liquefaction and the pulsating shear stress as in the case of loose sand. However, the test results also indicated that under cyclic stress application, no sudden failure occurred in dense sand, which was significantly different from the case of loose sand.

From the above mentioned investigations, it would be reasonable to summarize that for most sandy soils with a given void ratio under a given initial effective confining pressure, the number of stress cycles causing liquefaction increase as the applied pulsating shear stress decreases. In other words, the stiffness of such a soil is decreasing gradually until equal to zero during seismis shaking. In this regard, the stiffness of the soil foundation will be assumed an exponential function of time to account for the decaying property of shear strength of soil deposits during seismic excitation.

Let $k_f(t)$ be the decaying function of soil stiffness at liquefied (failure) zone. Then it can be expressed by the equation below.

$$k_f(t) = Q_f(t)\, k_{f0} \tag{5.2}$$

where "k_{f0}" is the bearing capacity of soil (initial soil stiffness) as indicated in Sect.3.6, and "$Q_f(t)$" is the characteristic function describing the process of liquefaction. Their expressions are shown as follows.

$$k_{f0} = c_k\, N_q\, \gamma \tag{5.3}$$

$$Q_f(t) = \begin{cases} \exp(-at/t_0) - (t/t_0)\exp(-a) & 0 \leqslant t \leqslant t_0 \\ 0 & t \geqslant t_0 \end{cases} \tag{5.4}$$

where c_k = Coefficient of soil stiffness, dependent upon the soil characteristics

N_q = Brinch Hansen bearing capacity factor

γ = Unit weight of soil

t_0 = Time required to cause liquefaction

a = Arbitrary constant for $Q_f(t)$

From observations(26,33,39), it was obvious that the seismic duration was much longer than the time required to cause the liquefaction. For one of liquefaction cases in the analysis, the coefficients of "a" and "t_0" are assumed to be 2.50 and "$0.2T_0$". "T_0" denotes the duration time of the earthquake. Note that both "a" and "t_0" are dependent upon the soil type and characteristics, and can be determined from laboratory tests such as triaxial, simple shear , shaking table tests, etc. A graph for characteristic function proposed was shown in Fig.5.6.

In reality, in the areas of non-liquefiable zone or near the liquefiable zone, the soil also loses its shear strength partially due to an increase in pore pressure during the earthquake. The characteristic function of soil stiffness at this region can be modified in the following expression.

$$Q_c(t) = \exp(-bt/T_0) \qquad (5.5a)$$

where "b" is a constant for "$Q_c(t)$", which is dependent on soil type. graphically, Eqn.5.5a is shown in Fig.5.7. It is noted that the decaying function of soil stiffness at unliquefied area is given as below.

$$k_c(t) = Q_c(t)\, k_{c0}$$

where "k_{c0}" is the initial stiffness of soil in the non-liquefiable zone. For simplification, "k_{c0}" is assumed to be equal to "k_{f0}" as expressed in Eqn.5.3.

Furthermore, a consideration on spatial effects is also required for the extended structures. It seems to be evident from observations that the effects of build-up of pore pressure which may cause liquefaction, attenuates with distance from the liquefied zone. A function further proposed for specifying the spatial and temporal effects is presented in the following manner.

As $0 \leqslant t \leqslant t_0$

$$Q_c(x,t) = \begin{cases} \exp(-\dfrac{\bar{b}xt}{l_c t_0}) - \dfrac{xt}{l_c t_0}\exp(-\bar{b}) ; & 0 \leqslant x \leqslant l_c \\ \exp\left\{-\dfrac{\bar{b}(l-x)t}{l_c t_0}\right\} - (\dfrac{l-x}{l_c})\dfrac{t}{t_0}\exp(-\bar{b}) ; & l_c + l_f \leqslant x \leqslant l \end{cases} \quad (5.5b)$$

As $t \geqslant t_0$

$$
Q_c(x,t) = \begin{cases} \exp(-\bar{b}x/l_c) - (x/l_c)\exp(-\bar{b}) \;; & 0 \leqslant x \leqslant l_c \\ \exp\left\{-\dfrac{\bar{b}(l-x)}{l_c}\right\} - \dfrac{l-x}{l_c}\exp(-\bar{b}) \;; & l_c + l_f \leqslant x \leqslant l \end{cases} \tag{5.5c}
$$

Note that

$$
k_c(x,t) = Q_c(x,t)\, k_{c0}
$$

where $\bar{b}$ = Coefficient dependent upon soil properties

l_c = Supported length of pipe in un-liquefied zone

l_f = Pipe length submerged in liquefied zone

l = Total length of pipe model

If we set $x = l_c$ or $x = l_c + l_f$, Eqn.5.5b will have a similar form to Eqn.5.4.

For examining the effects of the variation of soil stiffness outside the liquefied zone, a study was initiated by setting the stiffness constant all the time during an earthquake, and followed by replacing the decaying conditions of the soil stiffness.

5.4 Problem Description

An infinitely long pipeline was buried in a liquefiable region as shown in Fig.5.8. The soil deposits are considered as an elastic foundation with homogeneous properties and a constant soil stiffness of "k". Before the occurrence of an earthquake, the soil stiffness at both liquefied and un-liquefied zones are set equal to "k_{f0}" and "k_{c0}" respectively.

If an earthquake occurred at some depth and some distance away from the liquefiable region concerned, the seismic waves could be decomposed into two components, one horizontal and one vertical excitations. Based on some investigations(33,34,35), the soil deposits at the liquefiable zone are subjected to a train of upward propagation of shear waves from the underlying layers. The sandy soil is thus losing its shear strength gradually as the pore pressure of the soil element is building up. It also means that the soil stiffness of "k_f" is decreasing to zero in a very short time period, and the soil begins to be liquefied subsequently. As mentioned previously, the time period required to cause the liquefaction of soil deposits is usually much shorter than the duration time of earthquake. Therefore, the buried pipe is thus considered partially supported as shown in Fig.5.9. Furthermore, the horizontal wave propagation will cause incoherent motions along the pipe axis at both boundaries of the liquefied zone. Basically, the incoherent ground movements induce the pipe strains through soil restriction are likely to generate longitudinal forces (either tension or compression), and possibly cause the buckling/breaking failure of the pipe if the axial pipe forces are induced beyond the critical sustained load of the pipe.

The purpose of this study is to investigate the dynamic responses of the buried pipeline under a seismic environment of soil liquefaction, using a simplified model.

5.5 Proposed model of study

Fig.5.10 shows a model of pipe proposed for this research to investigate the dynamic responses of buried pipeline subjected to an end displacements in a liquefied environment. The simplified model is a long simply supported prismatic column resting on elastic foundations. The central segment of the pipe (column) was surrounded by liquefied soil.

In reality, the pipeline is unable to be buried in a perfectly straight condition due to inaccurate workmanship. It would be reasonable to assume the pipe is slightly curved in its natural state. Fig.5.10 shows the shape of the pipe axis that is assumed to be a sine imperfection curve at all times.

The axial load "N" is assumed to be produced by the incoherent motion and concentrated at two relative points on the pipe (i.e. points A and B as shown in Fig.5.10). The incoherent movements can be converted to relative movement (either contraction or elongation), during seismic shaking.

Under such circumstances, the pipe could be compressed or stretched longitudinally, and may be failed either in buckling or breaking. Note that the functions describing the induced relative displacements applied at the movable end B of the pipe can be linear, sinusoidal, pulse and random process functions etc. In this analysis, three types of relative axial displacements are applied at point B of the pipe to examine the dynamic behavior. These applied displacements are:

(a) Linear compresive displacement

(b) Sinusoidal displacement

(c) Recorded displacement of 1940 El Centro Earthquake

Several other conditions and assumptions adopted in this study are described as follows.

i) For most of the extended structures such as pipelines, tunnels and bridges etc., it is necessary to consider the spatial and temporal effects due to the dynamic responses during earthquake.

ii) Both axial and lateral inertia forces along the pipe were taken into consideration, but the rotatory inertia force was not included.

iii) Damping forces were not included in this analysis.

iv) The skin frictions induced in the concerned areas between pipe/soil were neglected.

v) The buried pipeline was kept stationary before excitation.

vi) Buoyancy forces of the soil were not taken into account in the liquefied region.

vii) The failure modes of cylindrical shell types were not included in this pipe analysis.

5.6 Basic Theoretical Derivations

The formal mathematical procedure for considering the behavior of an infinitely long pipe is by means of differential equations in which the position coordinates are taken as independent variables. Since time also is an indepemdent variable in a dynamic problem, the formulation of the equations of motion leads to a partial differential equation. It is apparent that because the pipeline is extended longitudinally, it is considered as beam- or rod-system in which it may be assumed that the physical properties (mass, stiffness, etc.) are expressed with reference to a single position variable along the central axis of the pipe. Therefore, the partial differential equations of these systems involves only two independent variables, time and distance.

5.6.1 Lateral Motion: Including Axial-Force Effects

The first case to be considered in the formulation of the continuum equations of motion is a straight, uniform beam supported on an elastic foundation as shown in Fig.5.11(a). The significant physical properties of the beam are assumed to be the flexural stiffness "EI" and the mass per unit length "m". The transverse loading w(x,t) is assumed to vary arbitrarily with position and time, and the transverse-displacement response y(x,t) also is a function of these variables. The end-support conditions for the beam are arbitrary, although they are pictured as simple supports for illustrative purposes.

The equation of motion of this simple system can readily be derived by considering the equlibrium of forces and moments acting on the differential segment of the beam shown in Fig.5.11(b). Summing the forces acting vertically leads to the first dynamic equlibrium relationship:

$$V + wdx - \left(V + \frac{\partial V}{\partial x} dx\right) - f_I dx - f_k dx = 0 \qquad (5.6)$$

in which "w" is the external force; "f_I dx" represents the distributed transverse inertia force and is given by the product of the differential mass and local acceleration:

$$f_I dx = mdx \frac{\partial^2 y}{\partial t^2} \qquad (5.7)$$

and f_k dx indicates the distributed transverse spring forces (elastic foundation) and is expressed by Eqn.5.8

$$f_k dx = kydx \qquad (5.8)$$

As indicated in Sect.5.3, soil stiffness is

$$k = \begin{cases} k_c(x,t) & \text{at un-liquefied zone} \\ k_f(t) & \text{at liquefied zone} \end{cases}$$

Substituting Eqn.5.7 and 5.8 into Eqn.5.6 and simplifying then gives

$$\frac{\partial V}{\partial x} = w - m\frac{\partial^2 y}{\partial t^2} - ky \qquad (5.9)$$

The second equilibrium relationship is obtained by summing moments about the elastic axis at the center point of the segment and neglecting the second order terms, as follows:

$$M + Vdx - N\frac{\partial y}{\partial x}dx - (M + \frac{\partial M}{\partial x}dx) = 0 \qquad (5.10)$$

where it has been noted that the distributed lateral force makes only a second-order contribution to the moment. Note that no inertia forces contribute in this case to the moment equilibrium. This simplifies directly to the standard static relationship among shear, moment and axial force

$$V = N\frac{\partial y}{\partial x} + \frac{\partial M}{\partial x} \qquad (5.11)$$

Differentiating Eqn.5.11 with respect to x and substituting into Eqn.5.9 yields, after rearrangement,

$$\frac{\partial^2 M}{\partial x^2} + \frac{\partial}{\partial x}(N\frac{\partial y}{\partial x}) + ky + m\frac{\partial^2 y}{\partial t^2} = w \qquad (5.12)$$

In practice, both the axial force "N" and soil stiffness "k" will vary as arbitrary functions of x and t in this analysis. Finally, introducing the basic moment-curvature relationship of elementary beam theory ($M = \partial^2 y/\partial x^2$) and setting "$w = 0$", leads to the partial differential equation of free vibration for the flexural beam including the effects of axial force

$$\frac{\partial^2}{\partial x^2}\left(EI\frac{\partial^2 y}{\partial x^2}\right) + \frac{\partial}{\partial x}\left(N\frac{\partial y}{\partial x}\right) + ky + m\frac{\partial^2 y}{\partial t^2} = 0 \qquad (5.13)$$

If the beam was laid with initial crookedness "y_0" which is independent to time "t", thus an expression including such initial crookedness could be presented by the following equation:

$$\frac{\partial^2}{\partial x^2}\left\{EI\frac{\partial^2}{\partial x^2}(y - y_0)\right\} + \frac{\partial}{\partial x}\left(N\frac{\partial y}{\partial x}\right) + k(y - y_0) + m\frac{\partial^2 y}{\partial t^2} = 0$$

(5.14)

in which both "EI" and "m" are assumed to be constants since the buried pipe is considered as an uniform beam resting on an elastic foundation.

5.6.2 Longitudinal Motion

A straight bar (pipe) in which the axial stiffness "AE" and mass per unit length "m" are assumed to be constants, is shown in Fig.5.12(a). The forces in the axial direction acting on a differential segment are indicated in Fig.5.12(b). Summing these forces leads to

$$N - f_i\,dx - \left(N + \frac{\partial N}{\partial x}dx\right) = 0 \qquad (5.15)$$

in which "f_i" represents the axial inertia force per unit length, and can be expressed as

$$f_i = m\frac{\partial^2 u}{\partial t^2} \qquad (5.16)$$

where "u" is the displacement in the axial direction. As indicated above, the "N" in Eqn.5.15 represents the time-varying axial force associated with varying axial strains produced from incoherent movement at both ends of the pipe.

Substituting Eqn.5.16 into Eqn.5.15 and simplifying leads to

$$\frac{\partial N}{\partial x} = - m\frac{\partial^2 u}{\partial t^2} \qquad (5.17)$$

This equation expresses the dynamic equilibrium of the pipe in the axial direction.

5.6.3 Effects of Axial Strains and Lateral Displacements

As depicted previously, the axial force is induced by the incoherent movement between points A and B as shown in Fig.5.10. For a perfectly straight column subjected to axial load, the axial strain can be expressed by Eqn.5.18

$$\varepsilon_1 = - \partial u/\partial x \qquad (5.18)$$

where the negative sign indicates compressive strain. However, the compressed pipe will displace laterally in a small amount and produce an appreciable shortenning along the original pipe axis. Therefore, the total change in pipe length along the initial pipe position can be determined in the following manner. Fig.5.14 show the geometric configuration of a finite-long pipe subjected to axial compression. From the Pythagorean theorem, as shown in Fig.5.13, the length of a differential element of arc, "ds", is

$$ds = (dx^2 + dy^2)^{1/2}$$

$$= \left\{1 + (dy/dx)^2\right\}^{1/2} dx \qquad (5.19)$$

By the "Binomial Series" displayed by the following equation

$$(1 + z)^{-m} = 1 - mz + \frac{m(m+1)}{2!} z^2$$

$$- \frac{m(m+1)(m+2)}{3!} z^3 + \ldots\ldots \qquad (5.20)$$

"ds" is expanded by letting $z=(dy/dx)^2$ and $m=-1/2$, as

$$ds = \left\{1 + (1/2)(dy/dx)^2 + \frac{(-1/2)(1/2)}{2}(dy/dx)^4 + \ldots.\right\} dx$$

$$(5.21a)$$

Because $(dy/dx)^2$ is so small (small deformation theory) that all higher-order terms in the series can be neglected. Thus Eqn.5.21a becomes

$$ds = \left\{1 + (1/2)(dy/dx)^2\right\}dx \qquad (5.21b)$$

The shortenning in this differential segment of the pipe is

$$\Delta e = ds - dx = (1/2)(dy/dx)^2 dx \qquad (5.22)$$

Therefore, the pipe strain due to lateral displacement of the pipe can be determined by dividing "dx" at both sides in the above equation.

$$\varepsilon_2 = \frac{\Delta e}{dx} = \frac{1}{2}(dy/dx)^2 \qquad (5.23)$$

Combining both effects "ε_1" and "ε_2" gives an expression for the induced axial force of the pipe.

$$N = (\varepsilon_1 - \varepsilon_2)EA$$

$$= \left\{- \frac{\partial u}{\partial x} - \frac{1}{2}\left(\frac{\partial y}{\partial x}\right)^2\right\}EA \qquad (5.24)$$

in which "A" is the cross-sectional area of the pipe.

For an inperfect pipeline, it would be reasonable to assume the pipe is slightly curved in its original natural state. Thus the axial pipe stress can be expressed in the following equation.

$$\frac{N}{AE} = - \frac{\partial u}{\partial x} - \frac{1}{2}\left\{\left(\frac{\partial y}{\partial x}\right)^2 - \left(\frac{\partial y_0}{\partial x}\right)^2\right\} \qquad (5.25)$$

Note that Eqn.5.25 can also apply to the case of a curved pipe subjected to axial tension, and the sign convention used in this equation will be adjusted automatically.

5.6.4 Summary for Theoretical Derivation

The equations of (5.14), (5.17) and (5.25) represent a complete set of fundamental equations for determining three unknown parameters, i.e. the lateral deflection "y", the axial displacement "u" and the axial force "N". All three parameters vary with position "x" and time "t".

Eqn.5.14 expresses equilibrium of the linearly elastic prismatic pipe (beam-type) in the lateral direction under the assumption of small deformation theory. Eqn.5.17

expresses equilibrium of the pipe (column-type) in the axial direction, and Eqn.5.25 determines the axial strain and the relief in stress caused by the increase in curvature of the pipe as the load is applied.

With regard to the sign convention used in this study, the positive quantities contain compressive force, upward deflection and rightward displacement.

5.7 Normalization of Fundamental Equations

To simplify the formulation of those fundamental equations appearing in Sect.5.6, a process of normalization is required.

Let

$$
\begin{array}{ll}
Y = y/r & P = N/AE \\
X = x/r & c^2 = E/\rho \\
U = u/r & m = \rho A \\
L = l/r & T = ct/r \\
K = k_o r^2/AE &
\end{array}
\qquad (5.26)
$$

where k_o = Initial tangent stiffness of the soil (Eqn.5.3)

r = Radius of gyration of the pipe

ρ = Mass density of the pipe

A = Cross-sectional area of pipe

c = The velocity of wave propagation

y_o = Initial crookedness of the pipeline

Substituting Eqn.5.26 into Equations (5.14), (5.15) and (5.25), gives the normalized equations as listed below.

$$\bar{Y}'''' + P'Y' + PY'' + K\bar{Y} + \ddot{Y} = 0 \qquad (5.27a)$$

$$P' = -\ddot{U} \qquad (5.27b)$$

$$P = -U' - \frac{1}{2}\left\{ (Y')^2 - (Y'_0)^2 \right\} \qquad (5.27c)$$

where $\bar{Y} = Y - Y_0$, and the prime and the dot denote differentiation with respect to "X" and "T" respectively.

5.8 Finite Difference Equations

The finite difference method(7,32) is a numerical technique for obtaining the approximate solutions to differential equations. The basis of the finite difference technique is that a derivative of a function at a point can be approximated by an algebraic expression consisting of the values of the function at that point and at several nearby points. In view of this fact, it is possible to replace the derivatives in a differential equation with algebraic expressions and thus transform the differential equation into an algebraic equation.

There are three approximations (i.e. forward, backward and central difference) for the derivatives in a differential equation. Of these three approximations, the central difference is the most accurate for a given spacing (ΔX or ΔT). The remaining discussion dealing with the approximation of higher derivatives will therefore be limited to the central difference method. The difference equations relating to the normalized equations (Eqn.5.27a-5.27c) are displayed as follows. Note that the index "i" and "j" indicate the array numbers of "X" and "T" respectively.

$$Y'_{i,j} = (Y_{i+1,j} - Y_{i-1,j})/2\Delta X \qquad (5.28a)$$

$$P'_{i,j} = (P_{i+1,j} - P_{i-1,j})/2\Delta X \qquad (5.28b)$$

$$U'_{i,j} = (U_{i+1,j} - U_{i-1,j})/2\Delta X \qquad (5.28c)$$

$$Y''_{i,j} = (Y_{i+1,j} - 2Y_{i,j} + Y_{i-1,j})/(\Delta X)^2 \qquad (5.28d)$$

$$\bar{Y}''''_{i,j} = (\bar{Y}_{i+2,j} - 4\bar{Y}_{i+1,j} + 6\bar{Y}_{i,j} - 4\bar{Y}_{i-1,j} + \bar{Y}_{i-2,j})/(\Delta X)^4$$

$$(5.28e)$$

$$\ddot{Y}_{i,j} = (Y_{i,j+1} - 2Y_{i,j} + Y_{i,j-1})/(\Delta T)^2 \qquad (5.28f)$$

$$\ddot{U}_{i,j} = (U_{i,j+1} - 2U_{i,j} + U_{i,j-1})/(\Delta T)^2 \qquad (5.28g)$$

Substituting Eqns.5.28a-5.28g into Eqn.5.27a, gives

$$Y_{i,j+1} = 2Y_{i,j} - Y_{i,j-1} - (\Delta T)^2 K_{i,j} \bar{Y}_{i,j}$$

$$- \frac{1}{4}\left(\frac{\Delta T}{\Delta X}\right)^2 (P_{i+1,j} - P_{i-1,j})(Y_{i+1,j} - Y_{i-1,j})$$

$$- \left(\frac{\Delta T}{\Delta X}\right)^2 P_{i,j} (Y_{i+1,j} - 2Y_{i,j} + Y_{i-1,j})$$

$$- \frac{(\Delta T)^2}{(\Delta X)^4} (\bar{Y}_{i+2,j} - 4\bar{Y}_{i+1,j} + 6\bar{Y}_{i,j}$$

$$- 4\bar{Y}_{i-1,j} + \bar{Y}_{i-2,j}) \qquad (5.29a)$$

Similarly to Eqn.5.27b and 5.27c

$$U_{i,j+1} = 2U_{i,j} - U_{i,j-1} - \frac{(\Delta T)^2}{2\Delta X} (P_{i+1,j} - P_{i-1,j}) \qquad (5.29b)$$

$$P_{i,j} = - \frac{1}{2\Delta X} (U_{i+1,j} - U_{i-1,j})$$

$$- \frac{1}{8(\Delta X)^2} (Y_{i+1,j} - Y_{i-1,j})^2$$

$$- (Y_{i+1,0} - Y_{i-1,0})^2 \qquad (5.29c)$$

where $\bar{Y}_{i,j} = Y_{i,j} - Y_{i,0}$

$K_{i,j} = K(i\Delta X, j\Delta T)$

For any particular moment "j+1", the lateral deflection and the axial displacement of the pipe can be determined by substituting the terms of the already known values at the moments of "j" and "j-1". The induced axial force is only dependent upon the lateral deflection and the axial displacement both function of "X" and "T", but not directly related to the time variable. A "computational molecules" in Fig.5.15 gives a pictorial representation of Eqns.5.29a-

5.29c. A numerical solution by applying the above technique is presented in CHAPTER VI.

5.9 Boundary and Initial Conditions

The following conditions are only suitable to the beam-column with simple supports at both ends.

(A) Lateral deflection

i) Initial crookedness

$$Y_{i,0} = Y_{i,-1} = a_0 \sin(i\Delta X\pi)$$

ii) Boundary conditions

a) $Y_{0,j} = Y_{m,j} = 0$

b) $Y_{1,j} = - Y_{-1,j}$

c) $Y_{2,j} = - Y_{-2,j}$

d) $Y_{m+1,j} = - Y_{m-1,j}$

e) $Y_{m+2,j} = - Y_{m-2,j}$

Here the subscript "m" denotes the coordinate number at the right end support of the pipe. If fixed end supports are taken into consideration instead of simple supports, only changing the signs of conditions (b)-(e) is required.

iii) Initial condition (No initial velocity)

$$\dot{Y}_{i,0} = \frac{1}{2\Delta T}(Y_{i,1} - Y_{i,-1}) = 0$$

Leads to

$$Y_{i,1} = Y_{i,-1}$$

(B) Axial displacement

i) Applied displacement at movable end

$$U_{m,j} = F(j\Delta T)$$

The function of F(T) could be linear, sinusoidal, impulse or any other function, e.g. random function as seismic wave.

ii) Boundary conditions

a) $U_{0,j} = 0$

b) $U_{m+1,j} = \frac{m+1}{m} U_{m,j}$

iii) Initial condition

$$U_{i,-1} = U_{i,0} = 0$$

iv) Initial linear strain along the pipe

$$U_{i,1} = \frac{i}{m} U_{m,1} \qquad i = 1,2,\ldots\ldots,m$$

(C) Axial force of the pipe

No axial pipe force existed before seismic shaking, i.e.

$$P_{i,0} = P_{i,-1} = 0$$

(D) Stiffness of the elastic foundation

i) At un-liquefied region

$$K = K_c \qquad 0 < i < m_1 , \quad m_r < i < m$$

ii) At liquefied region

$$K = K_f \qquad m_1 < i < m_r$$

iii) At boundaries of liquefied region along the pipe

$$K = (K_c + K_f)/2 \qquad i = m_1 \quad \text{or} \quad i = m_r$$

where "K_c" and "K_f" are varying with time. Both are also dependent upon the characteristics of the surrounding soil of the pipe, as defined in Sect.5.3 for this research. In addition, the index of "m_1" and "m_r" indicate the interface points of the central segment of the pipe submerged in the liquefied area as shown in Fig.5.11.

5.10 Summary and Discussions

Based on damage reports of past earthquakes, the pipelines buried in liquefiable regions were found seriously damaged during earthquakes. H.B. Seed and other investigators(34,35) have pointed out that for many deposits, soil liquefaction may be attributed to the upward propagation of shear waves from underlying layers. The soil liquefaction mechanism itself is not the object of this study.

By reviewing the failure modes of the pipe buried in the liquefiable zones, an initial idea may be acceptable to explain the pipe failures under such circumstances, that is, the pipe is also subjected to longitudinal wave propagation at the time of liquefaction of soil deposits. Normally, the longitudinal wave propagation (e.g. P-waves) may produce axial strains (stresses) that cause pipe buckling/breaking. In this study, the axial pipe strain can be induced by applying a relative movement between two particular points along the pipe.

The soil stiffness is a very important parameter influencing the dynamic behaviors of buried pipe during seismic shaking. Several characteristic functions incorporating spatial and temporal effects were proposed to describe the decaying properties of soil.

In the proposed model, a finite-long pipe simply supported at both sides was assumed to be rested on an elastic foundation. The central segment of the pipe was surrounded by liquefied soil. Actually, the pipe is extended infinitely long through the liquefiable zone. A further study investigating the effects of supported length of the pipe on an elastic foundation is required.

The equations of (5.14), (5.17) and (5.25) represent a complete set of fundamental equations for determining three unknown parameters: the lateral deflection "y", the axial displacement "u" and the axial pipe force "N". All three parameters are varying with position "x" and "t". In 1950, N.J. Hoff initiated a similar set of equations to investigate the dynamic buckling of an elastic column by using the Bessel-function method.

To obtain a closed-form solution for the buckling load of a buried pipe subjected to soil liquefaction and longitudinal wave propagation along the pipe, is quite difficult. A finite-difference technique is thus introduced to avoid such difficulties. The main disadvantage of this technique is that it gives numerical values of the unknown function at discrete points instead of an analytical expression that is valid for the entire system.

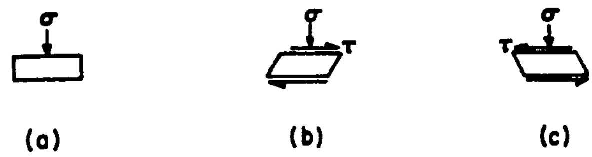

Fig.5.1 IDEALIZED STRESS CONDITIONS FOR ELEMENT OF SOIL BELOW GROUND SURFACE DURING AN EARTHQUAKE

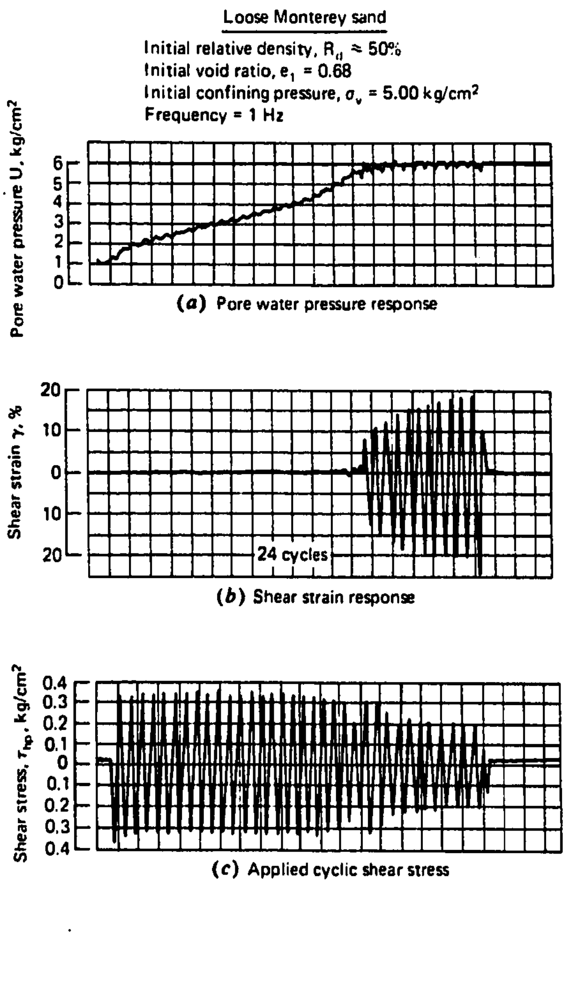

Fig.5.2

Record of a typical pulsating load test on loose sand in simple shear conditions. ***(After Peacock and Seed, 1968.)***

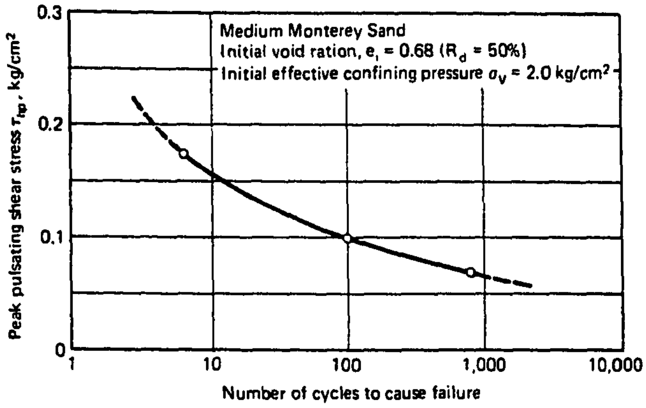

Fig.5.3 Typical form of relationship between pulsating shear stress and number of cycles to cause failure - simple shear conditions. (After Peacock and Seed, 1968.)

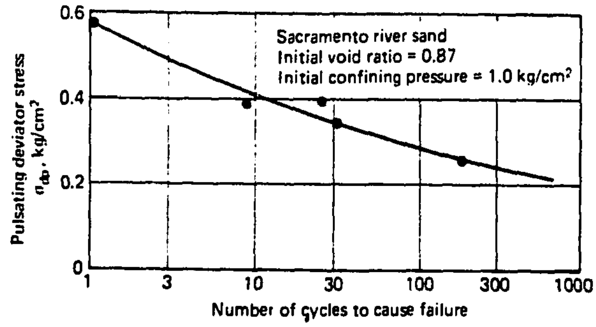

Fig.5.4 Relationship between pulsating deviator stress and number of cycles required to cause failure in loose sand. (After Seed and Lee, 1966.)

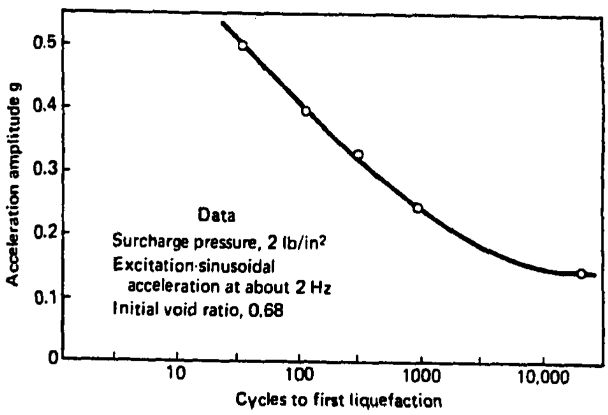

Fig.5.5 Effect of acceleration amplitude on resistance to liquefaction on vibration-table studies. (After Finn, 1972.)

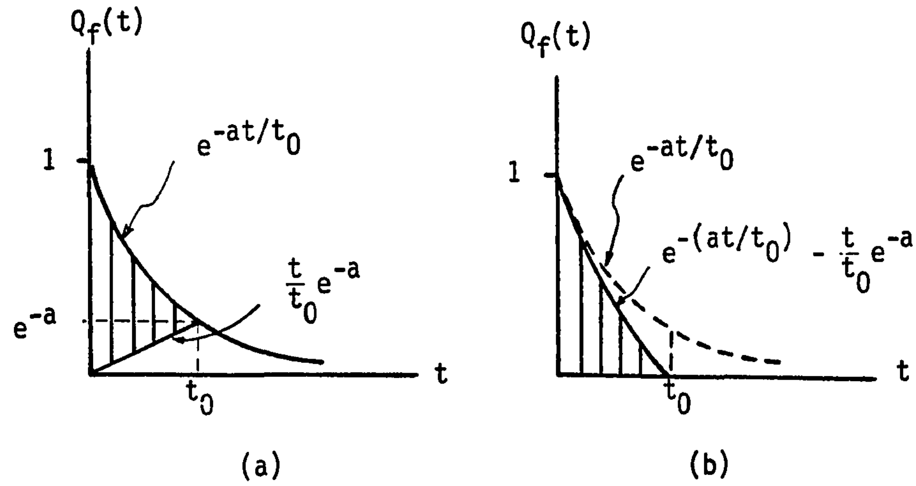

Fig.5.6 Characteristic function for liquefied zone.

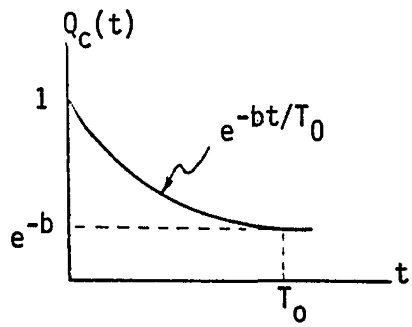

Fig.5.7 Characteristic function for un-liquefied zone.

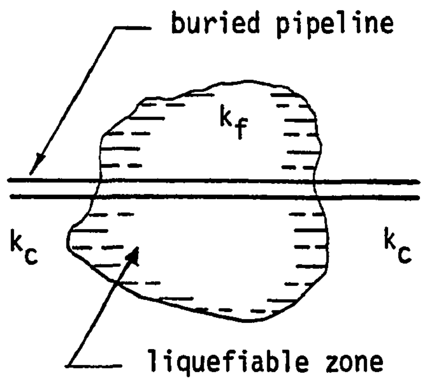

Fig.5.8 Pipeline buried through liquefiable zone.

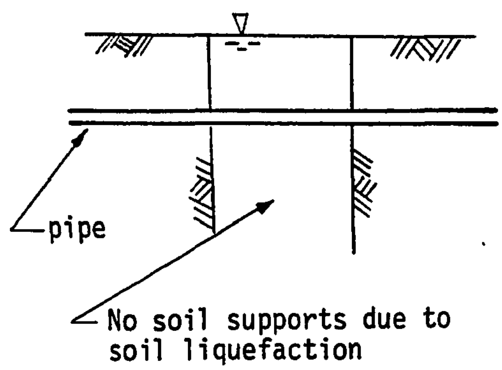

Fig.5.9 Proposed beam partially supported on elastic foundation.

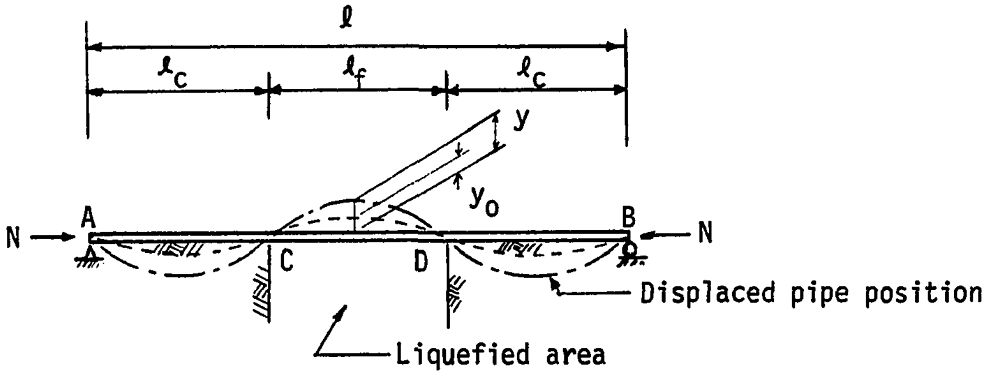

Fig.5.10 Proposed model of buried pipe

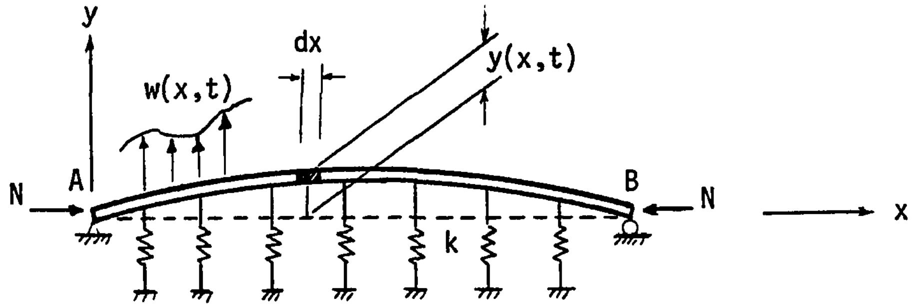

(a) Beam deflected due to loading

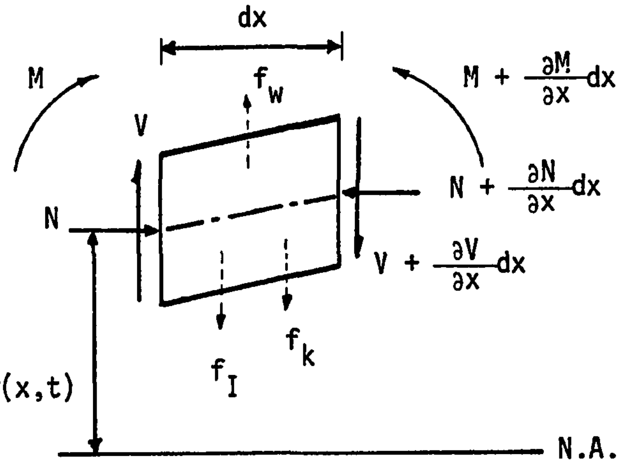

(b) Forces acting on differential element

Fig.5.11 Beam subjected to dynamic lateral deflections.

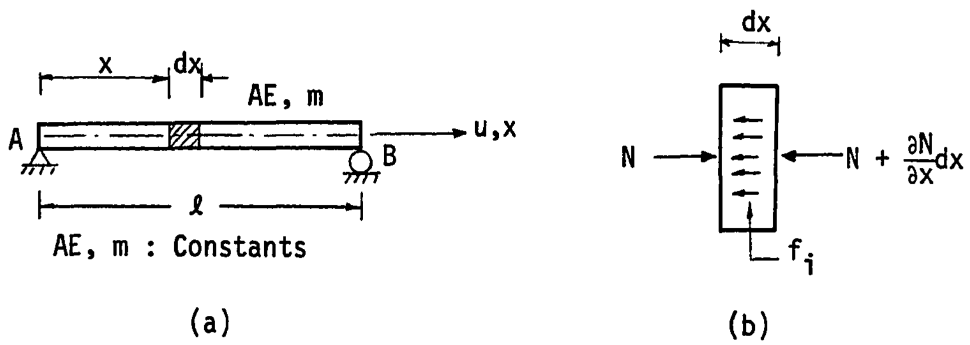

Fig.5.12 Bar subjected to dynamic axial deformations: (a) bar properties and coordinates; (b) forces acting on differential element.

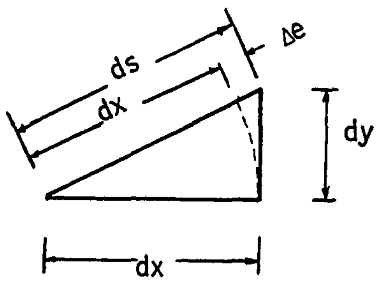

Fig.5.13 Relationship between "ds" and "dx".

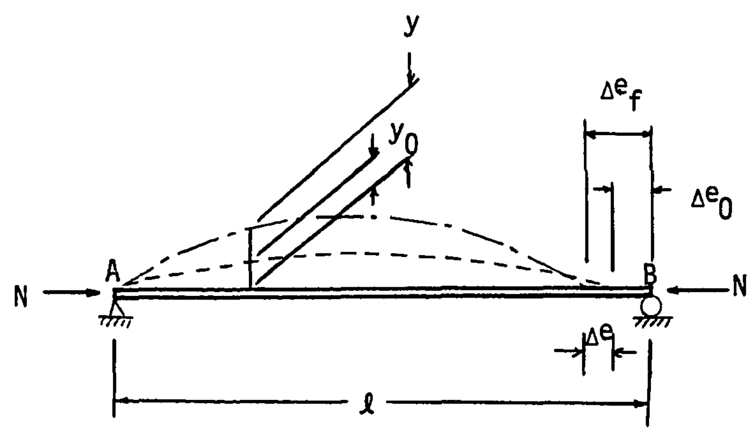

Fig.5.14 Column shortening due to axial compression and bending.

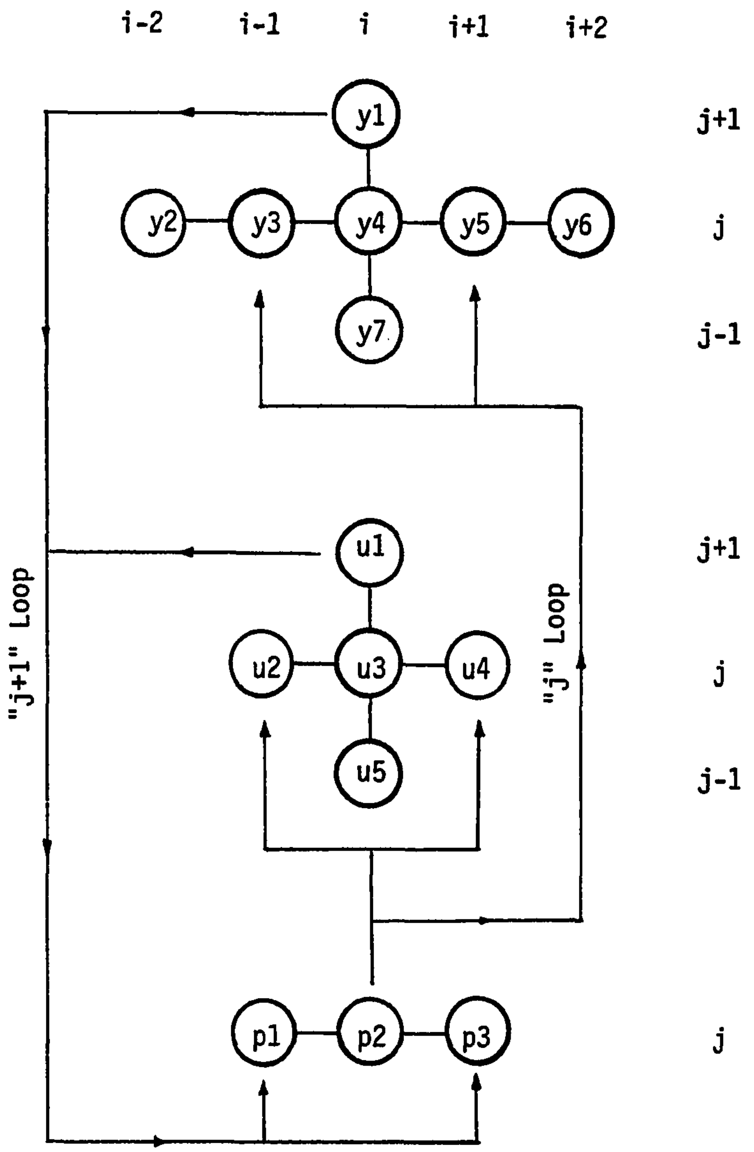

y1 = { $\underline{Y}_{i,j+1}$ }

y2 = { $\underline{Y}_{i-2,j}$ }

y3 = { $\underline{Y}_{i-1,j}, Y_{i-1,j}, P_{i-1,j}$ }

y4 = { $\underline{Y}_{i,j}$, $Y_{i,j}$, $K_{i,j}$ }

y5 = { $\underline{Y}_{i+1,j}$, $Y_{i+1,j}$, $P_{i+1,j}$ }

y6 = { $\underline{Y}_{i+2,j}$ }

y7 = { $Y_{i,j-1}$ }

u1 = { $U_{i,j+1}$ }

u2 = { $P_{i+1,j}$ }

u3 = { $U_{i,j}$ }

u4 = { $P_{i-1,j}$ }

u5 = { Ui,j-1 }

p1 = { $Y_{i-1,j}$, $Y_{i-1,0}$, $U_{i-1,j}$ }

p2 = { $P_{i,j}$ }

p3 = { $Y_{i+1,j}$, $Y_{i+1,j}$, $U_{i+1,j}$ }

Fig.5.15 Computational molecules for difference equations

CHAPTER VI

NUMERICAL SOLUTIONS FOR DYNAMIC RESPONSES OF BURIED PIPELINE IN A SOIL LIQUEFACTION ENVIRONMENT DURING EARTHQUAKES

6.1 Preface

By employing a digital computer and the finite-difference technique, a numerical procedure is developed to determine the dynamic responses of buried pipeline under soil liquefaction environment. The development of this numerical procedure is based mainly on the theoretical derivations and finite difference formulations from CHAPTER V - SEISMIC ANALYSIS FOR BURIED PIPELINE UNDER A SOIL LIQUEFACTION ENVIRONMENT. The finite-difference technique can also be applied to the case of Hoff's analysis(13), in which the Bessel-function method was used to determine the dynamic buckling of elastic columns. In this chapter, a comparative study using the numerical procedure is presented not only to illustrate the satisfactory agreement with the results obtained by Hoff (13), but also to delineate some characteristics of the dynamic behavior of pipeline buried in liquefiable regions during earthquakes.

To examine the effects of soil stiffness, all the soil characteristics discussed in Sect.5.3 are taken into consideration in the computation process.

The displacement applied at the movable end of the proposed pipe model is another important parameter in this procedure. Three typical displacements are employed to investigate their influences on the buckling of the pipe embedded in a liquefiable area. To be realistic, the integrated displacement of the 1940 El Centro Earthquake is also included in this study.

Additional parameters such as the initial crookedness of the pipe, the supported length of the pipe inside the un-liquefied area, etc. will be included in the discussions in the following sections.

6.2 Numerical Analysis

The formulation of the numerical procedure is mainly based on the finite difference method for the investigation of dynamic responses of pipeline buried in a liquefiable zone. As a rule, differential equations describe the behavior of continuous systems such as continuous pipelines, where as algebraic equations describe the behavior of lumped-parameter systems. The replacement of a continuous function in a differential equation with an algebraic expression consisting of the value of that function at several discrete points is equivalent to replacing a continuous system with one consisting of a discrete number of mass points.

In general, if a continuous system without the temporal variable is replaced by "n" discrete points, the unknown function is replaced by "n" simultaneous algebraic equations in terms of spatial variables only. The behavior of the continuous system can be obtained by solving these "n" simultaneous algebraic equations.

On the contrary, if a continuous system is involved in time-varying variables, a step-increment method is required to find the dynamic responses of the continuous system, instead of solving the simultaneous equations. A schematic representation of the step-increment method is shown in Fig.5.15. At the initial moment "j=0", the resulting value of the axial force "P" along the pipe can be obtained by replacing the values of "Y" and "U" which have been determined using the initial and boundary conditions. A detailed description of the initial and boundary conditions has been presented in Sect.5.9. From Eqn.5.29b, the axial displacement "U" at the time step "j=1" is thus acquired by substituting the known initial values of "U" and "P" at the time step of "j=0". A similar manner can be applied to determine "Y" (j=1) using Eqn.5.29a. After determining the values of "Y" and "U" with "j=1", the process is repeated to find "P" (j=1) values. Therefore, the step-iteration is repeated again as shown in Fig.5.15. In this respect, for any particular time step "j+1", the lateral deflection "Y", the axial displacement "U" and the induced axial force "P" at any arbitrary point on the pipe can be obtained by substituting the terms of the already known values at the time step of "j" and "j-1".

It should be noted that because the dynamic excitation (axial displacement) is applied at the movable end "B" of the pipe as shown in Fig.6.2b, the resulting "U^t" value of the movable end "B" at any time step "j" must be adjusted to match the input displacement. The difference between the resulting displacement, "U^t", and input displacement at point "B" is considered as an increment of the applied displacement for next time-increment calculation. The increment of the axial displacement is linearly distributed along the pipe, e.g. the mid point of the pipe is only subjected to a half of such an increment. An expression for such a distribution of displacement is given below.

$$U(X,T) = U^t(X,T) + \frac{X}{L}\left\{U_m(T) - U_m^t(T)\right\} \tag{6.1}$$

Eqn.6.1 can also be written in the other form similar to Eqn.5.29, as follows.

$$U_{i,j} = U^t_{i,j} + \frac{i}{m}(U_{m,j} - U^t_{m,j}) \tag{6.2}$$

where $U^t_{i,j}$ = Response axial displacement at point "i" on the pipe at the time step "j" (Eqn.5.29b).

$U_{m,j}$ = Applied axial displacement at point "B" of the pipe at the time step "j".

Note that when "j=1", "$U^t_{i,1}$" and "$U^t_{m,1}$" are equal to zero, based on the fact that the pipe is stationary before seismic excitation as depicted previously. Fig.6.3 graphically shows the applied axial displacement (increment) linearly distributed along the entire pipe. As shown in Fig.6.3, the initial input displacement, "$U_{m,1}$", applied at point "B" is linearly distributed along the pipe at the time step "j=1". "AD" represents the response curve, "$U^t_{i,2}$", of the pipe, obtained from Eqn.5.29(b). Although, at the time step "j=2", the axial displacement at point "B" increases to "$U_{m,2}$", the actual displacement increment applied at point "B" is "c" not "d". Here "c" is the difference between "$U^t_{m,2}$" and "$U_{m,2}$" and "d" is the difference between "$U_{m,2}$" and "$U_{m,1}$". The displacement increment "c" is also distributed linearly along the pipe. The triangle A'H'D shows such a kind of linear distribution. Therefore, the input value "$U_{i,2}$" of axial displacement at any arbitrary point "i" when "j=2" is the combination of "a" and "b" as shown in Fig.6.3. The procedure is repeated until the "j" value is equal to "n" which denotes the last time-step number of application of displacement increment.

6.3 Process of Computation

The computation is done by using the IBM 3081 at the University of Oklahoma. The computer program listing is given in the appendix D. The flow chart of the program is shown in Fig.6.1. Some steps of calculation are described as follows.

STEP (1) INPUT GIVEN DATA

The properties of structure and soil used in this computation are:

a) Pipe properties:

$D = 42$ in. $E = 30000000$ psi

$t_k = 0.562$ in. $\sigma_y = 72000$ psi

$I_x = 15710$ in.^{4} $A = 73.16$ in.^{2}

$r = 14.65$ in. $c = 200{,}000$ in./sec

b) Soil properties:

$\gamma = 110$ lb/ft.^{3} $N_q = 9.8$

c) Dimensionless parameter:

$l/r = 80, 150, 330, 450, 750, 900, 1050$ etc.

STEP (2) SELECT TYPE OF APPLIED AXIAL DISPLACEMENT

Three typical axial displacements applied at the movable end of the pipe model were used to examine the dynamic behaviors of the buried pipe. They are:

(a) Linear compressive displacement;

(b) Sinusoidal displacement;

(c) Recorded displacements of 1940 El Centro Earthquake.

Case (a) is employed to determine the dynamic buckling of a buried pipeline under a linearly increasing imposed end displacement for several distinct liquefaction conditions. Case (b) is an intermediate condition between a linearly increasing and randomly distributed ground motions for comparison purposes. Case (c) is to investigate the dynamic response of a buried pipe under a soil liquefaction environment during an earthquake. A series of integrated displacements based on the seismic records of 1940 El Centro Earthquake was taken into calculation.

STEP (3) INPUT INITIAL AND BOUNDARY CONDITIONS

The initial conditions are that the pipe has a small crookedness, and is stationary, and that no axial force exists along the pipe before seismic shaking. With regard to boundary conditions, both ends of the pipe model were assumed simply supported in this computation. Both initial and boundary conditions have been described in detail in Sect.5.9.

STEP (4) DEFINE CHARACTERISTIC FUNCTION OF SOIL STIFFNESS

Four different situations of soil stiffness were utilized in this calculation. These four cases are:

1) $Q_c = 1.0$ in un-liquefied zone

$Q_f = 0.0$ in liquefied zone

2) $Q_c = 1.0$

$Q_f = Q_f(t)$ as given in Eqn.5.4, in which constants $a = 2.50$ and $t_0 = 0.2\ T_0$.

3) $Q_c = \exp(-2t/T_0)$

$Q_f = Q_f(t)$ same as case (2)

4) $Q_c = Q_c(x,t)$ as given in Eqns.(5.5b) and (5.5c), in which $\bar{b} = 2.5$ and $t_0 = 0.2\ T_0$.

$Q_f = Q_f(t)$ same as case (2).

STEP (5) FINITE INCREMENT PROCEDURE - USING FINITE DIFFERENCE EQUATIONS

The difference equations including lateral deflection "Y", axial displacement "U" and axial pipe force "P", are expressed by Eqns.5.29a-5.29c in Sect.5.8. In this step, an increment procedure is required to determine numerical values of such functions of "Y", "U" and "P" at each discrete point on the X-axis and the T-axis. Based upon the discussion in Sect.6.2, an adjustment to the resulting values of "U" is needed for each time-increment calculation.

STEP (6) PRINT THE RESULTS

The results consist of three categories:

a) The resulting normalized lateral deflection.

b) The resulting normalized axial forces of the pipe.

c) The resulting normalized axial displacement of the pipe.

6.4 Comparison With Hoff's Analysis

In 1950, N.J. Hoff(13) initiated an analysis to investigate the dynamic buckling of an elastic column by using the Bessel-function method. In his study, as shown in Fig.6.2a, an elastic column with initial crookedness and simply supported at both ends, is longitudinally compressed. To find the dynamic buckling of the elastic column, the movable end "B" is subjected a leftward (compressive) displacement moving with a constant speed. Four governing differential equations derived by Hoff are listed below:

$$\ddot{u} = (E/\rho)\, u'' \tag{6.3}$$

$$EIy'''' + (Ny')' + \rho A\ddot{y} = 0 \tag{6.4}$$

$$N = -EA\, u' \tag{6.5}$$

$$\varepsilon_0 = vt/l \tag{6.6}$$

where u = axial displacement of the column

y = lateral deflection of the column

N = axial compressive force

ρ = mass density

ε_0 = compressive strain

v = moving speed at point "B"

A numerical example with following input data was performed by Hoff.

$$\Omega = \pi^8 (v/c)^2 (r/l)^6 = 2.25$$

$l/r = 370$ $\qquad\qquad$ $a_0 = (y_0)_{mid}/r = 0.25$

$v = 0.256$ in./sec $\qquad$ $c = 200{,}000$ in./sec

where "Ω" is the buckling index, and "c" is the wave propagation speed. The results of the numerical example are shown in Fig.6.3(a) and (b). From Fig.6.3(b) the dynamic buckling load is designated as "$1.725N_E$", the first peak value of the resulting curve. Here "N_E" is the Euler buckling load of the column.

The proposed method mentioned in CHAPTER V can also apply to Hoff's example. According to the Hoff's notion, two perfectly elastic columns are dynamically similar if the non-dimensional buckling index "Ω" defined previously is the same for both. In this regard, for comparison with Hoff's analysis, a numerical example using the finite difference method can be fulfilled by merely keeping the same buckling index (Ω=2.25). The other arbitrary data used in the numerical example are chosen as follows.

$l/r = 80$ $\qquad\qquad$ $a_0 = 0.25$

$A = 73.16$ in.^{2} $\qquad$ $v/c = 1.26835\times10^{-4}$

It should be noted that for Hoff's case, the effect of soil stiffness "K" must be excluded from Eqn.5.27a, i.e. K=0. The results of the finite difference analysis are shown in

Fig.6.5.

Fig.6.5a shows that due to the inertia effects, the dynamic lateral deflections "Y" oscillate within a certain amplitude. Such a phenomenon also occurs in Hoff's case. Furthermore, it is observed that the resulting "Y" values are consistent with those of Hoff. With regard to the induced axial force, a similar pattern is also found in Fig.6.5b, in which the dynamic buckling load is determined as "1.725 N_E". It would be easier to determine the dynamic buckling load of the pipe from Fig.6.5c, showing the relationship between the axial load ratio "N/N_E" and the lateral deflection "Y". In addition, as shown in Fig.6.5d, the axial displacement "U" is not significantly affected by the axial inertia of the pipe.

6.5 Pipe Responses to Longitudinal Compressive Displacement

To investigate the dynamic response of buried pipelines in a soil liquefaction environment, a numerical procedure has been presented in Sect.6.3. This section is to examine the parametric effects to the dynamic performances of pipeline embedded in the liquefiable zone. The important parameters affecting the pipe behavior are: a) soil resistant characteristics (stiffness), b) imposed ground displacement function, c) initial crookedness, and d) supporting length of the pipe inside the un-liquefied region. The effects of these influential factors will be discussed separately as follows.

6.5.1 Effect of Soil Stiffness

As mentioned in Sect.5.3, under a series of cyclic excitations, the soil behavior in the liquefiable region can be described by using a decaying property of the soil stiffness. A typical representation of a buried pipeline subject to an axial compressive displacement along the pipe under soil liquefaction environment is shown in Fig.6.2b. Four different situations of soil stiffness to be investigated are given in Table 6.1. The additional conditions are listed below.

$$L = 1/r = 450$$

$$v/c = 0.9572\times10^{-4}$$

$$a_0 = (y_0)_{mid}/r = 0.25$$

$$y_0/r = -a_0 \sin\left(\frac{X}{L/3}\pi\right) \qquad (6.7)$$

where "y_0" is the initial pipe crookedness which only varies with "x", and "X" is the non-dimensional form of the horizontal coordinate. Note that the input displacement function which is assumed to be linearly along the pipe is gradually applied at the movable end "B" of the pipe in a constant speed "v".

The dynamic responses of the pipe under four different conditions of soil stiffness are shown in Fig.6.6(a) and (b). It is obvious from Fig.6.6(b) that the lowest peak value of the axial load ratios appears in the first case. In addition, Several comparisons of cases (1)-(2), (2)-(3) and (2)-(4) are made to examine the influences of the variation of soil stiffness.

First, compare case (1) and (2). As shown in Fig.6.2(b), case (1) describes that a soil condition in the un-liquefied zone "AC" (or "DB") is unchanged at all time while the soil of the liquefiable zone "CD" is immediately liquefied at the beginning of earthquakes. In case (2), the soil condition in zone "AC" (or "DB") is same as case(1), but the soil of zone "CD" is losing its shear strength and completely liquefied after a very short period "t_0" as an earthquake occurs (Eqn.5.4). It can clearly be seen from Fig.6.6(b) that the first peak value of axial force increases from "3.38 N_E" of case(1) to "3.90 N_E" of case(2). The increase rate is nearly "15.4%". Here the "N_E" is the Euler buckling load of a simply supported column with "l/r=150" without elastic foundation as shown in Fig.6.2a.

Next is to examine the difference between case(2) and (3). In case(3), the soil condition in zone "CD" is the same as case(2), but the soil in zone "AC" (or "DB") is assumed partially losing its shear strength during the earthquake (as described by Eqn.5.5a). It is also found from Fig.6.6b that the first peak value of "N/N_E" decreases in a small amount.

The third comparison is made between case(2) and (4). In case(4), the soil condition in zone "CD" remains the same as case(2); the shear strength of soil in zone "AC" (or "DB") is affected by both temporal and spatial factors (as described by Eqns.5.5b and 5.5c in Sect.5.3), the effect of soil liquefaction attenuates with distance from the liquefied zone "CD". The results from the calculation show that the axial pipe decreases from "3.90 N_E" of case(2) to "3.66 N_E" of case(4). Table 6.1 lists the first peak values of the pipe associated with various soil conditions.

Another investigation for examining the effect of soil stiffness to the pipe buried in a liquefiable region has been carried out. The value of "Q_C" is kept unity all the time, while the values of "Q_f" varies from 0.0 to 0.12 for each calculation. Both "Q_c" and "Q_f" are independent of the time variable. As shown in Fig.6.7(a) and (b), the most critical situation in this investigation occurs at the case of "Q_f=0.0", where the lowest buckling load and the largest lateral deflection of the pipe occur. The first buckling load increases, but with decreasing rate as "Q_f" increases, as shown in Fig.6.7(b). The resulting numerical data of this investigation are listed in Table 6.2.

Based upon the above investigations, a conclusion can be made that the existence of soil foundation has a significant effect to the induced axial force of a pipe under an adverse seismic environment as shown in Fig.6.2b.

6.5.2 Effect of Imposed Axial Displacement (Strain or Loading Rate)

For evaluating the dynamic effect of longitudinal displacement (or strain rate) applied at one end of the pipe, an investigation is carried out. As shown in Fig.6.2b, the pipe buried in a liquefiable zone is gradually compressed by applying an axial displacement at the movable end of the pipe. The slenderness ratio of the pipe is 450. Six different moving (loading) speeds applied at the movable end of the pipe are chosen to evaluate their influences on the lateral deflection and axial load of the pipe.

The results of displacement and load response histories are shown in Fig.6.8. From Fig.6.8(a) and (b), it can be seen that the first peak value of lateral deflection at the mid-point of the pipe is nearly proportional to the moving speed of the movable end of the pipe. Similarly to the axial pipe load, as shown in Fig.6.8(c) and (d), the dynamic buckling load of the pipe increases with an increase in the moving speed as mentioned. Table 6.3 shows the applied loading speeds and the response data obtained from the calculations of the computer program which is given in the appendix D.

The dimensionless dynamic buckling load vs. dimensionless loading speed is plotted in Fig.6.9. One can see from this figure that when "v" is very small, as determined by interpolation method, the axial force of the pipe may closely approach the value of "$1.2N_E$" as shown in Fig.6.9. The 20% increase in the "static" buckling load of the pipe model can be considered as a contribution from the soil confinement at both side portions of the proposed pipe model. The new axial load ratios which is defined maximum dynamic buckling load to "static" buckling load of the same pipe are displayed and also enclosed in the quotation marks in Table 6.3.

6.5.3 Effect of Initial Crookedness of the Pipe

To study the effect of initial crookedness of the pipe model requires only changing the value of "a_0" in Eqn.6.6 during every calculation. The rest of the influential parameters such as soil stiffness, axial loading speed and supporting length of the pipe at un-liquefied zones etc. are kept constant for each calculation. The results of this parametric study is given in Fig.6.10.

It is observed from Fig.6.10(b) that the maximum dynamic buckling load decreases as the "a_0" value increases. All of the first peak values of pipe load (i.e. designated as maximum dynamic buckling load) are far beyond the Euler load of a pipe ($l/r=150$) which is simply supported without soil foundation. For the case of "$a_0=0.25$" as shown in Fig.6.10(b), the induced maximum axial load is "$3.71N_E$". With regard to the responses of lateral deflection of the pipe, it is apparent from Fig.6.10(a) that the maximum lateral deflection (first peak value) decreases as "a_0" increases. The results of such computations for various "a_0" values are shown in Table 6.4. Furthermore, a phenomenon of oscillation in both responses of the axial pipe load and the lateral deflection is also observed.

An investigation is also carried out to determine the initial pipe crookedness effect on the performance of a simply supported pipe without soil foundation as shown in Fig.6.2a. The pipe performance due to such effects can clearly be seen in Fig.6.11, indicating that small "a_0" values produce large values of "N/N_E" and "Y" during excitation. From the results of both investigations, the existence of an elastic foundation does not affect the oscillation patterns on both responses of lateral deflection and axial pipe force.

6.5.4 Effect of Supporting Length of the Pipe

In reality, a pipeline buried in a liquefiable region may be extended very long into both sides of the unliquefied zone. The pipe model proposed in Sect.5.5 is to simulate the real situation as mentioned above. For the purpose of further analyzing buried pipelines subjected to soil liquefaction, it is essentially important to select an adequate supporting length "l_c" for the pipe model as shown in Fig.6.2b. Six different pipe lengths are chosen to investigate their influences on the pipe performance under soil liquefaction environment.

It should be noted that based on the assumption of no friction between soil and pipe skin, the strain rate of pipe due to the application of an end displacement is equal to the amount of the end moving speed divided by the entire pipe length. For comparison, the strain rate of the pipe must be kept the same for each case. The related values of "l/r" and "v/c" are listed in Table 6.6.

In addition, it is also required to adjust the value of "a_0" in un-liquefied areas to better describe the sinusoidal shape of the initial pipe crookedness. A simple equation for such a adjustment is given below.

$$c_h = \frac{1}{2}\left(\frac{l/r - l_f/r}{l_f/r}\right) \tag{6.8}$$

where "l_f" is the pipe length submerged in a liquefied zone, which is set equal to "150r" in this investigation. After such an adjustment, Eqn.6.7 can be written in the following manners.

$$y_0/r = -(c_h a_0)\sin\left(\frac{X}{L/3}\pi\right) \tag{6.9}$$

For instance, in the case of "l/r=600" with "l_f/r=150", the value of "c_h" is determined as "1.5". A description detailing the variation of "c_h" along the entire pipe length is presented in Table 6.5.

Fig.6.12(a) and (b) show the pipe response to lateral deflection and axial load under the case of six different supporting lengths "l_c" of the pipe. It is found from Fig.6.12(b) that the resulting value of axial load increases slightly with an increase in the supporting length "l_c" of the pipe. The results obtained from the calculation involving the variation of the supporting length "l_c", are also presented in Table 6.6. Fig.6.13 shows the relationship between maximum axial load "N/N_E" and the slenderness ratio of the pipe model. It can be observed that the curve of axial load ratio - slenderness ratio becomes flatter as "l/r" exceeds 600, i.e. "$l_c/r=225$" and "$l_f/r=150$". It is obvious that the ratio of "l_c/r" to "l_f/r" is determined as "1.5". In this respect, it would be reasonable to do further analysis using this proposed model and taking "l_c" as 1.5 times "l_f". A simple example adequately determining the entire pipe length of the proposed model is given below.

<EXAMPLE>

Given $l_f/r = 160$

Thus $l_c/r = 1.5\ (l_f/r) = 240$

$L = l/r = 240\text{x}2 + 160 = 640$

6.6 Pipe Responses to Axially Sinusoidal Displacement

Basically, the dynamic behavior of a buried pipe subjected to an axially sinusoidal displacement are quite similar to the pipe responses described in Sect.6.5. The important parameters affecting the pipe performances still include (a) soil stiffness, (b) loading speed of pipe end, (c) initial pipe crookedness and (d) supporting length of "l_c".

For example, a typical pipe model with "$l/r=600$" and "$a_0=0.25$", is axially displaced by applying a sinusoidal displacement at point "B" as shown in Fig.6.2b. Such a sinusoidal diplacement can be expressed as follow.

$$U_m(T) = d_a \sin(2\pi T/T_0) \tag{6.10}$$

where "d_a" is the amplitude of sinusoidal displacement applied at the pipe end "B", and "T_0" is the period of the earthquake.

The applied axial displacement of any arbitrary point along the pipe model can be determined by using Eqn.6.1 or 6.2 as mentioned in Sect.6.2. For comparison, four different amplitudes of the sinusoidal displacement are employed for each calculation. It should be noted that within a given time period the large amplitude of a sinusoidal displacement will axially cause fast movement at the pipe end "B". As expected, the fast movement at point "B" of the pipe induces large value of "N/N_E", i.e. the larger the value of "d_a", the higher the maximum dynamic buckling load. point "B". Such phenomena can be easily found from Fig.6.14b which shows the response of axial force of the pipe subjected to various "d_a" effects. The notation "d_a" used in Fig.6.14(a) and (b) is a nondimensional amplitude of the sinusoidal displacement.

As shown in Fig.6.14a, the first peak values of lateral deflection are roughly proportional to the amount of "d_a".

Based on the results of Sect.6.5.2 and this Section, the fact that the fast axial movement at the movable end of the pipe induces large maximum dynamic buckling load of the pipe can be confirmed.

6.7 Pipe Response to 1940 El Centro Earthquake

Any realistic study of earthquake effects must be based on the ground motions during a destructive earthquake. Generally, actual measurements contain the records of ground acceleration which are called accelerograms. The ground velocity and displacement can be obtained by integrating the accelerogram once and twice respectively.

The number of destructive earthquakes for which measurements are available unfortunately is very small. The records of ground accelerations obtained from the 1940 El Centro Earthquake is used for the study. In this case, only the integrated displacements of the earthquake are of concern.

The investigation is to study the dynamic responses of a typical buried pipeline subjected to the 1940 El Centro Earthquake. The normalized pipe length and initial pipe crookedness are 600 and 0.25 respectively. The integrated displacements of the El Centro Earthquake are gradually applied at the movable end "B" of the pipe. The soil conditions of "Q_c" and "Q_f" are set 1.0 and 0.0 respectively.

Fig.6.15a shows the responses of lateral deflection oscillating approximately between "-1.3" and "2.7". Note that the unit used in the time-axis is equivalent to 0.05 seconds. The total duration time of the earthquake is 53.6 seconds.

Fig.6.15b shows the responses of axial load at the mid point of the pipe. The maximum compressive force along the pipe is "1.468 N_E", while the maximum tensile force of the pipe is "2.027 N_E". It is interesting to point out that the resulting curve of axial load ratio almost traces the curve of integrated displacements of the El Centro Earthquake, which is given in the Appendix B. A complete set of numerical data on such integrated displacements are also listed in the Appendix A. Furthermore, upon reviewing the case of that of a pipe subject to a sinusoidal displacement, it can be seen that the response curves of an axial load ratio, such as in Fig.6.14b, show a rough sinusoidal shape. Based upon both observations on Fig.6.14b and 6.15b, it can be concluded that the end displacement of the pipe significantly affects the induced axial force along the pipe in spite of the existence of axial inertia effects.

6.8 Summary

Under the adverse environment of soil liquefaction, the dynamic responses of the typical pipe model are significantly affected by such factors as (a) soil stiffness, (b) loading speed of pipe end, (c) initial pipe crookedness and (d) supporting length of the pipe segment inside the unliquefied regions. Their influences to pipe response are summarized as follows.

(1) The existence of a soil foundation along the pipe significantly increases the axial resistant capacity of the pipe.

(2) The smaller the initial pipe crookedness, the larger the axial pipe strength.

(3) The induced axial force along the pipe increases with an increase in the loading speed of pipe end.

(4) The induced axial force of the pipe increases slightly as the supporting segment of the pipe exceeds 1.5 times the central pipe segment submerged in the liquefied areas.

In addition, the proposed model using the finite difference method can also apply to the case of Hoff's study.

TABLES IN CHAPTER VI

Table 6.1 The dynamic behaviors of the pipe under four different liquefiable regions

Case	Soil Stiffness Q_c	Soil Stiffness Q_f	Responses at Buckling $(N/N_E)_{max}$	Responses at Buckling Y_F	Y_{max}
1	1.0	0.0	3.38	3.00	10.34
2	1.0	Eqn.5.4	3.90	2.79	11.07
3	Eqn.5.5a	Eqn.5.4	3.86	2.84	12.10
4	Eqn.5.5b Eqn.5.5c	Eqn.5.4	3.66	2.43	14.76

Note:

Q_c : Characteristic function of soil stiffness for un-liquefied zone.

Q_f : Characteristic function of soil stiffness for liquefied zone.

N : Axial load induced at mid-point of the pipeline. (1/r=450)

N_E : Euler load of the simply supported pipe without elastic Foundation. (Hoff's case, 1/r=150)

Y_F : Lateral deflection corresponding to dynamic buckling load.

Here the subscript "max" indicates the first peak value of the dyanmic responses.

Table 6.2 Dynamic responses of buried pipe under the effect of different values of Q_f while Q_c=1.0

Case	Q_f	$(N/N_E)_{max}$	Y_F	Y_{max}
1	0.0	2.94	2.60	9.05
2	0.04	5.05	2.50	6.60
3	0.08	6.58	2.37	5.28
4	0.12	7.53	1.87	4.28

* Additional conditions:

$L = l/r = 450$

$a_0 = (y_0)_{mid}/r = 0.25$ $v/c = 0.75x10^{-4}$

Table 6.3 Pipe responses to various moving speeds applied at the movable end of the pipe

Case	v/c	$(N/N_E)_{max}$	Y_F	Y_{max}
1	.000105	3.56 (2.97)	3.17	10.83
2	.000095	3.36 (2.80)	2.63	10.31
3	.000085	3.13 (2.61)	2.31	9.71
4	.000075	2.93 (2.44)	2.92	9.19
5	.000050	2.35 (1.96)	2.48	7.44
6	.000025	1.78 (1.48)	2.25	5.20

The value inside the quotation mark indicates $N_{max}/(1.2N_E)$.

* Additional conditions:

$L = l/r = 450$ $a_0 = 0.25$

$Q_c = 1.0$ $Q_f = 0.0$

Table 6.4 Pipe responses to various initial crookedness (a_0) of the pipe.

Case	a_0	$(N/N_E)_{max}$	Y_F	Y_{max}
1	0.25	3.71	2.70	10.83
2	0.50	3.11	2.40	9.91
3	0.75	2.75	2.76	9.35
4	1.00	2.48	3.00	9.02

Additional conditions:

$L = l/r = 450$ $v/c = 0.00009572$

$Q_c = 1.0$ $Q_f = Q_f(t)$ Eqn.5.4

t_0 = time required to cause liquefaction = $0.2\ T_0$

T_0 = duration time of earthquake

Table 6.5 Examples for describing the variation of "c_h" along the pipe while "$l_f/r=150$".

Example	l/r	l_c/r	$(c_h)_{AC}$	$(c_h)_{CD}$	$(c_h)_{DB}$
1	330	90	0.6	1.0	0.6
2	450	150	1.0	1.0	1.0
3	600	225	1.5	1.0	1.5

* Refer to Fig.6.2b.

Table 6.6 Pipe responses to various supporting lengths of the pipe at both sides of un-liquefied zones.

Case	l_c/r (l/r)	v/c	$(N/N_E)_{max}$	Y_F	Y_{max}
1	90 (330)	.000055	2.80	2.21	7.72
2	150 (450)	.000075	2.93	2.78	9.20
3	225 (600)	.000100	3.08	2.81	10.69
4	300 (750)	.000125	3.13	3.81	14.40
5	375 (900)	.000150	3.19	3.84	14.56
6	450 (1050)	.000175	3.23	3.87	17.49

Case (1) - (3) : dX=15; dT=20
Case (4) - (6) : dX=25; dT=25

* Additional conditions:

$a_0 = 0.25$ $(l/r):(v/c) = 6,000,000.$

$Q_c = 1.0$ $Q_f = 0.0$

$l_f/r = 150$

FLOW CHART FOR SOIL LIQUEFACTION

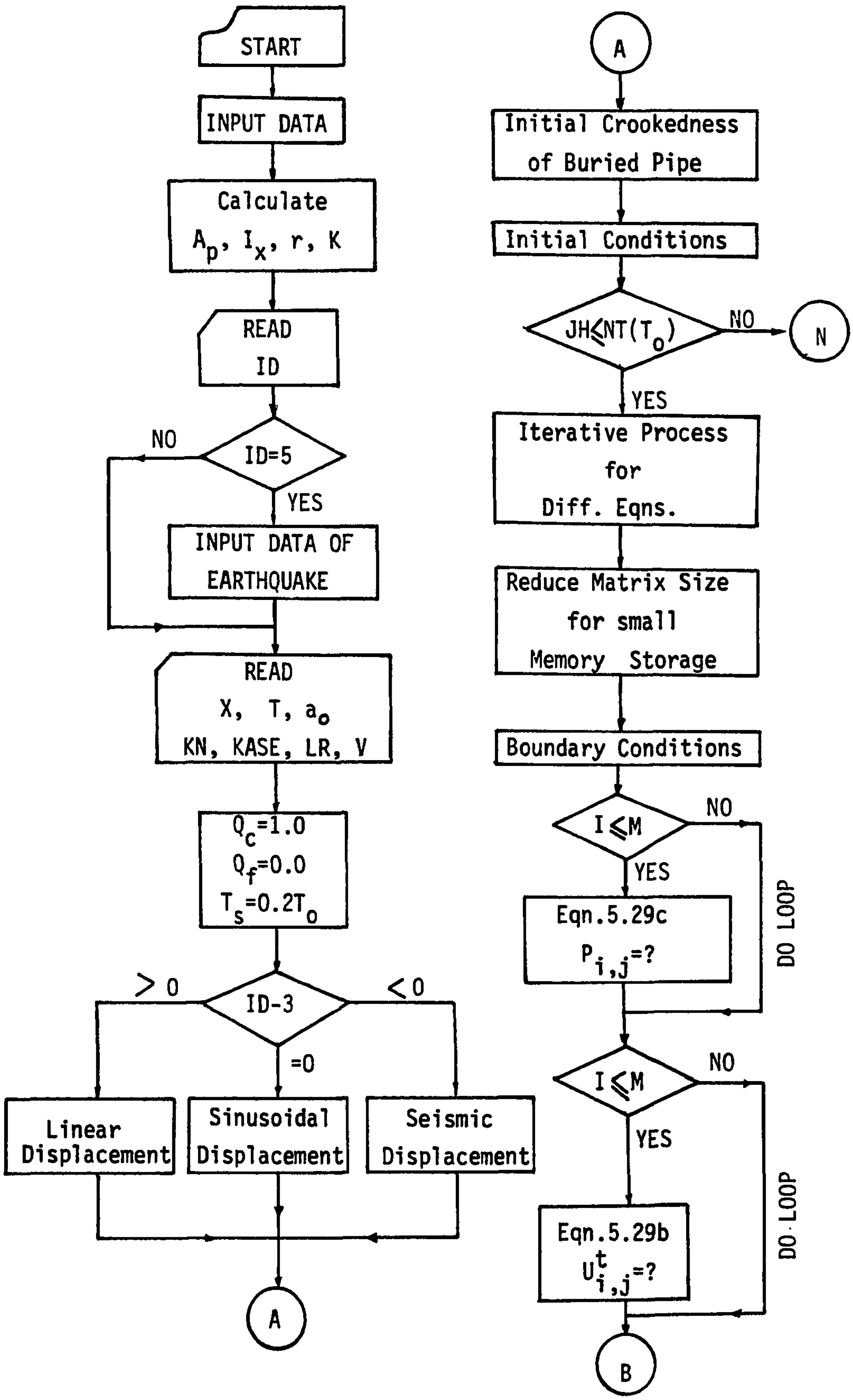

Fig.6.1

FLOW CHART FOR SOIL LIQUEFACTION (con't.)

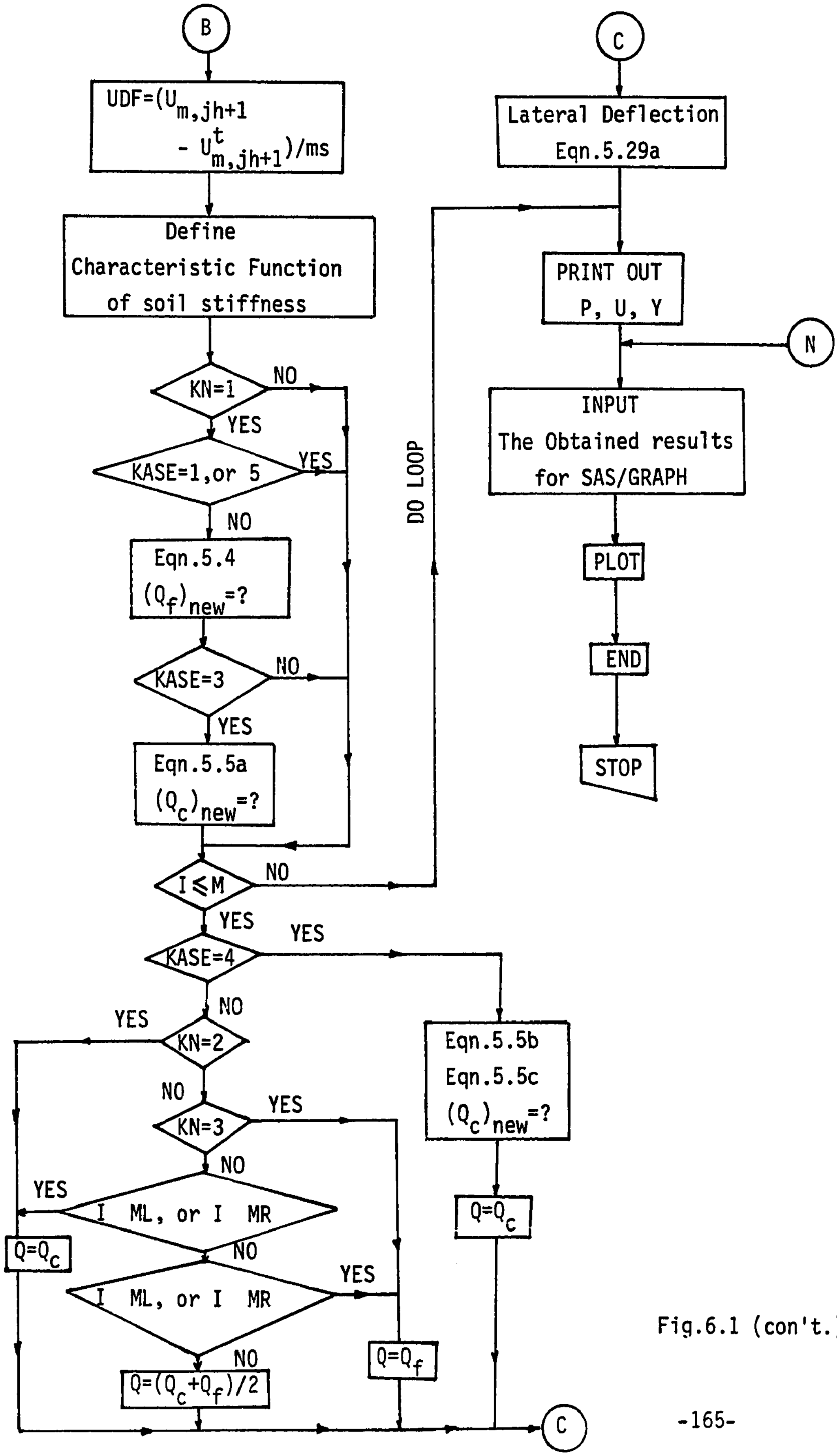

Fig.6.1 (con't.)

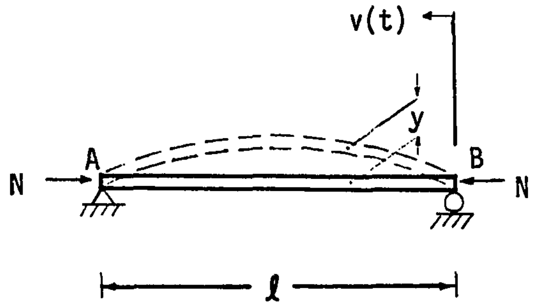

Fig.6.2a A pipe in a simple loading condition. (Hoff's case)

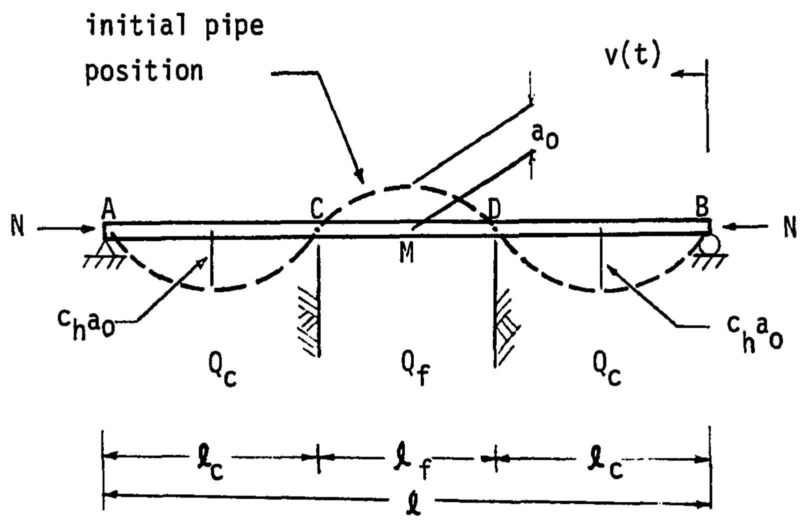

Fig.6.2b Proposed model of buried pipe with initial crookedness.

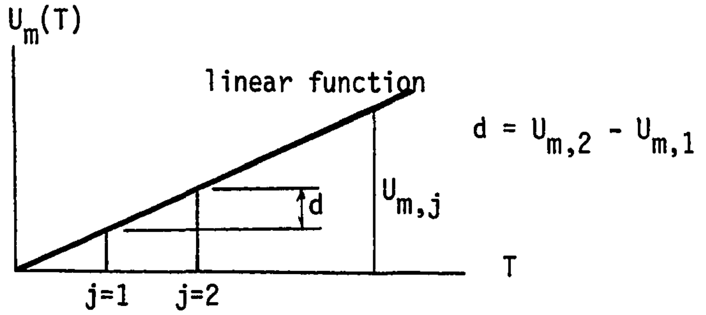

(a) Applied axial displacement at point B.

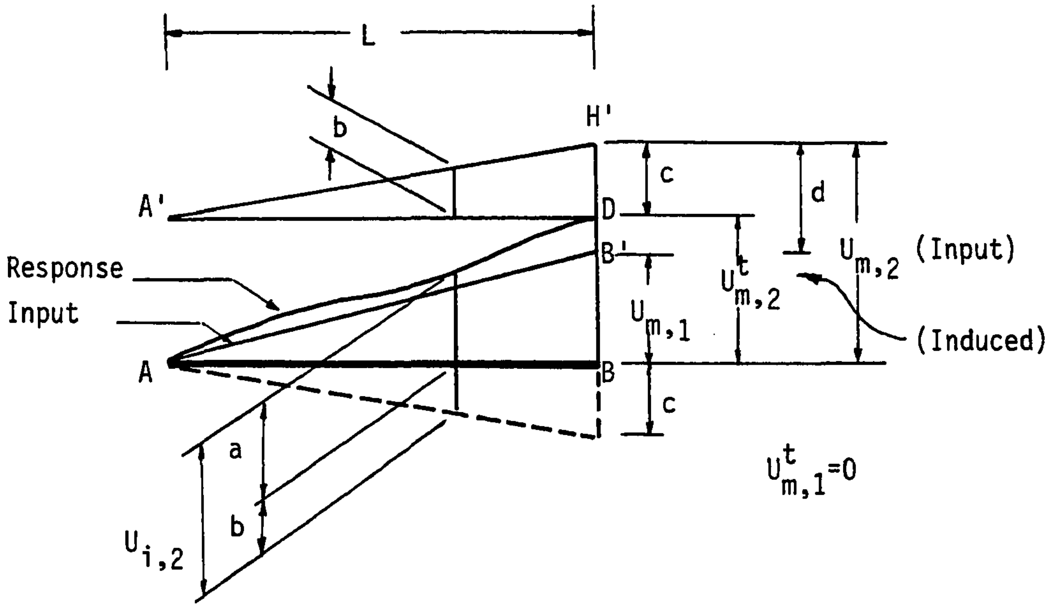

$$U_{i,j} = \overbrace{U^t_{i,j}}^{a} + \overbrace{\frac{i}{m}\left(\underbrace{U_{m,j} - U^t_{m,j}}_{c}\right)}^{b} \qquad j=2 \qquad (6.2)$$

$i = 1, 2, \ldots\ldots\ldots, m$ = Sequential number of "X".
$j = 1, 2, \ldots\ldots\ldots, n$ = Sequential number of "T".

(b) Increment distribution of applied axial displacement at point B for both cases in Fig.6.2 at the time step "j=2".

Fig.6.3

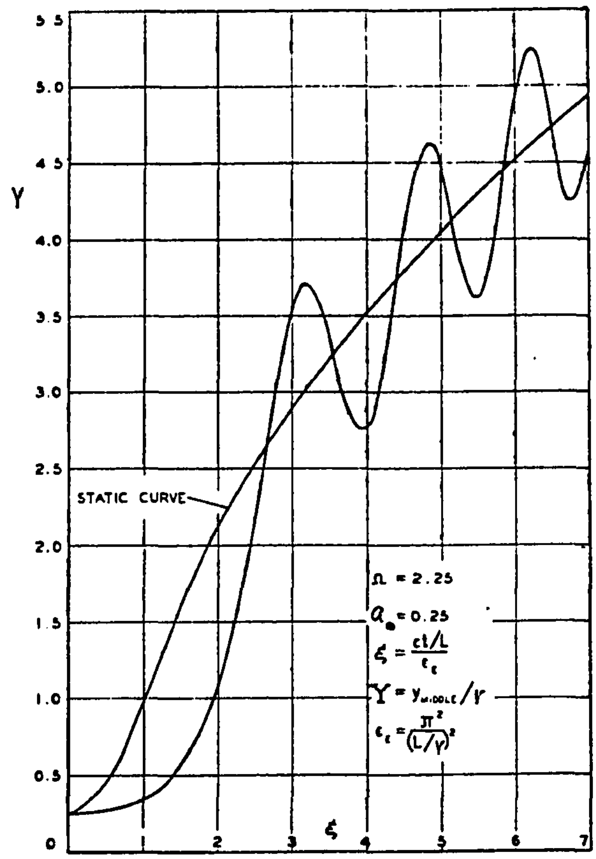

(a) Deflections of mid-point of beam

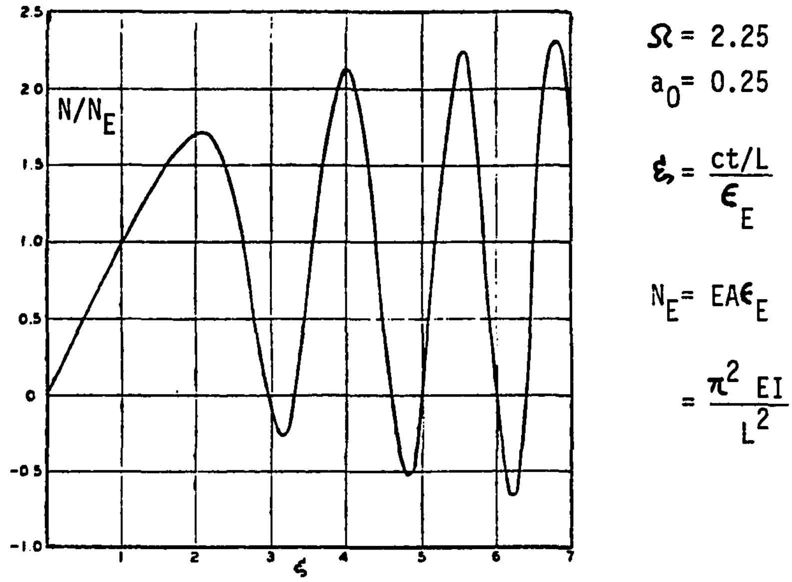

(b) Variation of axial compressive force

Fig.6.4 Dynamic responses of simple supported beam without elastic foundation. (After N.J. Hoff, 1950)

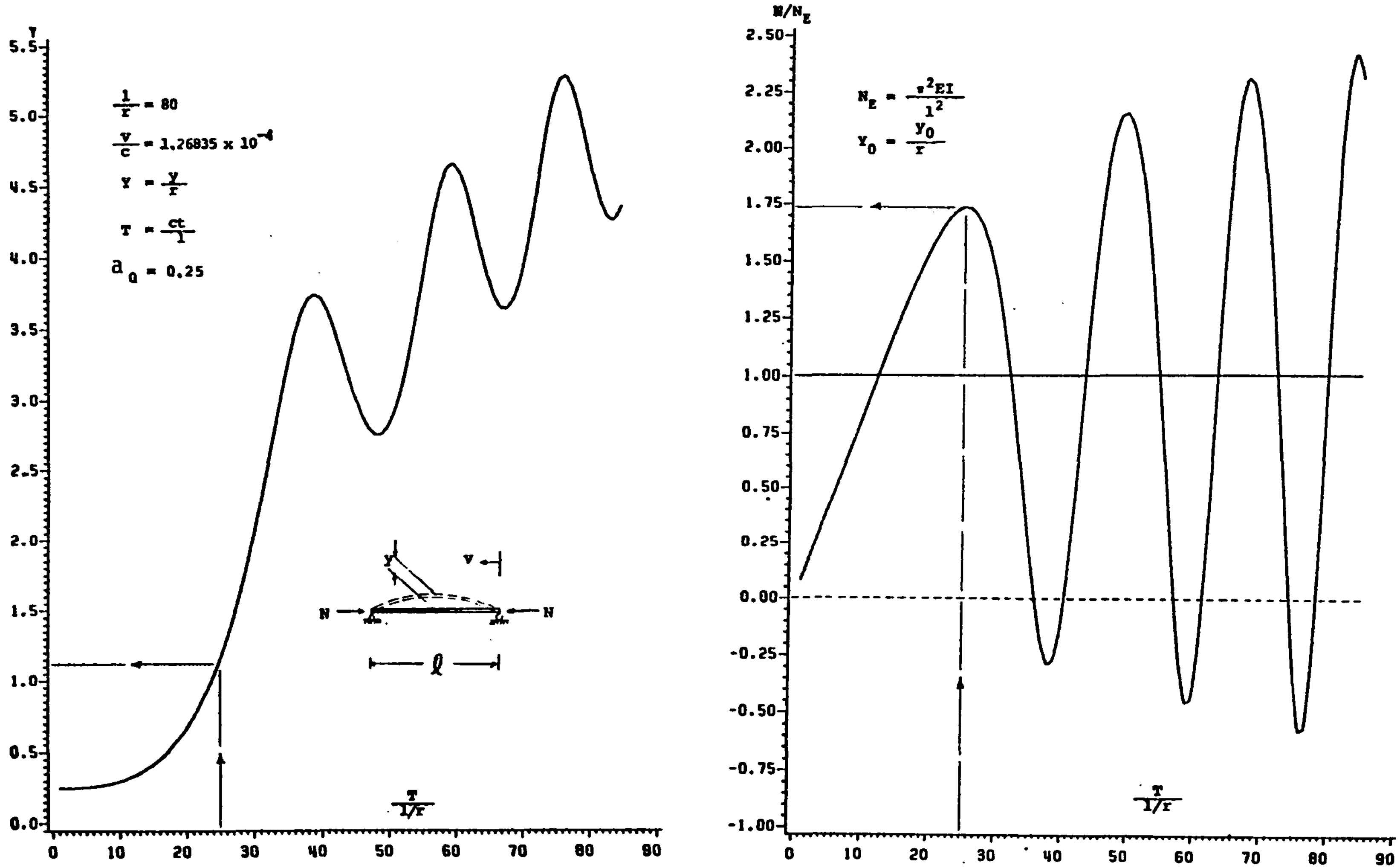

(a) Lateral deflections of mid point of the beam (pipe).

(b) Variation of axial compressive force.

Fig.6.5 Dynamic response of simply supported beam without soil foundation (Finite difference method).

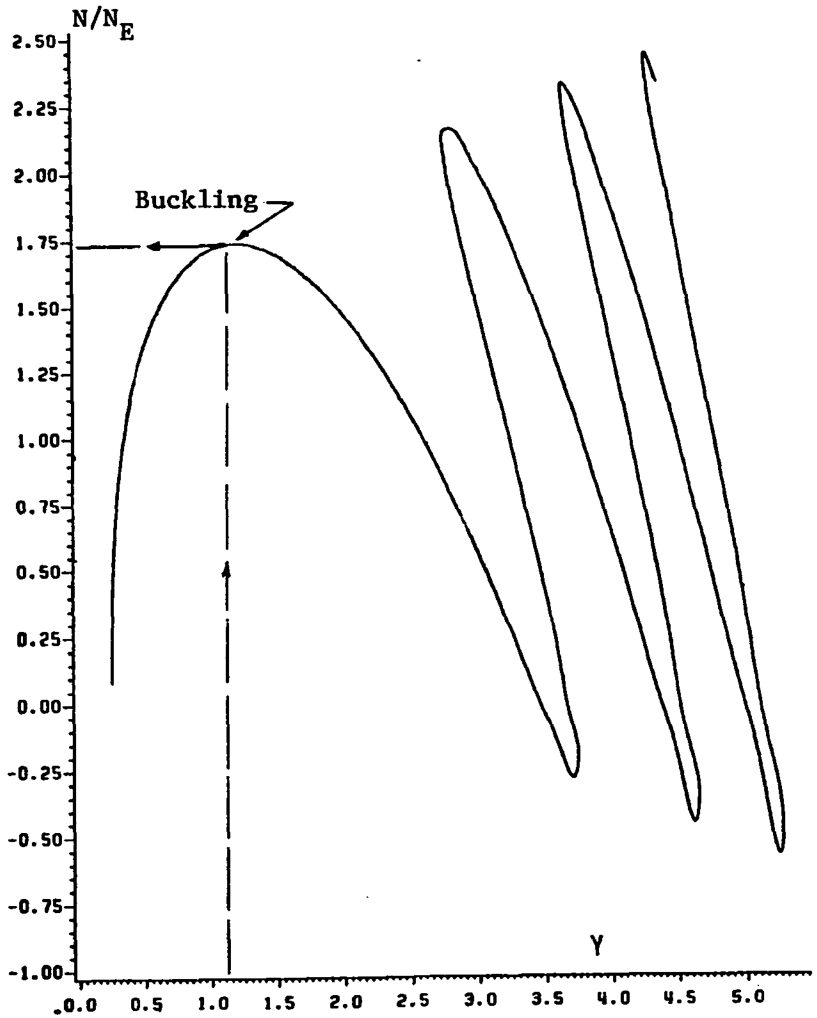

(c) Nondimensional load-deflection curve

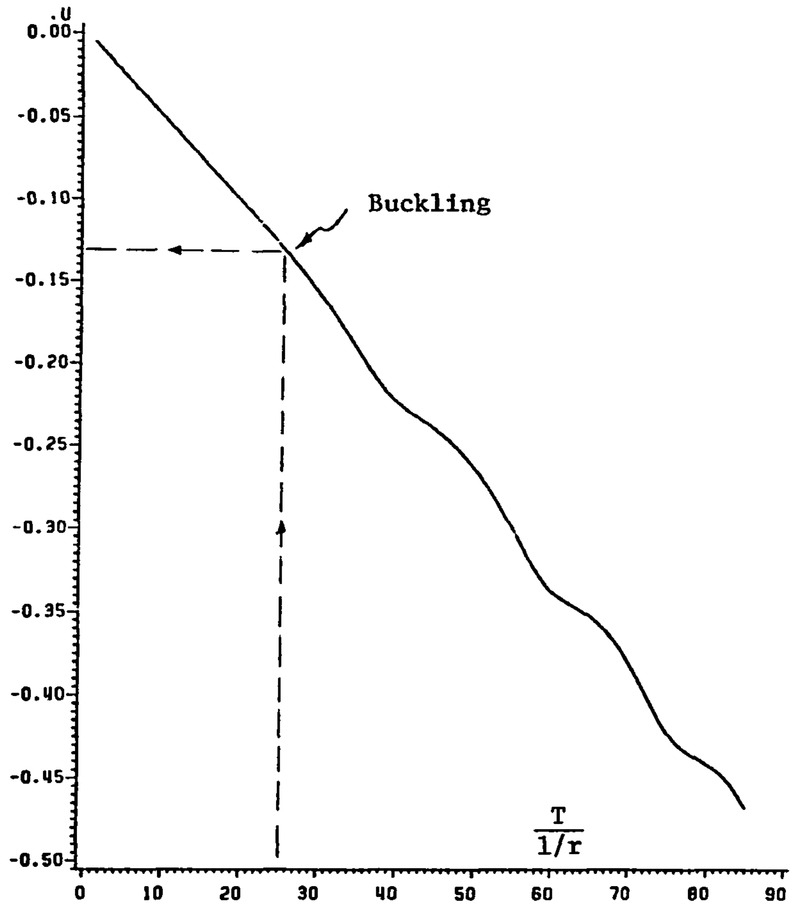

(d) Axial displacement at mid point of the beam (pipe).

Fig.6.5 (Con't)

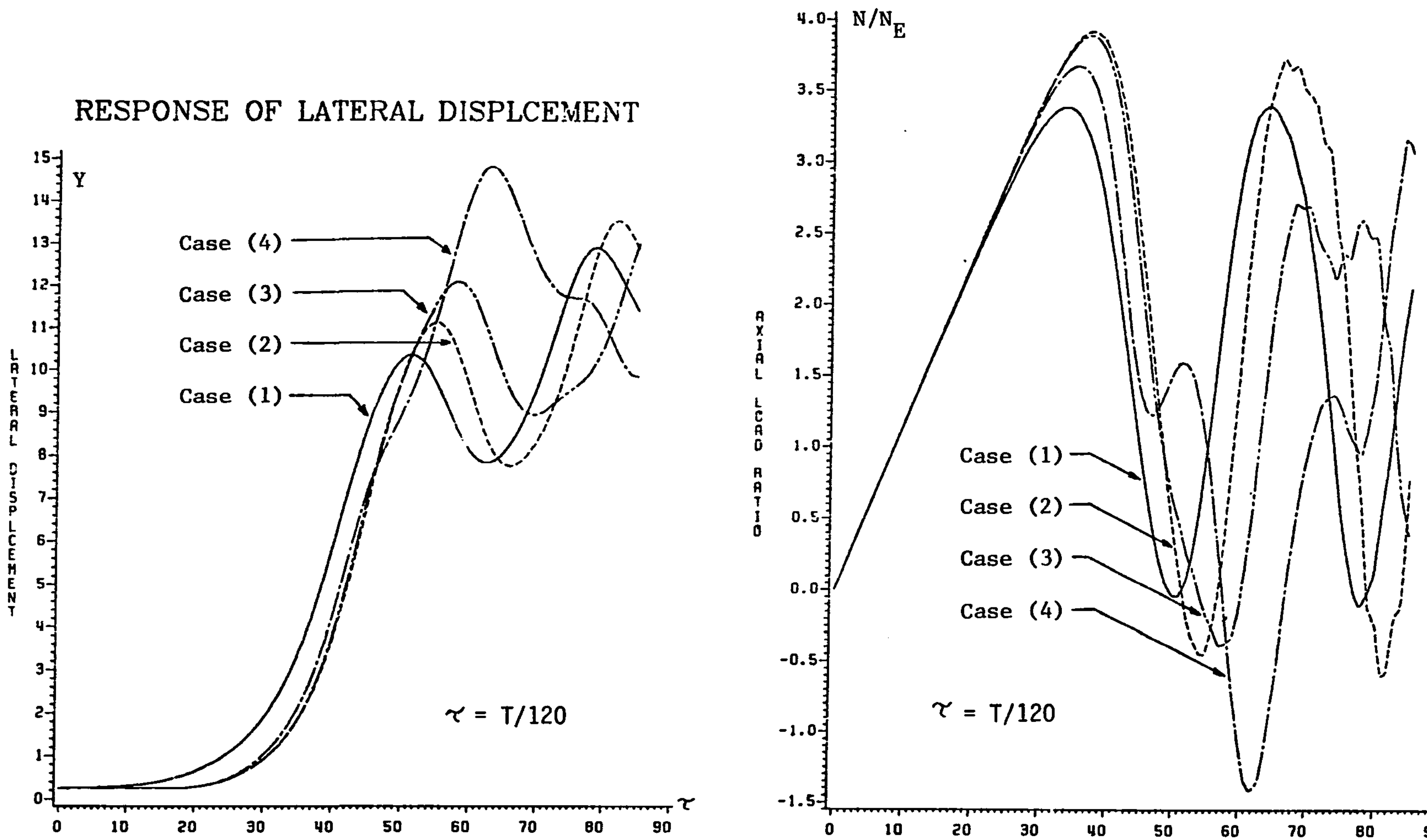

(a) Deflections of mod-point of pipe model.

(b) Variation of axial compressive force.

Fig.6.6 Dynamic responses of pipe model under the effect of different soil liquefaction environments.

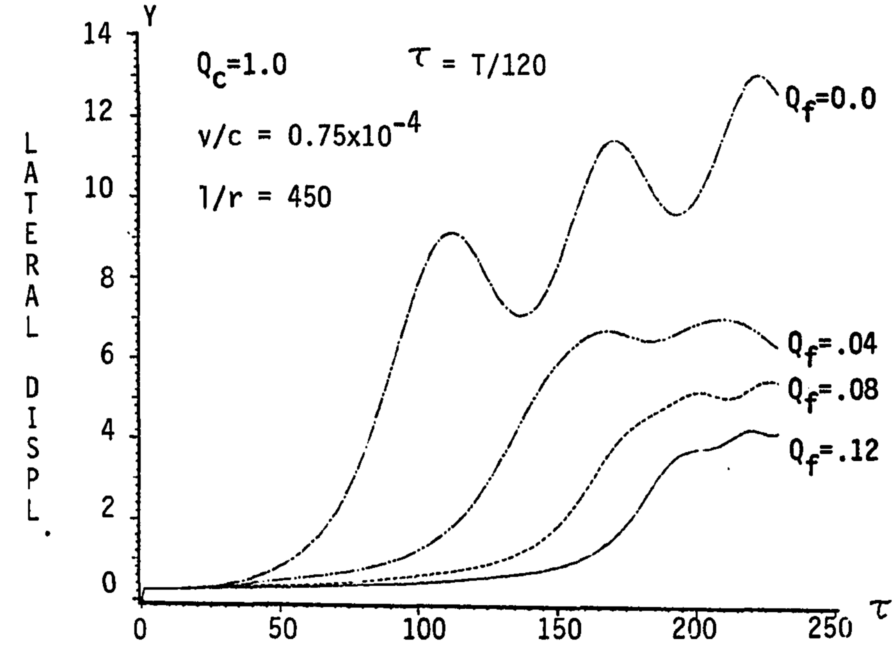

Fig.6.7a Response of lateral displacement under the effect of different soil stiffness at liquefiable zone during earthquake.

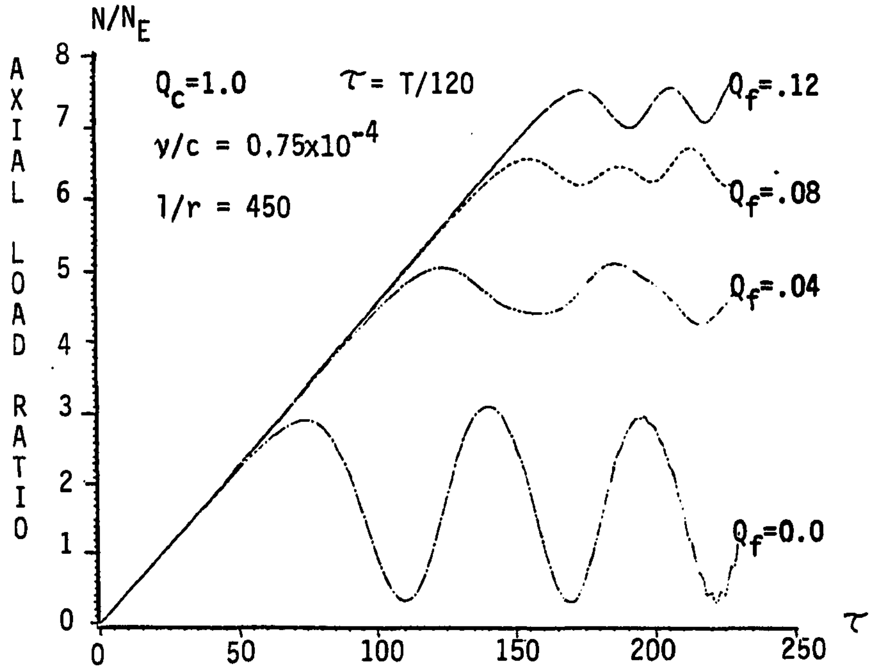

Fig.6.7b Response of axial load under the effect of different soil stiffness at liquefiable zone during earthquake.

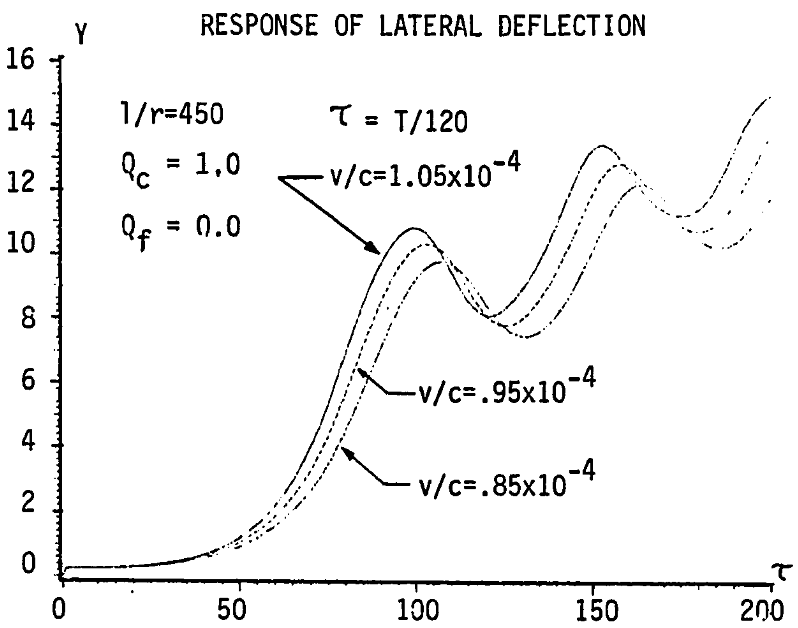

(a)

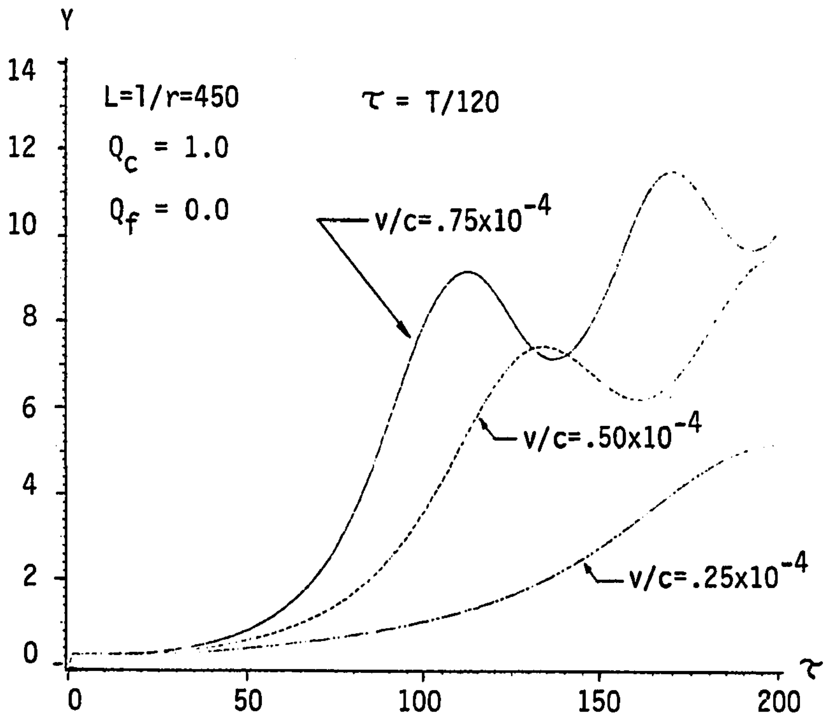

(b)

Fig.6.8 (a) & (b) Pipe response of lateral deflection under the effect of various moving speed applied at the movable end of the pipe.

DYNAMIC RESPONSE-AXIAL LOAD

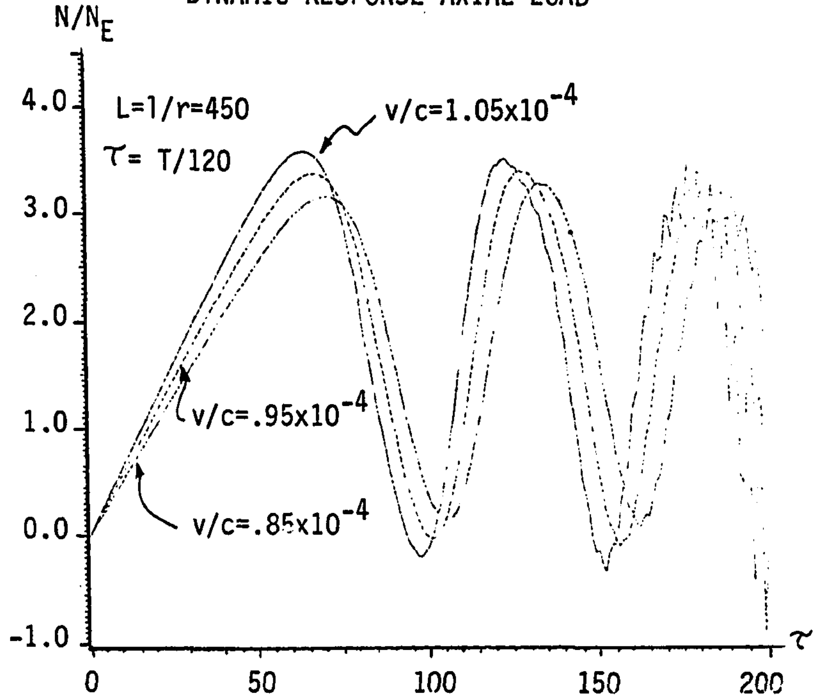

(c)

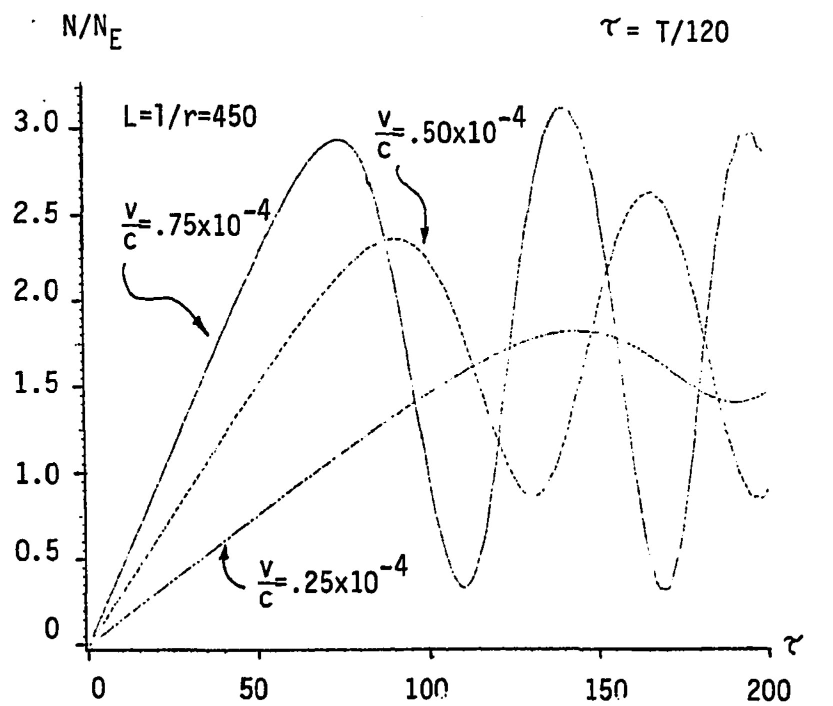

(d)

Fig.6.8 (c) & (d) Variation of axial pipe forces due to the effect of different moving speed applied at the movable end of the pipe.

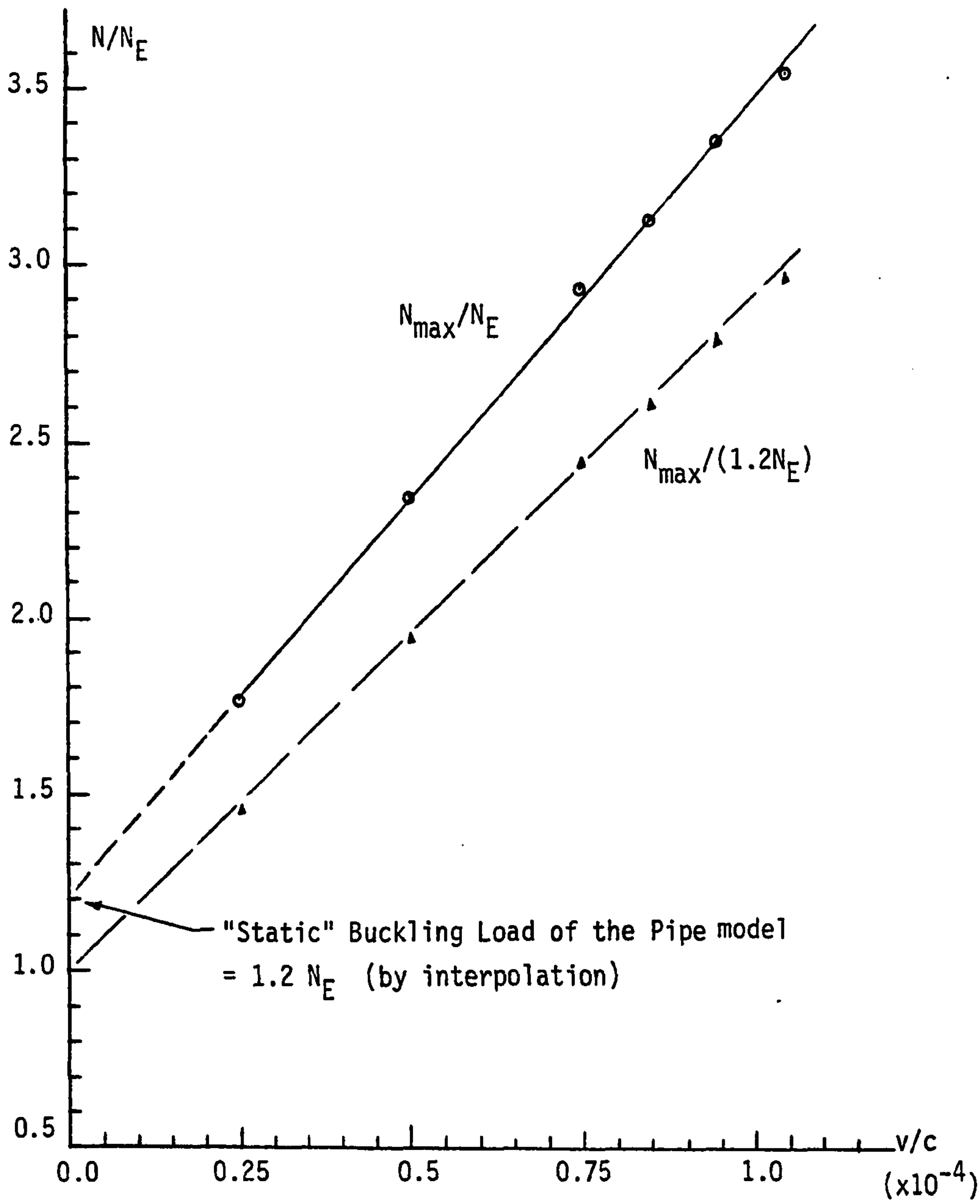

Fig.6.9 Relationship between N/N_E and v/c. (Refer Fig.6.8)

(3)

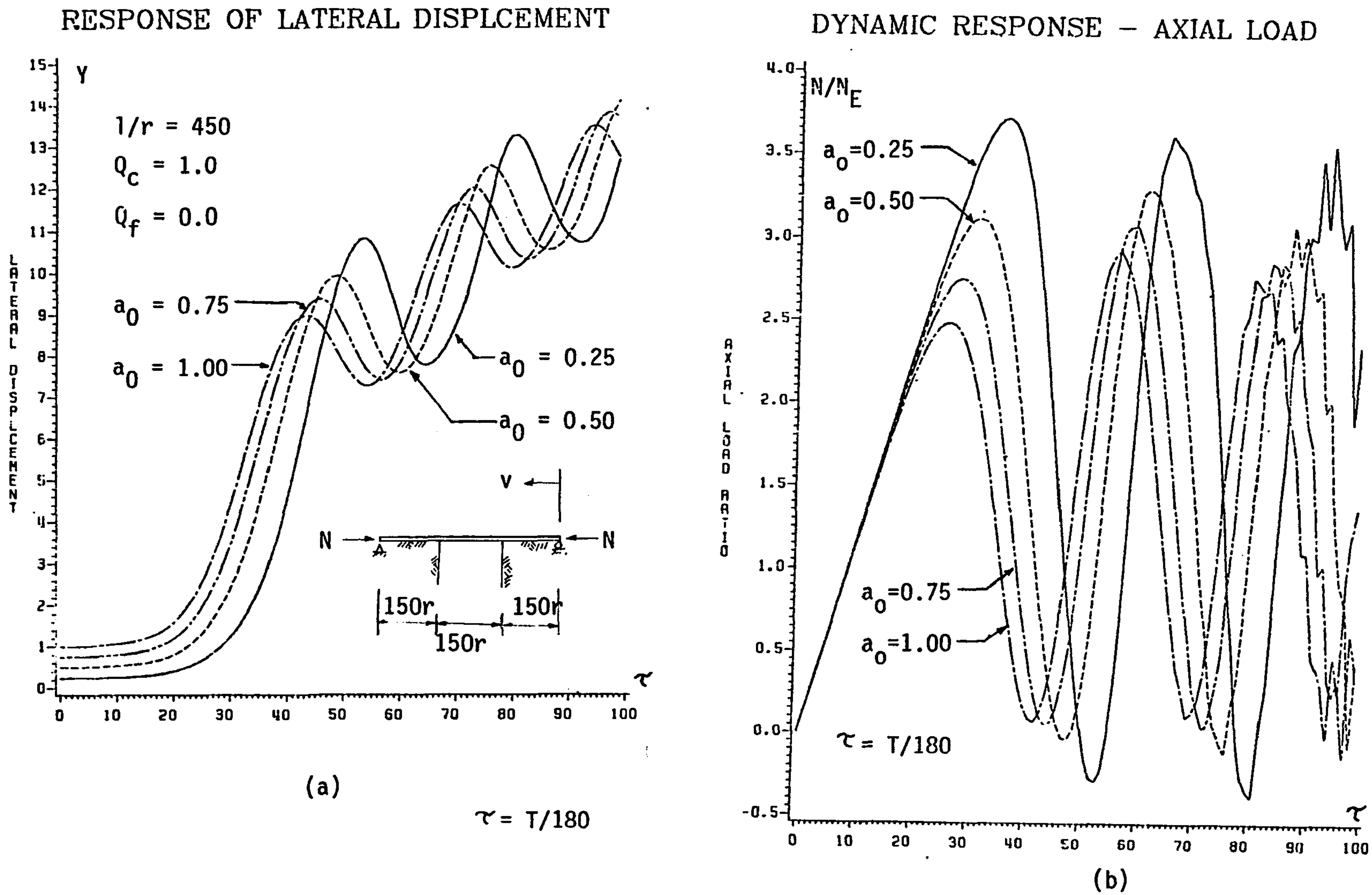

Fig.6.10 Pipe responses to the effect of initial pipe crookedness.

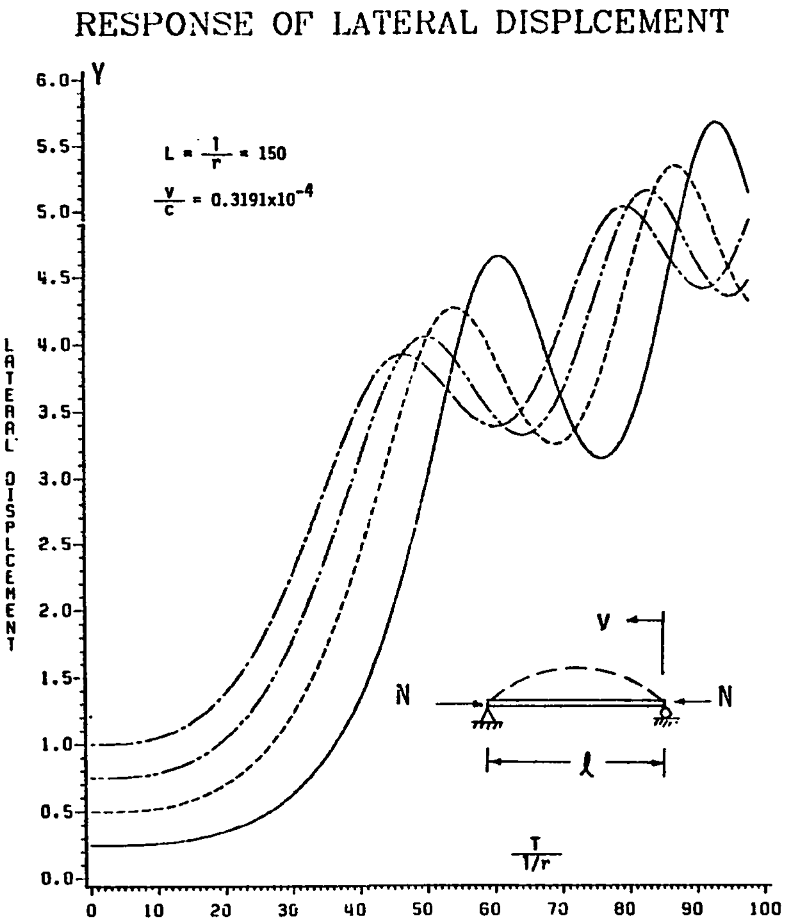

Fig.6.11a Under the effects of different initial crookedness of the pipe (Hoff's case).

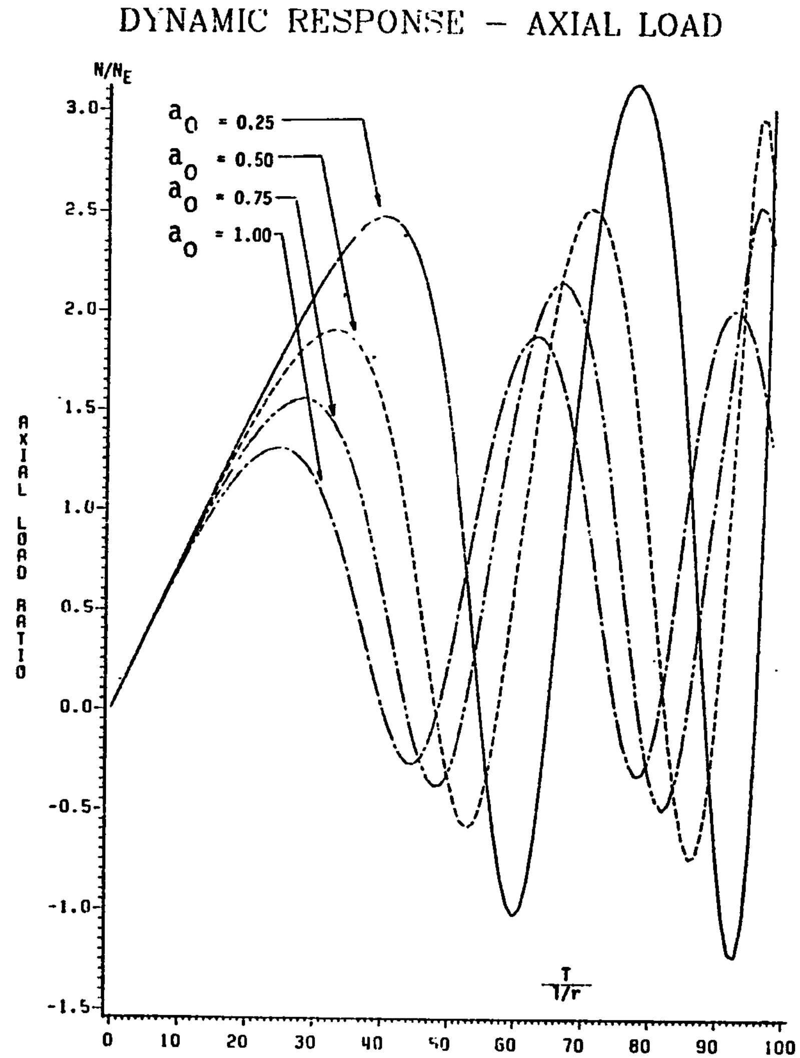

Fig.6.11b Under the effects of different initial crookedness of the pipe (Hoff's case)

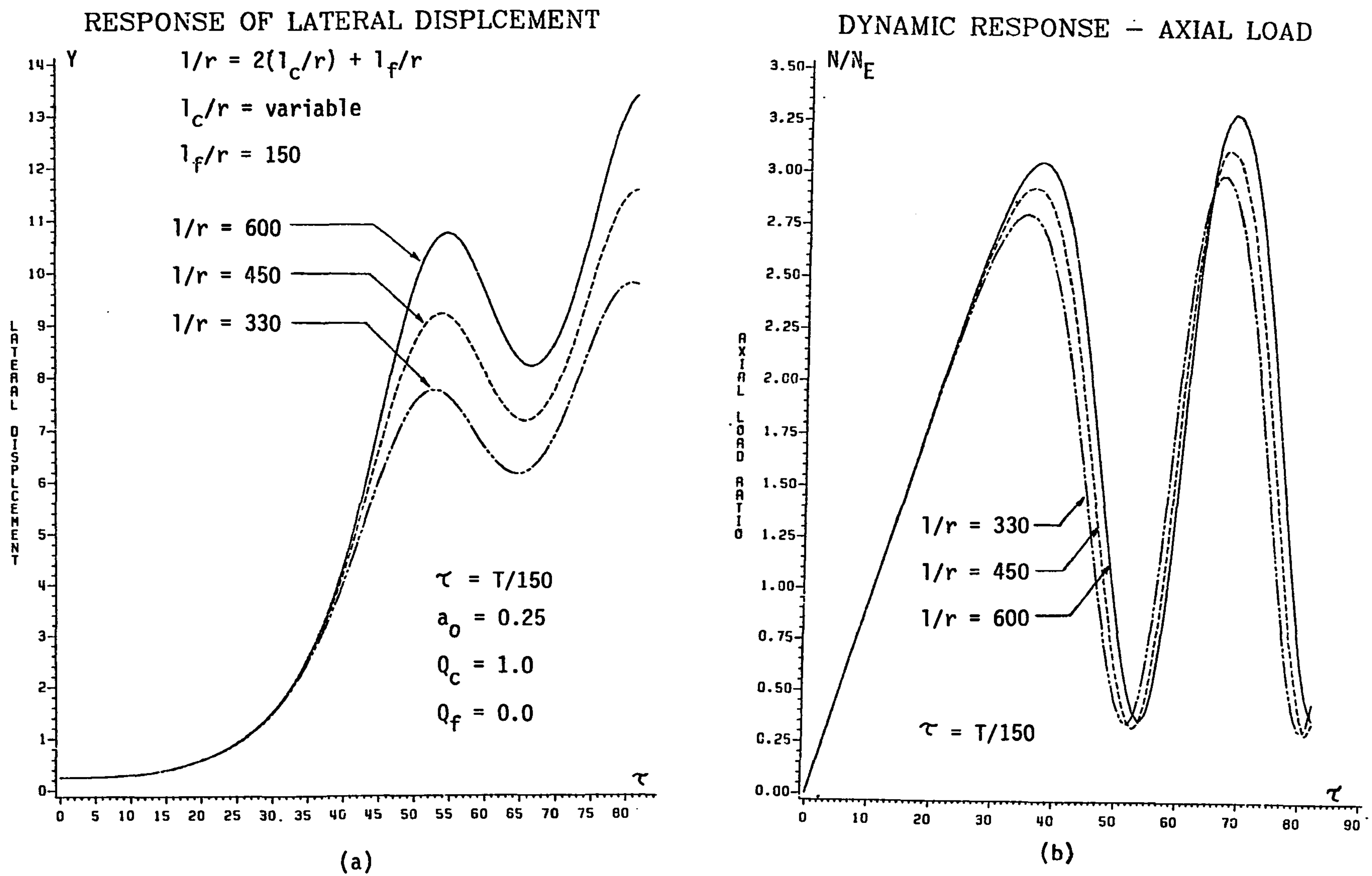

Fig.6.12 Pipe responses to the effect of the supporting length of pipe segment inside the un-liquefied zone.

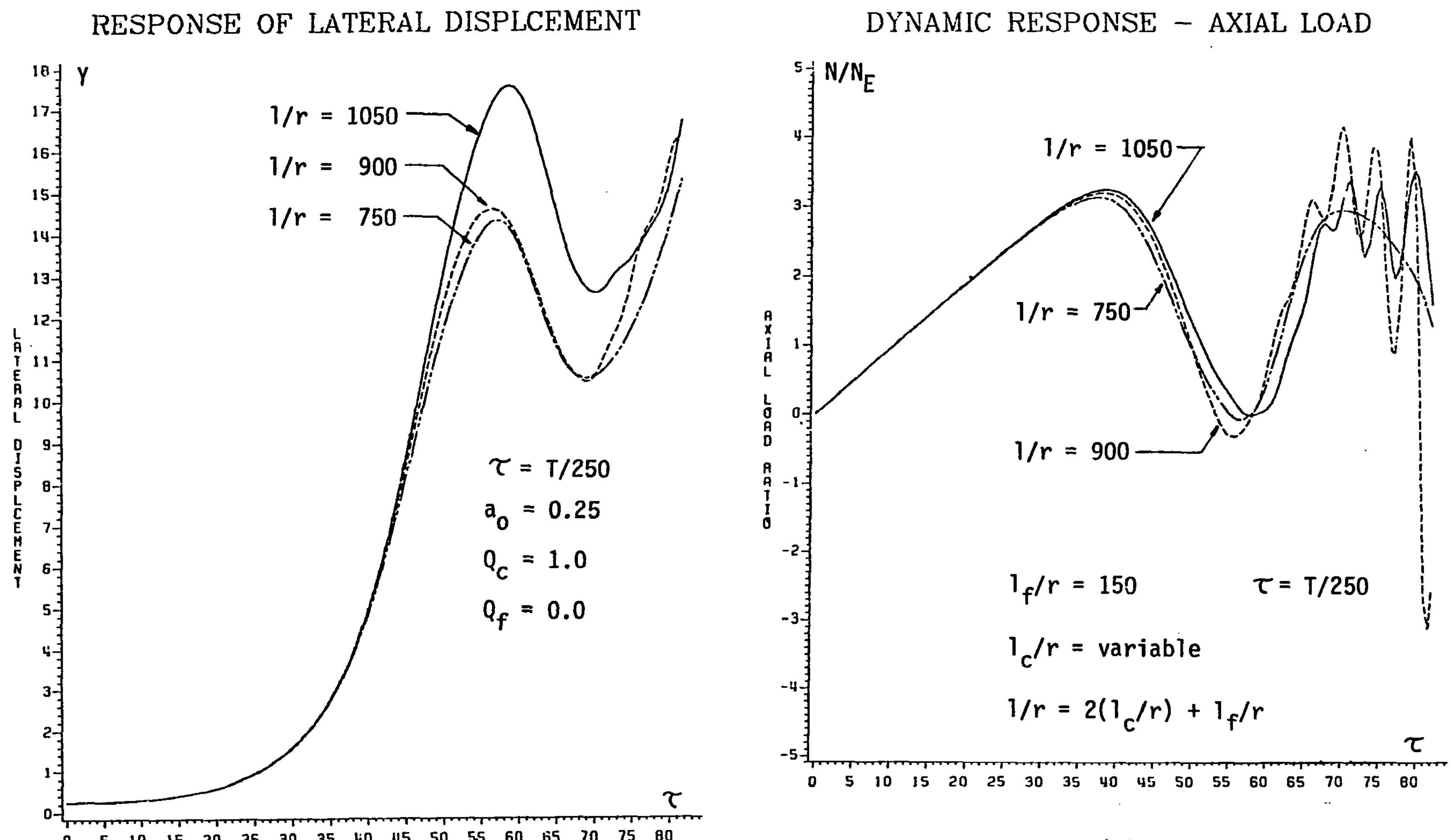

(c) (d)

Fig.6.12 (Con't.)

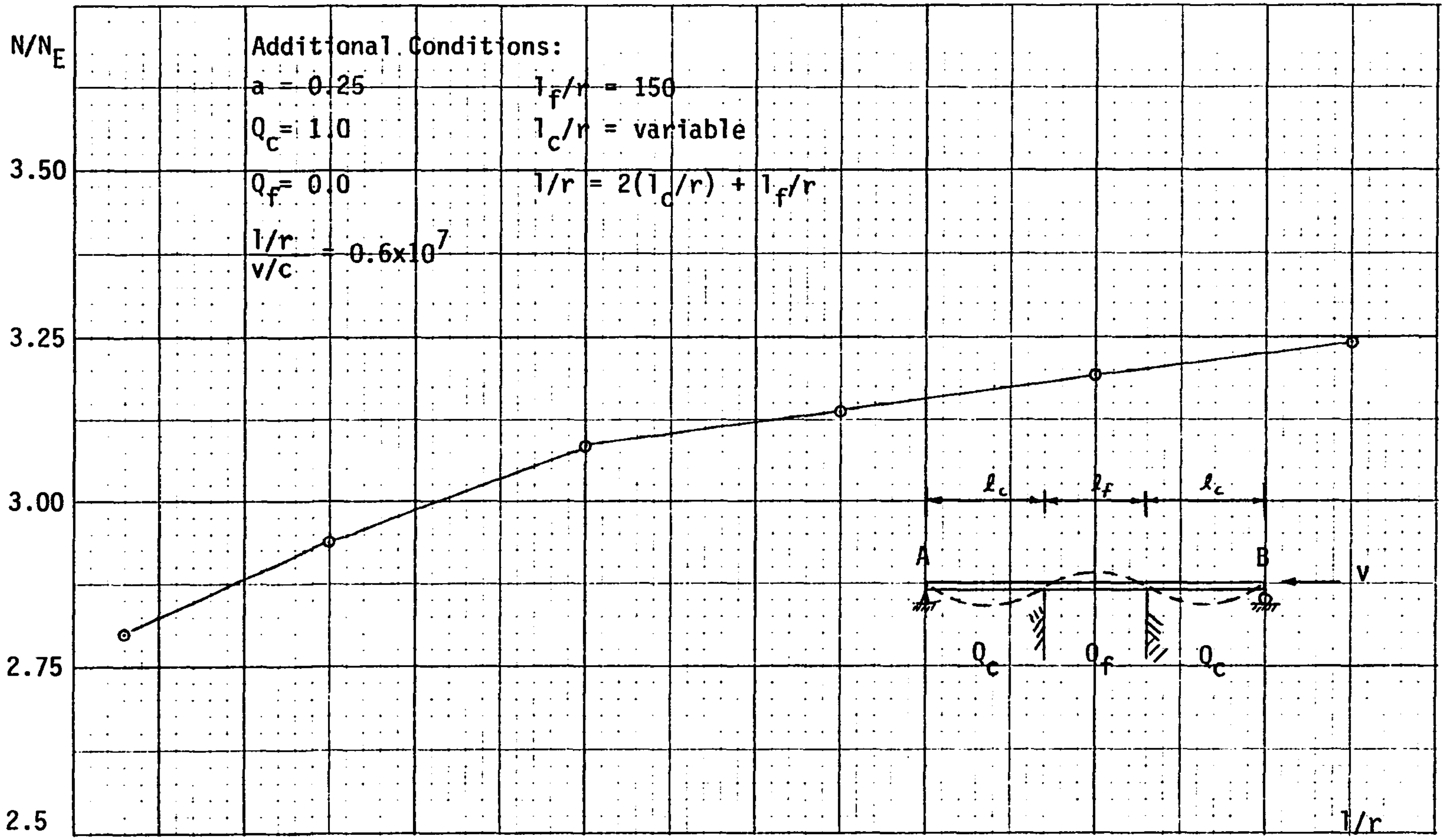

Fig.6.13 Relationship between maximum axial load and slenderness ratio of the proposed model.

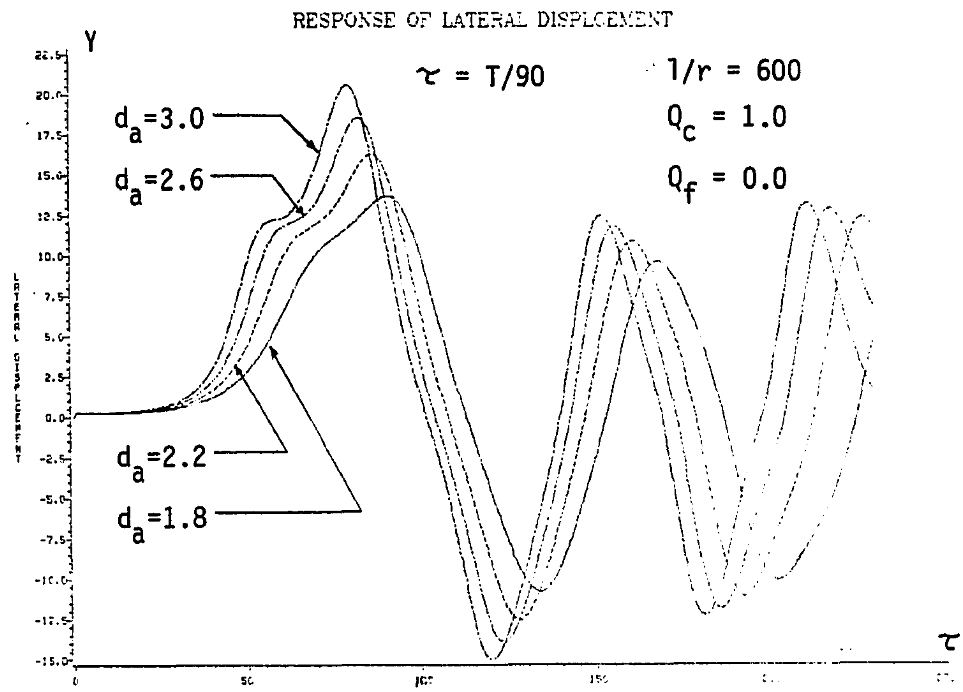

(a)

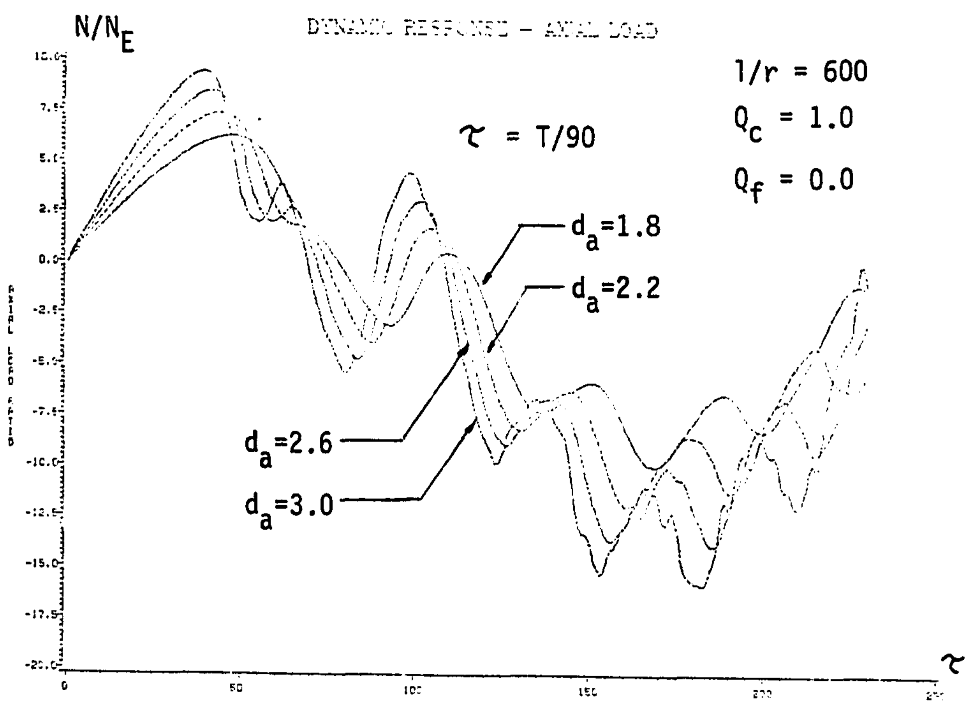

(b)

Fig.6.14 Pipe responses to various amplitues of axial sinusoidal displacement.

RESPONSE OF LATERAL DISPLCEMENT

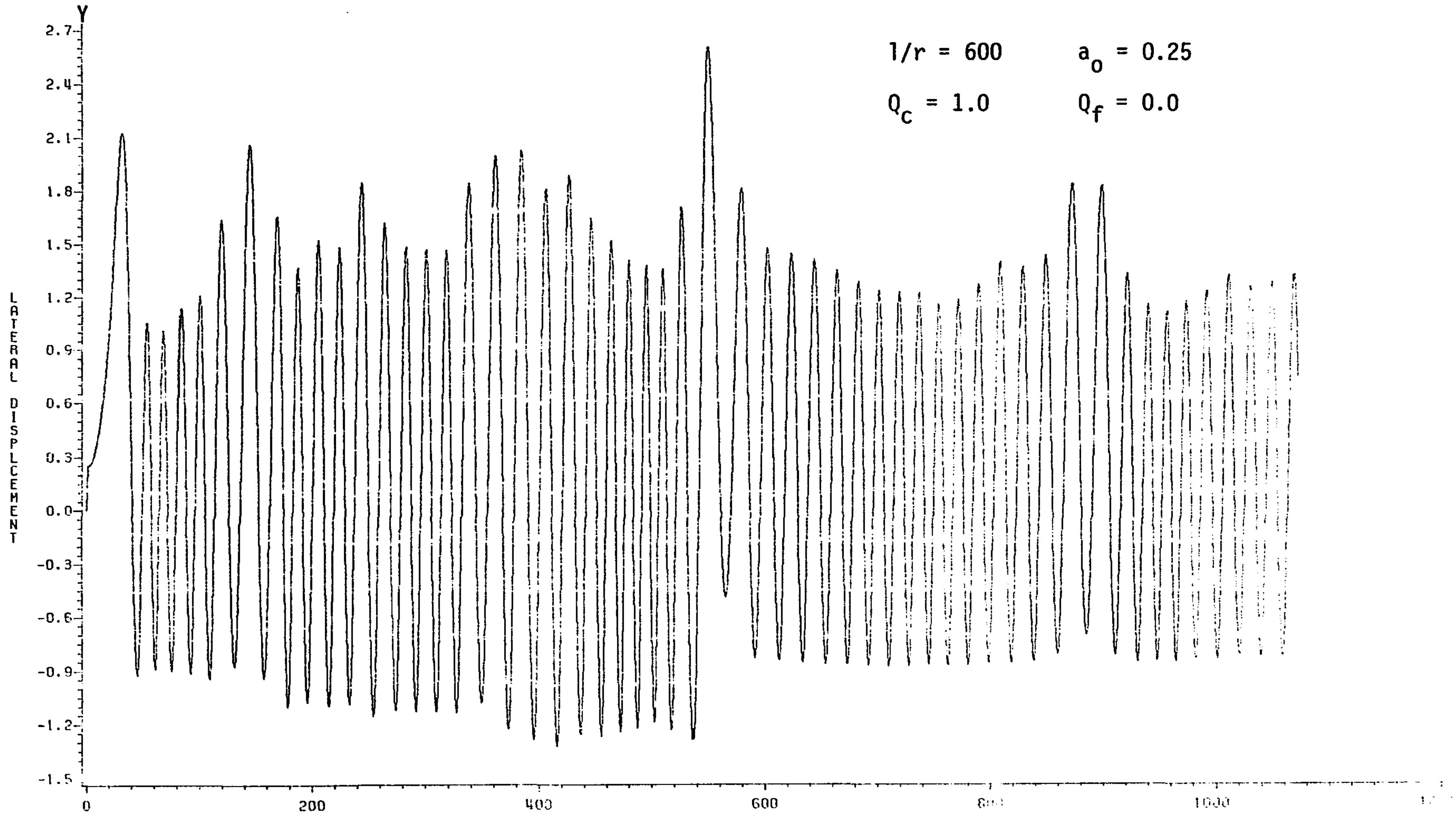

Fig.6.15a RESPONSE TO 1940 EL CENTRO EARTHQUAKE

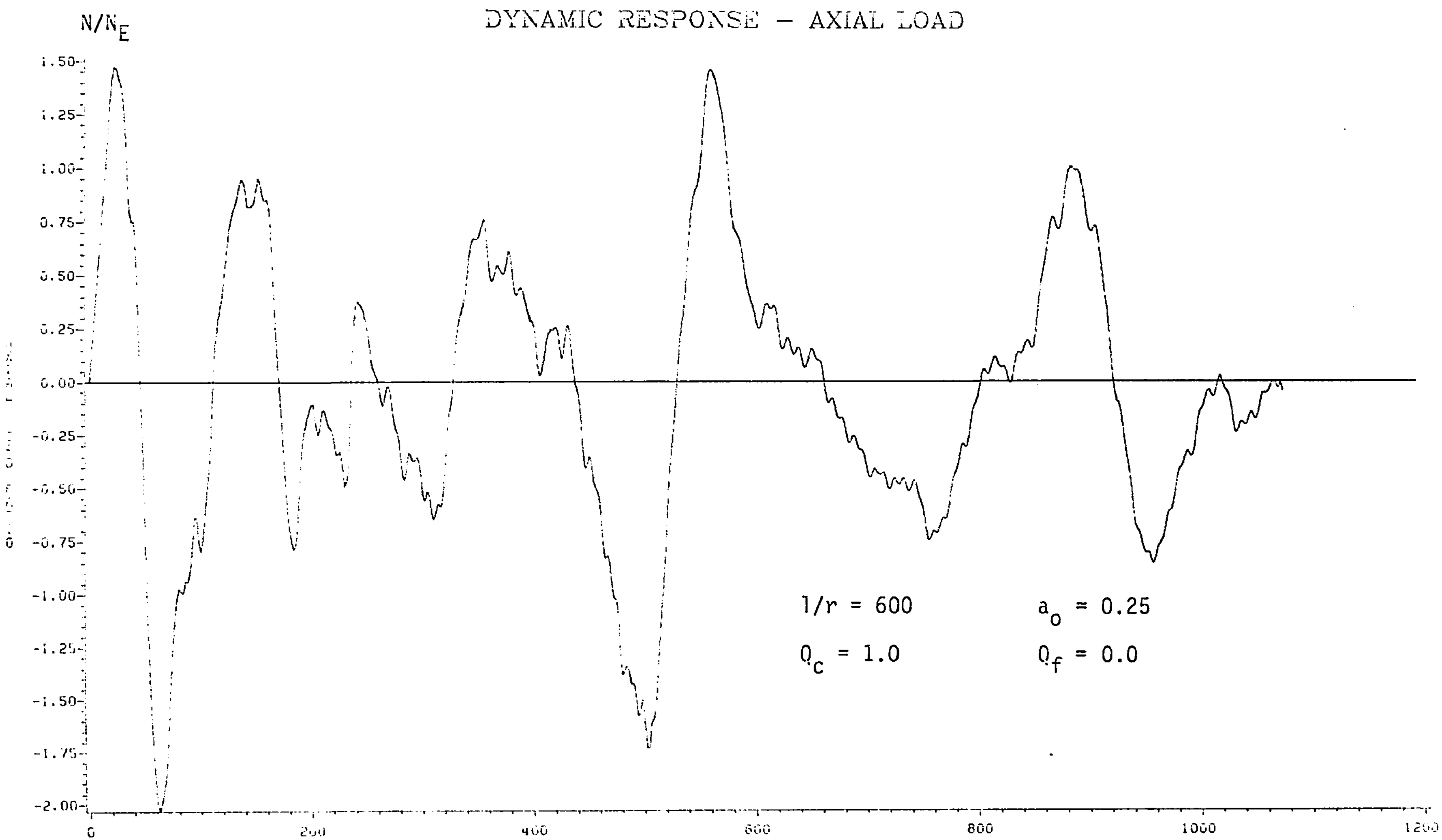

Fig.6.15b RESPONSE TO 1940 EL CENTRO EARTHQUAKE

CHAPTER VII

RECOMMENDATION FOR FUTURE STUDY

7.1 Fault Movement

CHAPTER III and IV present the analysis and results of a buried pipeline subjected to large tensile strike-slip causing pipe elongation (shown in Fig.2.2). The concepts of a pipe on elastic foundation and ultimate passive soil pressure are included in this analysis. An iterative method is used to solve the non-linear equations induced from the non-linearity of material and soil characteristics and large displacement.

The proposed analysis procedure can also be applied to a buried pipeline axially compressed by a compressive fault movement as shown in Fig.2.3. However, for most of compression members, the buckling phenomenon is the main failure mode, not the crushing or the yielding of material. Therefore, a further study on such a buckling phenomenon which has not been considered in this research is suggested. Future considerations on large fault movement effect may include the factors as depicted below.

1) The variation of radius of curvature, "R", of the curved pipe in the transition zone.

2) The effect of inelastic shear deformation in a curved pipe undergoing a large deflection.

7.2 soil Liquefaction

The investigation on the dynamic response of a pipeline buried in a liquefiable region during earthquakes has been presented in CHAPTER V and VI. By employing the finite-difference technique and a digital computer, an analysis procedure is established to determine such pipe performances of the lateral deflection and the induced axial force.

Because this is an initial study on the soil liquefaction effect, an elastic response of the pipe is only concerned. Furthermore, several other assumptions as described in sect.5.5 are also adopted to simulate the simplest real situation as mentioned previously. The suggestion for future research may contain those factors described as follows.

1) Stress wave propagation and reflection in an extended pipeline.
2) Inclusion of the skin friction between soil and pipe.
3) Slosh effect of the liquefied soil.
4) Failure mechanism of cylindrical shell.
5) Damping effect.
6) Inelastic dynamic behavior of a buried pipeline.

In addition, a study on the dynamic response for the segmented pipe (e.g. water main) is also suggested.

REFERENCES

1. Ariman, T., "A Review of the Earthquake Response and Aseismic Design of Underground Piping Systems", Proc. of Current State of Knowledge of Lifeline Earthquake Engineering, ASCE/LA, August, 1977.

2. Audibert, J.M.E and Nyman, K.J., "Soil Resistant Against Horizontal Motion of Pipes", Journal of the Geotechnical Engineering Division, ASCE, Vol.103, No.GT10, Oct., 1977

3. Beedle, Lynn S., "Secondary Design Problem", Plastic Design of Steel Frames, 2nd ed., John Wiley & Sons, Inc., N.Y., 1961.

4. Bolt, Bruce A., Earthquake- A Primer, W.H. Freeman and Company, S.F. 1978.

5. Cajina, A., "Managua Earthquake and Its Effects on the Water Supply System", Proc. Earthquake Engr. Res. Inst. Conf., Oakland, CA, Vol.2, pp.768-790, 1977.

6. Castro, C., "Liquefaction and Cyclic Mobility of Saturated Sands", Journal of Geotechnical Engineering, ASCE, Vol.101, No.GT6, June, 1975, pp.551-569.

7. Chajes, A., Principles of Structural Stability Theory, Prentice-Hall, Inc., Englewood Cliffs, N.J., 1974.

8. Clough, R.W. and J. Penzien, Dynamics of Structures, McGraw-Hill Book Company, New York, 1975.

9. Das, B.M. and Seeley, G.R., "Breakout Resistance of Shallow Horizontal Anchors", Journal of the Geotechnical Engineering Division, ASCE, Vol.101, No.GT9, Sept. 1975, pp.999-1003.

10. Finn, W.D.L., "Soil-Dynamics-Liquefaction of sands", Proc. First Int. Conf. Microzonation, Seattle, Vol.1, pp.87-111, 1972.

11. Hall, W.J. and Newmark, M.N., "Seismic Design Criteria for Pipelines and Facilities", Journal of the Technical Councils of ASCE, Vol.104, No.TC1, Nov. 1978, pp.91-107.

12. Hetenyi, M. "Beams on Elastic Foundation", University of Michigan Press, 1946.

13. Hoff, N.J.,"The Dynamics of the Buckling of Elastic Columns", Transactions of the American Society of Mechanical Engineers, ASME, 1951, pp.68-74.

14. Hoff, N.J., Nardo, S.V. and Erickson, B., "The Maximum Load Supported by an Elastic Column in a Rapid Compression Test", Proc. of The First U.S. National Congress of Applied Mechanics, Chicago, Illinois, 1951, pp.419-423.

15. Holzer, S.M. and R.A. Eubanks, "Stability of Columns Subjected to Impulsive Loading", Journal of the Engineering Mechanics Division, ASCE, Vol.95, No.EM4, Aug., 1969, pp.897-920.

16. Kachadorian, R., "Earthquake: Correlation Between Pipeline Damage and Geologic Environment", Journal of AWWA, March 1976, pp.165-167.

17. Kennedy, R.P., Chow,A.W. and Williamson, R.A., "Fault Movement Effects on Buried Oil Pipeline", Transportation Engineering Journal of ASCE, Vol.103, No.TE5, Sept. 1977, pp.617-633.

18. Kennedy, R.P., Darrow, A.C. and Short, S.A., "Seismic Design of Oil Pipeline Systems", Journal of the Technical Councils of ASCE, Vol.105, No.TC1, April 1979, pp.119-105.

19. Kubo, K. and Isoyama, R., "Damage to Buried Utility Pipes in the 1978 Miyagi-Ken-Oki Earthquake", Proc. of 7th World Conference on Earthquake Engineering", Istanbul, Turkey, Vol.8, Sept. 1980, pp.225-232.

20. Lawson, A.C., "The California Earthquake of April 18, 1906 - Report of the State Earthquake Investigation Commission", Washington, D.C., Carnegie Institute Washington Publication No.87, Vol.1, 1908.

21. Lee, K.L. and Seed, H.B., "Cyclic Stress Conditions Causing Liquefaction of Sand", Journal of the soil Mechanics and Foundations Division, ASCE, Vol.93, No.SM1, Jan. 1967, pp.47-70.

22. Liou, C.P., Streeter, V.L. and Richart, F.E., Jr., "Numerical Model for Liquefaction", Journal of the Geotechnical Engineering Division, ASCE, Vol.103, No.GT6, June 1977, pp.589-605.

23. Lubkin, S. and J.J. Stoker, "Stability of Columns and Strings Under Periodically Varying Forces", Quartly of Applied Mathematics, Vol.1, No.3, 1943, pp.215-236.

24. Meier, J.H., "On the Dynamics of Elastic Buckling", Journal of the Aeronautical Sciences, Vol.12, 1945, pp.433-440.

25. Newmark, N.M. and Hall, W.J., "Pipeline Design to Resist Large Fault Displacement", Proc. of the U.S. National Conference on Earthquake Engineering 1975, Earthquake Engineering Research Institute, Oakland, CA, June 1975.

26. Okamoto, S., "Disaster Prevention to Sewer Systems", Prevention of Civil Structures, (in Japanese), Kyoritsu Publishing Company, Japan, May 1970.

27. Okamoto, S., Introduction to Earthquake Engineering, John Wiley and Sons, Inc., New York, N.Y., 1973.

28. O'Rourke, T.D. and Trautmann, C.H., "Analytical Modeling of Buried Pipeline Response to Permanent Earthquake Displacement", Technical Report for NSF Grant No. PFR-7823096, July 1980.

29. O'Rourke, T.D. and Trautmann, C.H., "Buried Pipeline Response to Permanent Earthquke Ground Movements", Pressure Vessel and Piping Division, ASME, Century 2 Conference, 80-C2/PVP-78, S.F., August 1980.

30. Peacock, W.H. and Seed, H.B., "Sands Liquefaction under Cyclic Loading Simple Shear Conditions", Journal of the Soil Mechanics and Foundations Division, ASCE, Vol.94, No.SM3, May 1968, pp.689-708.

31. Prakash, S., Soil Dynamics, McGraw-Hill Book Company, New-York, N.Y., 1981.

32. Richtmyer, R.D. and Morton, K.W., "Difference Methods for Initial-Value Problems", 2nd ed., John Wiley & Sons, Inc., 1964.

33. Seed, H.B. and Idriss, I.M., "Analysis of Soil Liquefaction: Niigata Earthquake", Journal of the Soil Mechanics and Foundations Division, ASCE, Vol.93, No.SM3, May 1967, pp.83-108.

34. Seed, H.B. and Lee, K.L., "Liquefaction of Saturated Sands During Cyclic Loading", Journal of the Soil Mechanics and Foundations Division, ASCE, Vol.92, No.SM6, Nov. 1966, pp.105-134.

35. Seed, H.B. and W.H. Peacock, "Test Procedures for Measuring Soil Liquefaction Characteristics", Journal of the Soil Mechanics and Foundations Division, ASCE, Vol.97, No.SM8, Aug., 1971, pp.1099-1119.

36. Spangler, M.G. and Handy, R.L., "Soil Engineering", 3rd ed., Intext Press, Inc., New York, 1973.

37. Sun, S.P., "Earthquake Damage to Pipelines", Pressure Vessels and Piping Conference, ASME, 80-C2/PVP-156, San Francisco, CA, Aug. 1980, pp.1-4.

38. Taylor, C.L. and Cluff, L.S., "Fault Displacement and Ground Deformation Associated with Surface Faulting", Proc. of Current State of Knowledge of Lifeline Earthquake Engineering, ASCE/LA, August 1977.

39. Therashima, S., Tambo, N., Koyama, K., and M. Kobayashi, "Damage to the Water and Sewage Works caused by the 1968 Tokachi-Oki Earthquake", Report on the Tokachi-oki Earthquake 1968, (in Japanese), Nakanishi Photogravure Printint Company, Japan, March 1969, pp.553-578.

40. Timoshenko, S.P. and J.M. Gere, Theory of Elastic Stability, 2nd ed., McGraw-Hill, Inc., New York, 1961.

41. Wang, L.R.L. and O'Rourke, M.J., "State of the Art of Buried Lifeline Earthquake Engineering", Proc. of the Current State of Knowledge of Lifeline Earthquake Engineering, ASCE/LA, August 1977.

42. Yeh, Yaw-Huei, "Failure Mechanisms of Buried Pipelines Due to Fault Movement", Proc. of the 13th Southwestern Graduate Conference in Applied Mechanics, Norman, Oklahoma, April 1982.

43. Yeh, Yaw-Huei, "Seismic Designs of Buried Pipelines Subjected to Large Fault Movement", (in Chinese), Engineering Monthly, Taiwan, R.O.C., Oct. 1982.

APPENDICES

Appendix A

DISPLACEMENT OF 1940 EL CENTRO EARTHQUAKE

0.531496	1.015354	1.518503	2.052755	2.630709	3.223228
3.826772	4.464566	5.120472	5.623622	5.927559	6.030708
6.018503	6.059448	5.922441	5.361417	4.422834	3.522834
3.056692	2.881889	2.245275	1.074409	-0.333465	-1.576771
-2.945275	-4.094094	-5.179133	-6.249212	-7.113382	-7.661810
-7.788584	-7.684644	-7.340552	-6.936615	-6.379922	-5.620866
-4.779921	-4.260236	-3.933858	-3.726771	-3.629921	-3.574016
-3.527558	-3.652362	-3.468897	-2.984645	-2.498818	-2.454723
-2.712204	-2.801181	-2.637008	-2.305905	-1.877953	-1.280708
-0.412205	0.344094	0.822835	1.340550	1.785039	2.062598
2.295669	2.484252	2.723621	2.966920	3.181102	3.279921
3.434646	3.600787	3.757087	3.867716	3.824409	3.921260
3.830315	3.587795	3.574409	3.659055	3.590944	3.414567
3.348818	3.302755	3.136614	2.749999	2.159842	1.475984
0.764961	-0.195276	-1.087794	-1.638582	-2.118110	-2.599213
-2.932283	-2.926771	-2.611417	-2.124803	-1.568503	-1.087794
-0.795669	-0.572047	-0.503150	-0.431496	-0.303150	-0.400394
-0.563780	-0.584252	-0.531496	-0.520079	-0.583071	-0.740157
-0.884646	-0.962992	-1.013386	-0.909055	-1.024015	-1.485039
-1.902362	-1.696850	-0.853937	0.226772	0.974016	1.675590
1.998031	1.993306	1.702755	1.266929	0.995276	0.806693
0.542520	0.278346	0.099606	0.081102	0.086614	0.037795
0.033858	-0.033465	-0.121653	-0.303937	-0.564173	-0.847638
-1.004330	-1.137794	-1.282677	-1.438976	-1.366929	-1.302755
-1.317717	-1.307086	-1.364566	-1.409449	-1.451968	-1.636614
-1.838976	-1.924409	-2.088976	-2.273622	-2.371260	-2.348425
-2.214172	-2.021653	-1.771259	-1.342519	-0.899606	-0.594094
-0.272441	0.199213	0.650394	0.987402	1.378739	1.809842
2.112598	2.273622	2.371260	2.486613	2.609055	2.690945
2.724015	2.743307	2.823228	3.032677	3.012598	2.796850
2.551181	2.313779	2.146063	2.112598	2.103149	2.129921
2.111417	2.146456	2.370078	2.495275	2.423622	2.353936
2.212204	1.962992	1.697638	1.569685	1.557874	1.427559
1.167322	1.053937	0.990945	0.801968	0.713779	0.609055
0.528346	0.712992	1.020078	1.172047	1.048819	0.979134
1.042126	1.048819	1.085039	1.200000	1.177559	1.011810
0.731890	0.454331	0.089370	-0.191339	-0.423228	-0.733071
-1.025984	-1.206299	-1.325590	-1.449212	-1.661811	-1.770079
-1.995669	-2.198818	-2.446456	-2.760236	-2.971653	-3.214172
-3.483858	-3.711417	-3.885433	-4.119684	-4.545276	-4.960236
-5.103936	-5.198818	-5.184645	-5.356298	-5.499212	-5.633858
-5.784252	-5.711023	-5.763730	-6.155512	-6.563388	-6.603150
-6.252361	-5.958661	-5.550393	-5.143701	-4.565353	-3.844488
-3.239763	-2.564960	-1.681496	-0.939764	-0.293307	0.092520
0.370866	0.773228	1.148031	1.612991	2.139370	2.612991

3.113385	3.658661	4.237795	4.707479	5.117323	5.393307
5.592126	5.708661	5.709449	5.646063	5.561417	5.425983
5.243306	5.017323	4.790551	4.490944	4.228346	3.966928
3.669291	3.399212	3.131495	2.822834	2.568897	2.312204
2.048031	1.807480	1.611417	1.458661	1.437401	1.448424
1.411811	1.321653	1.296456	1.375196	1.442913	1.417716
1.381889	1.378346	1.336614	1.184645	1.048425	0.983465
0.931102	0.868504	0.769292	0.659055	0.595276	0.588583
0.628346	0.670472	0.654331	0.647638	0.648031	0.617717
0.605512	0.568897	0.505512	0.455512	0.383465	0.271260
0.124409	-0.013386	-0.113779	-0.229921	-0.390551	-0.532284
-0.599213	-0.636221	-0.671654	-0.724803	-0.761811	-0.798819
-0.870473	-0.984252	-1.081495	-1.133464	-1.189369	-1.270865
-1.329921	-1.379133	-1.449212	-1.525984	-1.567717	-1.589764
-1.595275	-1.622046	-1.635039	-1.630315	-1.644881	-1.680708
-1.700787	-1.731890	-1.779921	-1.780708	-1.757874	-1.740945
-1.724409	-1.703543	-1.698424	-1.721259	-1.781495	-1.876771
-2.012992	-2.190157	-2.348818	-2.470078	-2.581101	-2.655511
-2.699212	-2.703149	-2.666928	-2.617322	-2.524409	-2.399212
-2.245275	-2.078346	-1.917716	-1.758661	-1.614961	-1.473228
-1.316141	-1.157086	-1.023228	-0.901181	-0.769292	-0.635433
-0.507480	-0.391339	-0.254724	-0.078740	0.116929	0.289764
0.429527	0.520079	0.562598	0.546063	0.503937	0.464567
0.410630	0.353543	0.318110	0.308661	0.320472	0.354331
0.416535	0.494094	0.545669	0.575984	0.616535	0.683071
0.751575	0.805905	0.881496	0.994882	1.147637	1.352362
1.594094	1.850787	2.112205	2.371260	2.627559	2.865747
3.065747	3.216141	3.314173	3.406693	3.509842	3.633070
3.758267	3.857874	3.923621	3.941731	3.926771	3.888976
3.825590	3.725984	3.634252	3.549212	3.453543	3.340550
3.196457	3.016535	2.775590	2.472441	2.139370	1.811024
1.479134	1.127559	0.770472	0.434252	0.129921	-0.140945
-0.403543	-0.671260	-0.956299	-1.240551	-1.522440	-1.800393
-2.061023	-2.298819	-2.519685	-2.709449	-2.862992	-2.972047
-3.042126	-3.074016	-3.070079	-3.038976	-3.000393	-2.970078
-2.922441	-2.814960	-2.661417	-2.480708	-2.289370	-2.090551
-1.904330	-1.748031	-1.624803	-1.525590	-1.429527	-1.333071
-1.253149	-1.184252	-1.097637	-0.974410	-0.819291	-0.662205
-0.517323	-0.387795	-0.274409	-0.179528	-0.096457	-0.011811
0.069291	0.138189	0.176772	0.170472	0.094094	0.022047
-0.069685	-0.206299	-0.340945	-0.469291	-0.572441	-0.648819
-0.689370	-0.703937	-0.703150	-0.679921	-0.621654	-0.531102
-0.440157	-0.360630	-0.298425	-0.242913	-0.198425	-0.156299
-0.107087	-0.050000	0.029921	0.123622	0.213780	0.272835
0.322047	0.000000				

* Unit: in.

‡ Time interval: 0.1 second

Appendix B

The integrated displacement of 1940 EL CENTRO EARTHQUAKE.

EL CENTRO (N90E)

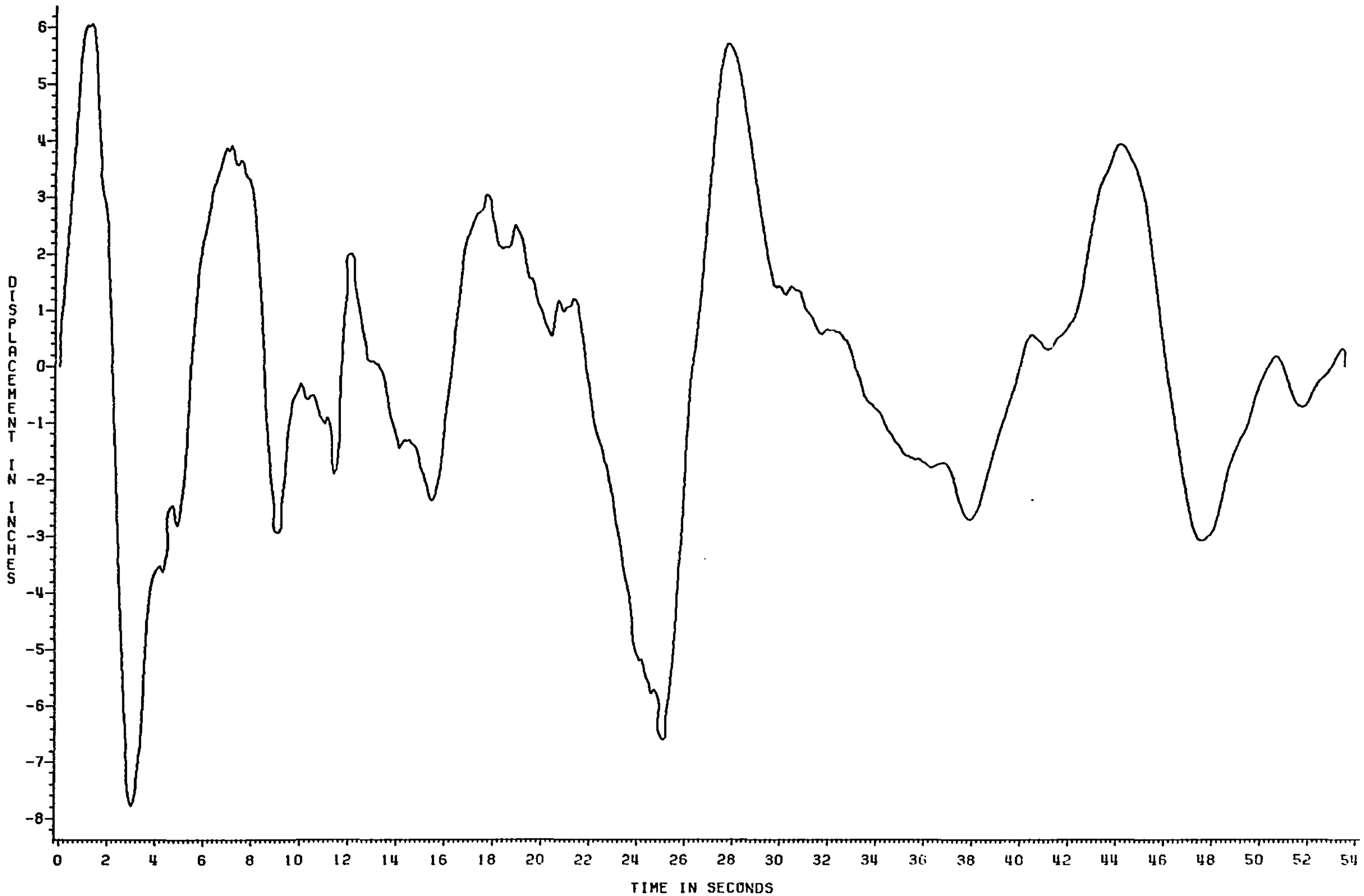

APPENDIX C

Computer Program for Fault Movement

```
C.............................................................C
C                                                             C
C     DETERMINATION OF RESISTANT CAPACITY OF A BURIED PIPE    C
C     TO LARGE FAULT MOVEMENT BY USING ITERATIVE METHOD       C
C                                                             C
C.............................................................C
      DIMENSION ALPHA(1000),P(1000),V(1000),R(1000),CK(1000)
      REAL NQ,LG,LP,LY1,LY2,KS,IX,LAMDA,MOM
      DATA PI,E1,SD,SN/3.14159,3.0E+7,0.02,-0.02/
      DATA XK,DX/0.5,100./
      DATA YS,YSS,STD,STDN/45000.,60000.,0.25,-0.30/
      SD2=4.*SD
      READ(5,150) BETA1,DELTA1,PHI1,GAMMA1
  150 FORMAT(4F10.5)
      READ(5,250) ID
      READ(5,250) M
      READ(5,250) NG
      READ(5,250) N
  250 FORMAT(I5)
      READ(5,270) YI,YII
  270 FORMAT(2F10.2)
C..... UNIT CONVERSION ......
      BETA=BETA1*PI/180.
      PHI=PHI1*PI/180.
      GAMMA=GAMMA1/(12.**3.)
      DELTA=DELTA1*12.
      WRITE(6,160) BETA1,DELTA1,PHI1
  160 FORMAT('1',' *** THE GIVEN DATA ***'/
     ,5X,'ANGLE OF CROSSING A FAULT =',F10.5,2X,'DEG.'/
     ,5X,'LENGTH OF FAULT MOVEMENT =',F10.5,1X,'FT.'/
     ,5X,'FRICTIONAL ANGLE BETWEEN SOIL/PIPE =',F10.5,1X,'DEG.')
C
         NP=1
      DO 800 K5=1,NP
      READ(5,220) NQ,Z,D,THK
  220 FORMAT(4F10.5)
      AP=PI*(D-THK)*THK
      IX=0.25*PI*((D/2.)**4.-(D/2.-THK)**4.)
      SX=2.*IX/D
```

```
      ZP=(D**3.-(D-2.*THK)**3.)/6.
      WRITE(6,230)Z,D,THK,AP,IX,SX,ZP
  230 FORMAT(5X,'DEPTH TO CENTER OF PIPE =',F8.3,1X,'IN.'/
     ,5X,'OUTSIDE DIAMETER OF PIPE =',F10.5,1X,'IN.'/
     ,5X,'THICKNESS OF PIPE =',F10.5,1X,'IN.'/
     ,5X,'CROSS-SECTIONAL AREA OF PIPE =',F8.3,1X,'SQ.IN.'/
     ,5X,'MOMENT OF INERTIA OF PIPE =',F15.4,1X,'IN.**4'/
     ,5X,'ELASTIC SECTION MODULUS, SX=',F12.2,1X,'IN.**3'/
     ,5X,'PLASTIC SECTION MODULUS =',F10.2,1X,'IN.**3')
C
      QR=GAMMA*Z*D
      PP=NQ*QR
      FP=PP*TAN(PHI)
      PS=QR*PI*(1.+XK)/2.
      FS=PS*TAN(PHI)
      KS=1000.*NQ*GAMMA*D
      LAMDA=(0.25*KS/(E1*IX))**0.25
      WRITE(6,240)NQ,GAMMA1,PP,FP,PS,FS,XK,KS,LAMDA
  240 FORMAT(/5X,'**** SOIL CHARACTERISTICS ****'/
     ,5X,'BEARING CAPACITY FACTOR =',F8.3/
     ,5X,'UNIT WEIGHT OF SOIL =',F10.5,1X,'LB/CU.FT.'/
     ,5X,'PASSIVE PRESSURE PP =',F15.5,1X,'LB/IN.'/
     ,5X,'SOIL FRICTION DUE TO PP- FP =',F15.5,1X,'LB/IN.'/
     ,5X,'STATIC SOIL PRESSURE,PS =',F10.3,1X,'LB/IN.'/
     ,5X,'SOIL FRICTION DUE TO PS, FS =',F10.3,1X,'LB/IN.'/
     ,5X,'COEFFICIENT FOR PS, XK =',F6.3/
     ,5X,'STIFFNESS OF SOIL FOUNDATION, KS =',F15.6/
     ,5X,'CHARACTERISTIC FACTOR, LAMDA =',F15.7)
C.....ITERATIVE PROCESS......
C
      DO 800 J=1,N
      LY1=YI/E1
          LY2=0.04
      E2=(YII-YI)/(LY2-LY1)
      EM1=SX*YI
      EM2=SX*YII
      ZMOM=ZP*YII
      YTAU=0.6*YII
      WRITE(6,280) J,E1,E2,YI,YII,YTAU,LY1,LY2
  280 FORMAT(//5X,'..... PROPERTIES OF MATERIAL NO.',I3/
     ,5X,'FIRST MODULUS OF ELASTICITY =',F12.3,1X,'PSI'/
     ,5X,'SECOND MODULUS OF ELASTICITY =',F12.2,1X,'PSI'/
     ,5X,'FIRST YIELD STRESS =',F12.3,1X,'PSI'/
     ,5X,'SECOND YIELD STRESS =',F12.3,1X,'PSI'/
     ,5X,'SHEAR STRESS AT 2ND YIELD POINT =',F12.3,1X,'PSI'/
     ,5X,'FIRST YIELD STRAIN =',F10.5,1X,'IN./IN.'/
     ,5X,'SECOND YIELD STRAIN =',F10.5,1X,'IN./IN.')
      WRITE(6,290) ZMOM,EM1,EM2
  290 FORMAT(5X,'PLASTIC RESISTING MOMENT =',F12.2,1X,'LB-IN.'/
     ,5X,'1ST ELASTIC RESISTING MOMENT =',F12.2,1X,'LB-IN.'/
     ,5X,'2ND ELASTIC RESISTING MOMENT =',F12.2,1X,'LB-IN.')
```

```
C
      AST=PI/36.
      IF(DELTA1.LT.9.8) AST=PI/60.
      IF(DELTA1.GT.22.5) AST=PI/24.
            IDR=1
      IA=2000
      K=0
          JRE=100
          EEN=0.02
      THETAB=0.
        ER=E1
        ER2=EM2/(EM1/E1+(EM2-EM1)/E2)
               WRITE(6,296)ER2
  296 FORMAT(5X,'REDUCED MODULUS OF ELASTICITY, ER2 =',F12.3,
     ,1X,'PSI')
C
  300 K=K+1
      WRITE(6,302) K
  302 FORMAT(/6X,'............. ITERATION NO.',I4)
      AL=PI/9000.
      ANG=AL
      ACL=AL/2.
      ADL=AL/3.
      AEL=AL
      IF(YI.GT.YS) ANG=ACL
      IF(YI.GT.YSS) ANG=ADL
      IDS=3
          NCK=2
      IDX=1
      DMIN=1000.
      AH=AST
               JCT=0
C
      DO 500 I=1,M
  305 CONTINUE
      IF(IDX.EQ.2) GO TO 500
      ALPHA(I)=AH*180./PI
      IF(ID.EQ.2) GO TO 310
C............SUBJECT TO TENSILE EFFECTS......................
        BB=BETA-THETAB
        XX=0.5*DELTA*(SIN(BB)+COS(BB)*TAN(THETAB))
        YY=1.-COS(AH)+SIN(AH)*TAN(THETAB)
        R(I)=XX/YY
      MOM=ER*IX/R(I)
        TM=1./R(I)+LAMDA*COS(THETAB)*TAN(AH)
        TN=FP*R(I)*(TAN(AH)-AH)
        TT=1.-COS(AH)-SIN(AH)*TAN(AH)
        P(I)=PP*R(I)+(TM*MOM-TN)/TT
        V1=(PP*R(I)-P(I))*SIN(AH)
        V2=FP*R(I)*(1.-COS(AH))-LAMDA*COS(THETAB)*MOM
        V(I)=(V1+V2)/COS(AH)
```

```
C..     ............GEOMETRIC ELONGATION......................
        GG=R(I)*SIN(AH)-0.5*DELTA*COS(BB)
        LG=2.*(R(I)*AH-GG/COS(THETAB))
      GO TO 320
C............SUBJECT TO COMPRESSIVE EFFECTS..................
  310   BC=BETA+THETAB
        XX=SIN(BC)-COS(BC)*TAN(THETAB)
        YY=1.-COS(AH)+SIN(AH)*TAN(THETAB)
        R(I)=0.5*DELTA*XX/YY
      MOM=ER*IX/R(I)
        CA=1./R(I)+LAMDA*COS(THETAB)*TAN(AH)
        CB=FP*R(I)*(AH-TAN(AH))
        CC=SIN(AH)*TAN(AH)+COS(AH)-1.
      P(I)=-PP*R(I)+(MOM*CA-CB)/CC
        V1=(P(I)+PP*R(I))*SIN(AH)
        V2=FP*R(I)*(1.-COS(AH))+LAMDA*MOM*COS(THETAB)
        V(I)=(V1-V2)/COS(AH)
C..     ..............GEOMETRIC SHORTENING....................
        CG=R(I)*SIN(AH)+0.5*DELTA*COS(BC)
        LG=2.*(COS(THETAB)-R(I)*AH)
  320 CONTINUE
C.....PERMISSIBLE ELONGATION OR SHORTENNING.....
      FA=P(I)/AP
        IF(I.LT.M.OR.FA.LT.YII) GO TO 322
              NCK=5
          WRITE(6,321)
  321 FORMAT(5X,'......RE-SELECT THE VALUE OF ALPHA(I).....')
  322   CONTINUE
      VA=V(I)/AP
      IF(FA.GE.YII) GO TO 490
      F5=P(I)*COS(AH)+PP*R(I)*(1.-COS(AH))
      F6=V(I)*SIN(AH)+FP*R(I)*SIN(AH)
      FB=(F5-F6)/AP
      RR=R(I)
      IF(FA.LT.YI) GO TO 350
C.....MAX. AXIAL STRESS INDUCED IN INELASTIC REGION.....
      PX=P(I)
      VX=V(I)
      IF(FB.LT.YI) GO TO 330
      AF=0.
        AG=AH
        S1=AH*R(I)
        H1=(VX+FP*RR)*(COS(AH)-1.)
        H2=PX*SIN(AH)+PP*RR*(AH-SIN(AH))
        EL1A=(H1+H2)*RR/(E2*AP)
        EL1B=RR*AH*YI*(1./E1-1./E2)
        EL1=EL1A+EL1B
        EL2=0.
        SP=(FB-YI)*AP/FS
        ELP=(FB*SP-0.5*FS*SP*SP/AP)/E2
        SE=YI*AP/FS
```

```
        ELE=(YI*SE-.5*FS*SE*SE/AP)/E1
        S3=SP+SE
        EL3=ELP+ELE
        GO TO 380
  330 CALL ANGLE(PX,VX,FP,PP,AP,RR,YI,AG,PI,NG,DX)
      S1=AG*R(I)
      H1=(V(I)+FP*R(I))*(COS(AG)-1.)
      H2=P(I)*SIN(AG)+PP*R(I)*(AG-SIN(AG))
        EL1A=R(I)*(H1+H2)/(E2*AP)
        EL1B=R(I)*AG*YI*(1./E1-1./E2)
        EL1=EL1A+EL1B
      V3=FP*R(I)*(1.-COS(AG))+PP*R(I)*SIN(AG)
      V4=P(I)*SIN(AG)+V(I)*COS(AG)
      VT=V3-V4
      PT=YI*AP
      TMOM=(P(I)-PT)*R(I)-FP*R(I)*R(I)*AG
      GO TO 360
C.....MAX. AXIAL STRESS INDUCED IN ELASTIC REGION.....
  350 S1=0.
      EL1=0.
      AG=0.
      ANG=AEL
      VT=V(I)
      PT=P(I)
  360 IF(FB.GE.0.) GO TO 365
        FB=0.
        CALL ANGLE(PT,VT,FP,PP,AP,RR,FB,AF,PI,NG,DX)
        GO TO 366
  365 AF=AH-AG
  366 S2=AF*R(I)
      H5=(VT+FP*R(I))*(COS(AF)-1.)
      H6=PT*SIN(AF)+PP*R(I)*(AF-SIN(AF))
      EL2=(H5+H6)*R(I)/(E1*AP)
      S3=FB*AP/FS
      EL3=(FB*S3-0.5*FS*S3*S3/AP)/E1
      IF(FB.LE.0.) EL3=0.
  380 LP=2.*(EL1+EL2+EL3)
C.....COMPARISON......
      DIF=(LP-LG)/LP
      CK(I)=DIF
      DIFA=ABS(DIF)
        JCT=JCT+1
      IF(DIF.GT.STD) GO TO 445
      WRITE(6,390) I,R(I),FA,FB,VA
  390 FORMAT(/6X,I4,6X,'R =',F12.3,6X,'FA =',F10.3,5X,'FB =',
     ,F10.3,6X,'VA =',F10.3)
      AB=THETAB*180./PI
      A1=AG*180./PI
      A2=AF*180./PI
      WRITE(6,420) ALPHA(I),A1,A2,AB
  420 FORMAT(12X,'ALPHA =',F8.3,10X,'A1 =',F8.3,7X,'A2 =',F8.3,
```

```
     ,5X,'THETA =',F7.3,1X,'DEG.')
      PERT=DIF*100.
      WRITE(6,440) EL1,EL2,EL3,LG,LP,PERT
  440 FORMAT(14X,'EL1 =',F10.2,7X,'EL2 =',F8.2,6X,'EL3 =',F10.2/
     ,15X,'LG =',F10.2,1X,'IN.',4X,'LP =',F8.2,1X,'IN.',
     ,20X,F8.2,'% OFF')
          IF(DIF.LE.STDN) GO TO 480
      IK=I-1
          IF(JCT.EQ.1.AND.I.GE.2) CK(IK)=0.
      IF(DMIN.LE.SD) GO TO 445
      IF(DIF.GT.0.) GO TO 445
          DCK=CK(IK)-CK(I)
          HK=40.0*DCK
          ACK=ABS(DCK)
          IF(ACK.LE.SD) HK=1.1
      IF(CK(IK).EQ.DMIN.AND.DIFA.GT.DMIN) GO TO 460
  445 IF(DIFA.GT.DMIN) GO TO 480
        DMIN=DIFA
        IA=I
        UG=LG
        UP=LP
        SMOM=MOM
        SL=S3/12.
        FBB=FB
        AE=AF*180./PI
        AIN=(AH-AF)*180./PI
        IF(DIF.GE.SD2) GO TO 480
        IF(DIFA.LT.SD) GO TO 480
          DCK=CK(IK)-CK(I)
          HK=40.0*DCK
          ACK=ABS(DCK)
          IF(ACK.LE.SD) GO TO 480
        IF(DIF.GE.0.) GO TO 470
          IA=5000
          IF(ID.EQ.2) IA=6000
  460     AH=AH-ANG/HK
          CK(IK)=CK(I)
          GO TO 305
  470     AH=AH+ANG/HK
          CK(IK)=CK(I)
          GO TO 305
  480 CONTINUE
      IF(DIF.LE.STD) IDS=5
        IF(DIF.LT.-0.15) IDX=2
      IF(IDS.EQ.5) AL=ANG
  490 CONTINUE
      AH=AH+AL
      THETAB=0.5/(LAMDA*R(I))
  500 CONTINUE
          IF(NCK.EQ.5) GO TO 550
C
```

```
      TB=THETAB
      IF(IA.EQ.2000) GO TO 650
      IF(IA-5000) 510,760,780
  510 THETAB=0.5/(LAMDA*R(IA))
      DFS=(THETAB-TB)/THETAB
      IF(K.GT.100) GO TO 800
      IF(DFS.GT.SD) GO TO 300
      FA=P(IA)/AP
      TAU1=V(IA)/AP
      TAU2=LAMDA*SMOM/AP
      BS=SMOM*D/(2.*IX)
      TA=ALPHA(IA)*PI/180.
      DIS=R(IA)*TA-UG/2.
      IF(ID.EQ.2) DIS=DIS+UG
      DIST=DIS/12.
      TG=THETAB*180./PI
      RC=R(IA)/12.
      GCL=UG/12.
      PCL=UP/12.
      SM=SMOM/12000.
      ZM=ZMOM/12000.
      WP=FBB/YII
      WM=SMOM/ZMOM
        AWP=PI*WP/2.
        WPC=COS(AWP)
C
          IF(SMOM.GT.ZMOM) GO TO 550
          IF(SMOM.GT.EM1) IDR=2
          IF(IDR.EQ.2) GO TO 542
C
  515 WRITE(6,520)FA,TAU1,FBB,TAU2,BS,SM,ZM
  520 FORMAT(/15X,'................... FINAL SOLUTION ......',
     ,'...............'/
     ,15X,'A. STRESSES'/
     ,18X,'1. AXIAL STRESS AT POINT A =',F12.2,1X,'PSI'/
     ,18X,'2. AVERAGE SHEAR STRESS AT POINT A =',F10.2,1X,'PSI'/
     ,18X,'3. AXIAL STRESS AT POINT B =',F10.2,1X,'PSI'/
     ,18X,'4. AVERAGE SHEAR STRESS AT POINT B =',F10.2,1X,'PSI'/
     ,18X,'5. BENDING STRESS AT POINT B =',F12.2,1X,'PSI'/
     ,18X,'6. BENDING MOMENT AT POINT B =',F12.4,1X,'KIP-FT.'/
     ,18X,'7. PLASTIC RESISTING MOMENT OF PIPE =',F12.4,
     ,1X,'KIP-FT.')
      WRITE(6,530) RC,GCL,PCL,DIST,SL
  530 FORMAT(/15X,'B. LENGTHS'/
     ,18X,'1. RADIUS OF CURVATURE =',F10.3,1X,'FT.'/
     ,18X,'2. GEOMETRIC ELONGATION =',F10.3,1X,'FT.'/
     ,18X,'3. PERMISSIBLE ELONGATION =',F10.3,1X,'FT.'/
     ,18X,'4. DISTANCE FROM FAULT TO POINT B =',F10.3,1X,'FT.'/
     ,18X,'5. AFFECTED LENGTH IN ELASTIC FOUNDATIIN =',F10.3,
     ,1X,'FT.')
      WRITE(6,540) ALPHA(IA),AIN,AE,TG,WP,WM,WPC
```

```
  540 FORMAT(/15X,'C. ROTATIONS'/
     ,18X,'1. SUBTENDING ANGLE (ALPHA) =',F8.3,1X,'DEG.'/
     ,18X,'2. SUBT. ANGLE IN INELASTIC ZONE =',F8.3,1X,'DEG.'/
     ,18X,'3. SUBT. ANGLE IN ELASTIC ZONE =',F8.3,1X,'DEG.'/
     ,18X,'4. ROTATION AT POINT B =',F8.3,1X,'DEG.'/
     ,/15X,'D. RATIOS'/
     ,18X,'1. RATIO OF PB/PY =',F7.3/
     ,18X,'2. RATIO OF MB/MZ =',F7.3/
     ,18X,'3. RATIO OF MPC/MZ =',F7.3/
     ,15X,'.............................................')
      IF(K.LT.100) GO TO 800
C
C.....REDUCTION OF MODULUS OF ELASTICITY
  542  IF(SMOM.GT.EM2) GO TO 544
      IF(SMOM.GT.EM1.AND.SMOM.LE.EM2) GO TO 546
          RME=E1
          GO TO 548
  544          RME=ER2*(ZMOM-SMOM)/(ZMOM-EM2)
                GO TO 548
  546               RME=SMOM/((EM1/E1)+(SMOM-EM1)/E2)
  548 DRME=(ER-RME)/RME
      ARME=ABS(DRME)
          WRITE(6,549)DRME,RME,SMOM
  549 FORMAT(10X,'DIFFERENCE RATIO OF "ER" =',F7.3/
     ,10X,'REDUCED MODULUS, RME =',F12.2/
     ,10X,'INDUCED MOMENT AT POINT "B" =',F12.2)
      IF(ARME.LE.0.05) GO TO 515
          CRE=1.0-EEN*K
          IF(DRME.LT.0.0) GO TO 901
          IF(JRE.EQ.100) GO TO 902
          EEN=EEN/2.0
          CRE=PRE-EEN
          GO TO 902
  901     JRE=50
          EEN=EEN/2.0
          CRE=PRE+EEN
  902     PRE=CRE
          ER=CRE*E1
         GO TO 300
C
  550 WRITE(6,560)
  560 FORMAT(/3X,'***** THE ITERATION IS NOT CONVERGENT *******')
      GO TO 800
  650 WRITE(6,660)
  660 FORMAT(/16X,'..... WRONG ..........')
      GO TO 800
  760 WRITE(6,770)
  770 FORMAT(/16X,'..... TENSILE FAILURE OCCURS ..............'/)
      GO TO 800
  780 WRITE(6,790)
  790 FORMAT(/16X,'..... COMPRESSIVE FAILURE OCCURS ........'/)
```

```
 800 CONTINUE
     STOP
     END
     SUBROUTINE ANGLE(G,H,FP,PP,AP,RR,SF,AG,PI,NG,DX)
     AD=PI/9000.
     A=0.
     IND=5
     DO 2100 J1=1,NG
     IF(IND.EQ.6) GO TO 2100
2060 CONTINUE
       C1=G*COS(A)-H*SIN(A)
       C2=PP*RR*(1.-COS(A))-FP*RR*SIN(A)
       YG=(C1+C2)/AP
     DEL=YG-SF
     IF(DEL.GT.-100.) GO TO 2080
       A=A-AD/4.
       GO TO 2060
2080 A=A+AD
       IF(ABS(DEL).LT.DX) IND=6
2100 CONTINUE
     AG=A-PI/9000.
     IF(IND.EQ.5) AG=10000.
     RETURN
     END
c........DATA SET........
  70.0      30.0      20.0     110.0
    1
  800
  600
    1
  72000.    85000.
   9.8      57.0      42.0       0.562
```

APPENDIX D

Computer Program for Soil Liquefaction

```
c.......................................................
c                                                      c
c     Dynamic response of pipeline subjected to soil   c
c     liquefaction during earthquake                   c
c     (Under Effects of Various Different Soil Stiffness) c
c                                                      c
c......................................................c
      dimension y(45,25),u(45,25),ut(45,25),p(45,25),
     ,pr(45,25),ps(6,700),ys(6,700),us(6,700),pd(6,700)
      dimension uk(2500),um(2500)
      real ix,lr,nq,ks
      data r,gam,thk,pi/21.0,6.3657e-2,0.562,3.14159/
      data el,sl,cp,vs/3.0e+7,10.0,2.0e+5,0.256/
      data nq,clr,as,stress/9.8,150.0,2.50,72000.0/
      d=2.0*r
      aa=pi*(d-thk)*thk
      ix=pi*(d**4-(d-thk*2.)**4)/64.
      rg=(ix/aa)**0.5
      ks=200.*nq*gam
      sk=ks*rg**2/(aa*el)
c
               read(5,50)id
   50 format(i5)
               write(6,55)id
   55 format(/5x,'index for displacement input, id=',i3)
      if(id.ne.5) go to 75
c
c.....Input data of 1940 El Centro Earthquake
      ueq=0.0
      uk(3)=0.0
      do 70 i=1,41
            j=i*60
            jq=j-60
                  read(5,60)uk(j)
                  write(6,60)uk(j)
   60             format(f12.7)
            dis=(uk(j)-uk(jq))/60.
               do 70 kz=1,60
                    jk=jq+kz
```

```
                        uk(jk)=ueq+dis
                        ueq=uk(jk)
   70 continue
   75    continue
c
      nu=1
                  read(5,85)dx,dt,a
                  read(5,95) kn,kase
                  read(5,80)m,nt,ml,mr
                  read(5,90)lr,v
   80 format(4i5)
   85 format(3f10.2)
   90 format(f10.2,e15.5)
   95 format(2i5)
            es=(pi/clr)**2
            strain=stress/el
            pratio=strain/es
      write(6,100) aa,ix,rg,lr,a,es,strain,pratio,v
  100 format('1',5x,'..........the giving data...........'/
     ,5x,'cross-sectional area of rod, aa=',e12.4,1x,'sq.in.'/
     ,5x,'moment of inertia of rod, ix=',e12.4,1x,'in**4'/
     ,5x,'radius of gyration, rg=',e12.4,1x,'in.'/
     ,5x,'slenderness ratio of rod, lr=',f10.3/
     ,5x,'initial crookedness of pipe, a=',f10.3/
     ,5x,'buckling strain of pipe, es=',e12.4/
     ,5x,'yielding strain of pipe=',f10.4/
     ,5x,'ratio of yield-load/buckling-load =',f10.3/
     ,5x,'speed ratio of vs/cp, v=',e12.4)
      m1=m+1
      m2=m-1
      m3=m+2
      m4=m-2
      nt1=nt+1
      ms=m-3
      np=nt-3
      mp=ms/2+3
                 write(6,106) kn
  106 format(/5x,'condition of supporting foundation, kn =',i3)
                 write(6,110) ms,np
  110 format(5x,'number of rod segment, ms=',i4/
     ,5x,'number of time interval, np=',i4)
      if(id.eq.5) go to 112
            write(6,132)dt
  112 continue
      do 360 k=1,4
c
c.....soil stiffness conditions
      qc=1.0
          qf=0.12-(k-1)*0.04
          if(kase.eq.1) qf=0.0
      ts=0.2*np
```

```
      nb=np/5 + 3
      ab=-as/ts
      bpz=exp(-as)/(ml-3)
c
c.....initial conditions......................
c
      if(id-3)115,125,131
c.....(1) linear function for axial displacement
  115  do 120 j=3,nt
         um(j)=-v*dt*(j-3)
  120 continue
      go to 135
c
c.....(2) sine function for axial displcement
  125         read(5,126)dr
  126 format(f10.3)
              write(6,127)dr
  127 format(5x,'amplitude of sinusoidal displacement, dr=',f10.3)
      do 130 j=3,nt
         xi=2.0*pi*(j-3)/np
         um(j)=-dr*sin(xi)
  130 continue
          go to 135
c
c.....(3) Displacement of 1940 El Centro Earthquake
c
  131     dt=cp*0.1/(rg*60.)
          write(6,132)dt
  132     format(5x,'nondimensional time interval =',f10.3)
             do 134 j=3,nt
                um(j)=(uk(j)/rg)*lr/(3.0*clr)
  134        continue
c
c.....initial crookedness of the buried pipe...............
c
  135 um(nt1)=um(nt)
      do 150 i=3,m
         cc=1.0
      if(i.ge.ml.and.i.le.mr) go to 140
         xi=-(i-3)*pi/(ml-3)
         if(i.gt.mr) xi=-(i-mr)*pi/(m-mr)
             cc=0.5*(lr-clr)/clr
         go to 145
  140    xi=(i-ml)*pi/(mr-ml)
  145    y(i,3)=cc*a*sin(xi)
         y(i,2)=y(i,3)
         y(i,4)=y(i,2)
         u(i,3)=0.
         u(i,2)=0.
         u(i,4)=(um(4)*(i-3))/ms
         p(i,3)=0.
```

```
        pr(i,3)=p(i,3)/es
  150 continue
          y(3,3)=0.
          y(3,2)=0.
          y(m1,3)=0.
           y(m1,2)=0.
          y(mr,3)=0.
           y(mr,2)=0.
      y(m,3)=0.
      y(2,3)=-y(4,3)
      y(1,3)=-y(5,3)
      y(m1,3)=-y(m2,3)
      y(m3,3)=-y(m4,3)
      u(2,3)=-u(4,3)
      u(m1,3)=0.
      p(2,3)=0.
c
                write(6,160)
  160 format(/5x,'the dynamic responses of rod...........')
      write(6,161) kase
  161 format(5x,'soil stiffness conditions, kase =',i4)
      ji=0
           if(k-2) 162,164,166
  162 write(6,292)ji,(u(i,3),i=3,m,5)
      write(6,294)ji,(pr(i,3),i=3,m,5)
      write(6,296)(y(i,3),i=3,m,5)
                go to 180
  164    write(6,280)ji,(u(i,3),i=3,m,5)
         write(6,285)ji,(pr(i,3),i=3,m,5)
         write(6,290)(y(i,3),i=3,m,5)
                     go to 180
  166 write(6,280)ji,u(3,3),u(6,3),u(9,3),u(14,3),
     ,u(19,3),u(22,3),u(25,3)
      write(6,285)ji,pr(3,3),pr(6,3),pr(9,3),pr(14,3),
     ,pr(19,3),pr(22,3),pr(25,3)
      write(6,290)y(3,3),y(6,3),y(9,3),y(14,3),y(19,3),
     ,y(22,3),y(25,3)
  180 continue
c
c.....iteration process for finite difference..............
c
      do 350 jh=4,nt
      j=jh
      jp=jh+1
      jn=jh-3
      if(jh.gt.20) go to 185
          j2=j-1
          j1=j+1
          if(j1.gt.20) j1=j1-10
          go to 190
  185             kh=(jh-11)/10
```

```
               j=jh-kh*10
               j2=j-1
               if(j2.le.10) j2=j2+10
               j1=j1+1
               if(j1.gt.20) j1=j1-10
  190 continue
      u(3,j)=0.
      u(2,j)=-u(4,j)
      u(m1,j)=(um(jh)/(m-3))*(m-2)
      y(3,j)=0.
      y(m,j)=0.
      y(2,j)=-y(4,j)
      y(1,j)=-y(5,j)
      y(m1,j)=-y(m2,j)
      y(m3,j)=-y(m4,j)
c
      do 200 i=3,m
         i1=i+1
         i2=i-1
         up=(u(i1,j)-u(i2,j))/(2.*dx)
         ypa=(y(i1,j)-y(i2,j))**2
         ypb=(y(i1,3)-y(i2,3))**2
         yp=(ypa-ypb)/(8.*(dx**2))
         p(i,j)=-yp-up
         pr(i,j)=p(i,j)/es
  200 continue
      p(m1,j)=p(m,j)
      pr(m1,j)=p(m1,j)/es
c
      if(nu.eq.0) go to 230
      do 220 i=4,m
         i1=i+1
         i2=i-1
         uu=2.*u(i,j)-u(i,j2)
         pu=(dt**2)*(p(i1,j)-p(i2,j))/(2.*dx)
         ut(i,j1)=uu-pu
  220 continue
      udf=(um(jp)-ut(m,j1))/ms
  230 continue
c
c.....Defines characteristic function of soil stiffness
c
          if(kn.ne.1) go to 240
      if(kase.eq.1.or.kase.eq.5) go to 240
      at=-ab*(jh-3)
      qf=exp(at)-exp(-as)*(jh-3)/ts
          if(jh.ge.nb) qf=0.0
      if(kase.ne.3) go to 240
         bk2=2.0*(jh-3)
         bq=-bk2/np
         qc=exp(bq)
```

```
  240 continue
c
      do 270 i=4,m
      i1=i+1
      i2=i-1
      i3=i+2
      i4=i-2
c
c.....stiffness of elastic foundation
           if(kase.eq.4) go to 255
      if(kn.eq.2) go to 251
      if(kn.eq.3) go to 252
      if(i.lt.ml.or.i.gt.mr) go to 251
      if(i.gt.ml.or.i.lt.mr) go to 252
      q = 0.5*(qc + qf)
      go to 265
  251 q=qc
      go to 265
  252 q=qf
      go to 265
  255 bc=ab/(ml-3)
        bce=bpz*(jh-3)/ts
      if(i.le.ml) go to 257
      if(i.ge.mr) go to 258
           q=qf
      go to 265
  257 if(jh.ge.nb) go to 2571
      bcq=-(bc*(i-3))*(jh-3)
              qc=exp(bcq)-bce*(i-3)
      go to 260
 2571   bct=bc*ts*(i-3)
        qc=exp(bct)-bpz*(i-3)
      go to 260
  258 if(jh.ge.nb) go to 2581
      bcr=-(bc*(m-i))*(jh-3)
          qc=exp(bcr)-bce*(m-i)
      go to 260
 2581   bcx=bc*ts*(m-i)
        qc=exp(bcx)-bpz*(m-i)
  260   q=qc
  265 continue
c
c.....Difference equations for lateral deflection
c
      yl=2.0*y(i,j)-y(i,j2)
      yi=y(i,j)-y(i,3)
      yi1=y(i1,j)-y(i1,3)
      yi2=y(i2,j)-y(i2,3)
      yi3=y(i3,j)-y(i3,3)
      yi4=y(i4,j)-y(i4,3)
      yk=yi*sk*(dt**2)*q
```

```
      y2=(dt/dx)**2*(p(i1,j)-p(i2,j))*(y(i1,j)-y(i2,j))/4.
      y3=(dt/dx)**2*p(i,j)*(y(i1,j)-2.*y(i,j)+y(i2,j))
      ya=yi3-4.*yi1+6.*yi-4.*yi2+yi4
      y4=ya*dt**2/(dx**4)
      y(i,j1)=y1-(y2+y3+y4)-yk
         u(i,j1)=ut(i,j1)+udf*(i-3)
  270 continue
c
      jk=jn/6
      jt=jk*6
      if(jn.ne.jt) go to 300
      if(jk.gt.120) go to 300
         jx=jk/2
         jy=2*jx
         if(jk.ne.jy) go to 300
               if(lr.lt.500.) go to 274
  272            write(6,292)jk,(u(i,j),i=3,m,5)
                 write(6,294)jn,(pr(i,j),i=3,m,5)
                 write(6,296)(y(i,j),i=3,m,5)
      go to 300
  274       write(6,280)jk,(u(i,j),i=3,m,5)
            write(6,285)jn,(pr(i,j),i=3,m,5)
            write(6,290)(y(i,j),i=3,m,5)
                     go to 300
  276 write(6,280)jk,u(3,j),u(6,j),u(9,j),u(14,j),
     ,u(19,j),u(22,j),u(25,j)
      write(6,285)jn,pr(3,j),pr(6,j),pr(9,j),pr(14,j),
     ,pr(19,j),pr(22,j),pr(25,j)
      write(6,290)y(3,j),y(6,j),y(9,j),y(14,j),y(19,j),
     ,y(22,j),y(25,j)
  280 format(/5x,i5,4x,'u=',7(1x,e12.4))
  285 format(5x,'(',i4,')',2x,'pr=',7(1x,e12.4))
  290 format(14x,'y=',7(1x,e12.4))
  292   format(/1x,i5,4x,'u=',9e12.4)
  294   format(1x,'(',i4,')',2x,'pr=',9e12.4)
  296   format(10x,'y=',9e12.4)
  300 continue
      if(jn.ne.jt) go to 350
      pd(k,jk)=pr(mp,j)/y(mp,j)
      ys(k,jk)=y(mp,j)
      ps(k,jk)=pr(mp,j)
      us(k,jk)=u(mp,j)
  350 continue
         do 360 i=3,m
         y(i,3)=0.0
  360 continue
c
c.....graphs for resulting data.......................
c
      nm=np/6
c
```

```
      do 400 i=0,nm
         write(18,450)i,(ys(k,i),ps(k,i),k=1,4)
  400 continue
  450 format(i5,8(2x,e12.4))
      stop
      end
c.......DATA SET.......
   3
  15.0      15.0      0.25
   1   5
  43 1383   18   28
  600.0       1.00000e-4
  3.000
  3.000
  3.000
  3.000
  450.0       1.05000e-4
  450.0       0.95000e-4
  33 1383   13   23
  450.0       0.75000e-4
  25 2463    9   19
  330.0       0.55000e-4
  33 1023    5   13   23
  150.0       0.31907e-4
c........SAS/GRAPH
data;
infile fred;
input t y1 p1 y2 p2 y3 p3 y4 p4;
label y1=lateral displcement;
goptions hsize=6.4 vsize=4.95;
proc gplot;
title response of lateral displcement;
footnote response to different stiffness at liquefiable zone;
plot y1*t y2*t y3*t y4*t/haxis=0 to 250 by 50 overlay;
symbol1 i=spline c=1;
symbol2 i=spline l=3 c=1;
symbol3 i=spline l=15 c=1;
symbol4 i=spline l=9 c=1;
proc gplot;
goptions hsize=6.4 vsize=4.95;
plot p1*t p2*t p3*t p4*t/haxis=0 to 250 by 50 overlay;
label p1=axial load ratio;
title dynamic response - axial load;
footnote response to different stiffness at liquefiable zone;
symbol1 i=spline c=1;
symbol2 i=spline l=3 c=1;
symbol3 i=spline l=15 c=1;
symbol4 i=spline l=9 c=1;
```